DOCTORAL (Ph.D.) DISSERTATION

Colloidal stability in the presence of ionic liquids: Tuning interactions in particle dispersions

Dóra Takács

Supervisor:
Dr. István Szilágyi
associate professor

Doctoral School of Chemistry
Faculty of Science and Informatics
Department of Physical Chemistry and Materials Science
University of Szeged

Szeged
2024

Table of contents

List of abbreviations

AFM	Atomic force microscopy
AL	Amidine latex particle
BMIM	1-butyl-3-methylimidazolium
BMPIP	1-butyl-1-methylpiperidinium
BMPL	1-butyl-1-methylpyrrolidinium
BMPY	1-butyl-1-methylpyridinium
CCC	Critical coagulation concentration
DLS	Dynamic light scattering
DLVO	Derjaguin, Landau, Verwey and Overbeek
EAN	Ethylammonium nitrate
EDL	Electric double layer
IEP	Isoelectric point
IFT	Indirect Fourier Transformation
ILs	Ionic liquids
IP-2	Polyimidazolium ionic liquid polymer
LDH	Layered double hydroxide
SAXS	Small-angle X-ray scattering
SL	Sulphate latex particle
SWAXS	Small- and wide-angle X-ray scattering
TEM	Transmission electron microscopy
XRD	X-ray diffraction

1. Introduction

Ionic liquids (ILs) have emerged as a pioneering class of tuneable solvents that are composed entirely of ions yet maintain a liquid state below 100 °C [1]. They possess a variety of advantageous properties and therefore hold significant potential for various applications in areas such as materials synthesis, catalysis, and electrochemical processes [2]. ILs play an important role in particle dispersions, acting either as the main medium or as additives [3-6], and they have a major impact on the outcome of applications. It is obvious that in heterogeneous particle-IL systems, colloidal stability is one of the most critical parameters. The interplay of attractive and repulsive forces determines the aggregation processes of the particles and thus the stability of the dispersion [7]. However, since ILs are ionic by nature, they add complexity to our understanding of electrostatic forces in such systems. The strong ionic character of ILs screens long-range repulsive forces, necessitating a deeper knowledge of the interactions between IL components and dispersed particles for effective utilisation of IL-containing dispersions.

Despite significant progress in the physicochemical characterisation of ILs in bulk phases, the study of their interfacial properties and their influence on colloidal stability is a recent endeavour [8]. The aim of the present work is therefore to investigate and map the charge and aggregation relations between different particles in heterogeneous IL-based systems. Factors such as water and salt content are scrutinised to determine the physicochemical parameters that influence colloidal stability in IL media and how these parameters can be adjusted to achieve optimal results. In addition, ion specificity has a significant impact on the stability of IL-containing dispersions, which may hinder their applicability. Thus, this problem was also addressed by investigating basic charging and aggregation processes in aqueous IL solutions while systematically modifying the IL structures.

Furthermore, ILs have proven to be promising alternatives to conventional solvents for the delamination of layered materials [9]. They facilitate the exfoliation in one-step in a liquid phase and the subsequent stabilisation of the resulting 2D nanosheets in dispersions. Therefore, the interactions between IL components and layered materials – namely, layered double hydroxides (LDH) – were investigated in both aqueous and pure IL media. The overall findings can help to support the selection of suitable ILs based on their structural and physicochemical properties and to optimise the choice of solvents for specific applications.

2. Literature review

2.1. Ionic liquids

ILs are defined as a liquid below 100°C and – in contrast to conventional solvents – they are composed entirely of ions, which gives them a unique property profile [1, 8, 10]. The steric imbalance between the composing ions leads to poor coordination and weaker Coulombic forces, which prevents their arrangement in a regular crystal structure and causes unusually low melting temperatures. ILs typically consist of a bulky organic cation paired with a compact organic or inorganic anion. The structure of the most commonly described IL cations and anions is depicted in Figure 1.

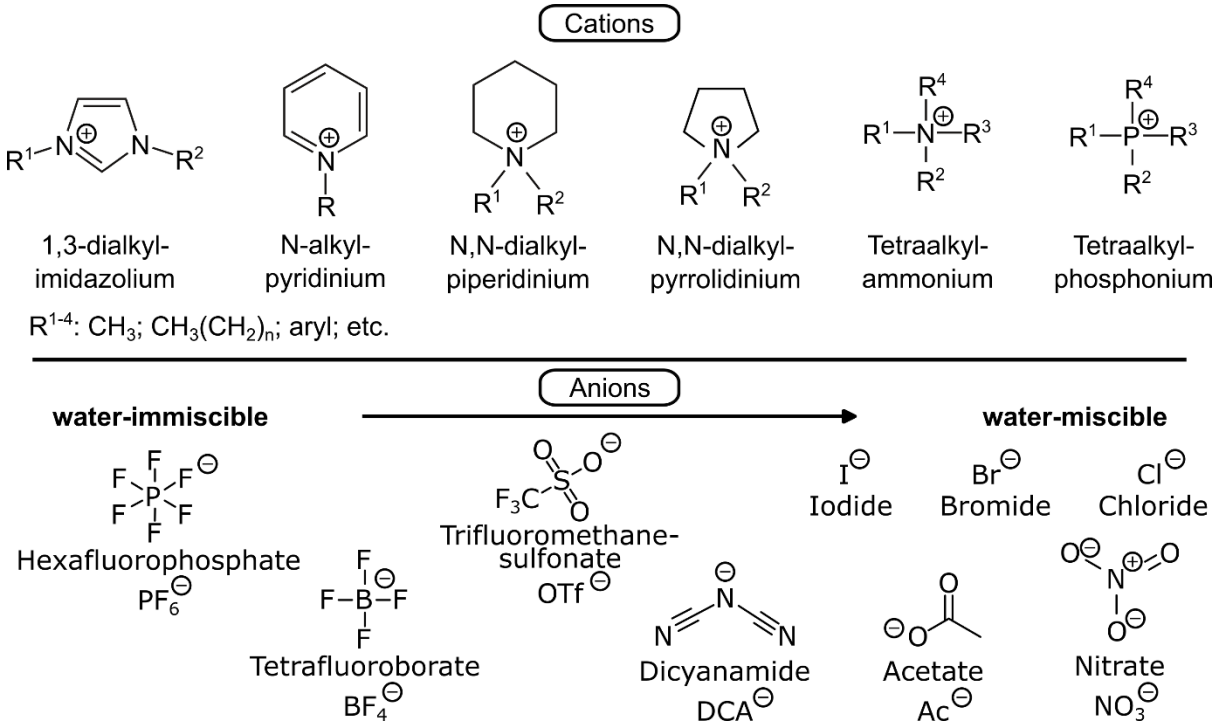

Figure 1. The chemical structures and names of the cations and anions that make up the commonly used ILs.

Research in the field of ILs has experienced a significant upswing in recent decades, although they were discovered much earlier. The reason for this lies in the specific physicochemical properties of ILs. Accordingly, they do not vaporise, thus the upper limit of their operational temperature range is determined by their thermal decomposition temperature [11]. The negligible vapour pressure of ILs at ambient conditions – compared to volatile organic solvents – is a strong ecological advantage. In addition, the lower volatility of these solvents and their non-flammability contribute to the operational safety of a given process, as mixtures of volatile

organics and air are always associated with explosion hazards. However, the actual environmental friendliness of ILs is generally doubtful, given the lack of clarity regarding their direct toxicity and environmental behaviour [12].

The term "designer solvent" has been coined for ILs due to the possibility of gradually changing their physicochemical properties by adjusting cations and anions, as well as their diversity [1, 13]. The combination of different types of cations and anions enables not only the continuous production of novel ILs with new qualities, but also a finer tuning of specific properties such as viscosity, thermal stability, vapour pressure, and hydrophobicity, making ILs valuable materials for a wide range of chemical processes. In rheological studies of ILs, altering either the cation or anion structure while keeping the other constant, is a common approach to tuning dynamic viscosity, lubricity, and solvation properties. These studies have shown that higher charge localisation leads to higher viscosity in ILs. Thus, factors such as ion size and charge delocalisation are crucial parameters that influence viscosity [14]. This relationship also applies to the density of ILs. Even a seemingly minor structural change, such as replacing a C8 chain with a C10 chain on an alkylimidazolium moiety (see Figure 1), affects the physicochemical properties of the resulting IL [15].

The physicochemical properties of ILs depend strongly on their bulk structure and their intrinsic ionic nature [8, 16]. Most researchers suggest that the bulk structure of IL is similar to that of a highly concentrated salt solution or a molten salt. However, recent models propose that ILs are structured solvents ranging from supramolecular (ion pairs, ion clusters) to mesoscopic (H-bond networks, micelle-like, and bicontinuous morphologies) length scales. Imidazolium-based ILs, for example, form networks of cations and anions connected by hydrogen bonds [17]. The ionicity in ILs reflects the fraction of dissociated species that avoid clustering, and it strongly depends on the structural composition of the IL [16]. The higher the dissociation of an IL, the more it exhibits unique properties that make it a special class of solvent.

As a consequence of this unusual range of properties, ILs are highly attractive from both fundamental and practical perspectives [2, 13, 18-20]. They are used in electrochemical [19] (e.g., batteries, sensors, electrodeposition, dye-sensitised solar cells), chemical [21] (e.g., organic reactions, nanoparticle synthesis, catalysis) and extraction processes (e.g., enhanced oil recovery [22], microextraction [23]). ILs are also used as additives, such as lubricants [24], surfactants [25], and shale [26] or corrosion inhibitors [27]. In most of these applications, the

physical arrangement of the ions at the interfaces plays a key role in determining the process efficiency (see Figure 2), as it controls processes as diverse as amphiphilic adsorption, colloidal stability, lubrication, heterogeneous catalysis or charge transfer [28].

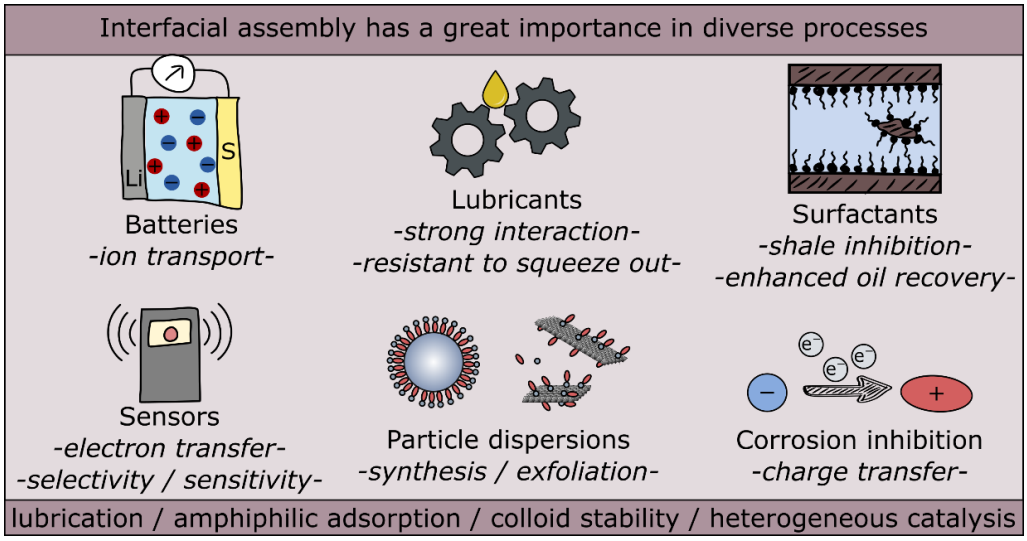

Figure 2. The importance of interfacial layering of IL compounds in various applications.

Regarding IL applications, the use of particle dispersions containing ILs – either as the main medium or as an additive – is receiving considerable attention (as discussed in more detail later in section 2.4) [3]. With the increasing importance of IL dispersions, it becomes imperative to focus on understanding the mechanisms behind the stabilisation of (nano)particles in ILs, since colloidal stability plays a crucial role in the success of these applications. A better understanding of the interactions in IL-containing dispersions enables the development of tailored materials with improved performance and durability, paving the way to fully exploit their potential [29].

2.2. Colloidal stability

The applications described above make it clear that it is crucial to know and adjust the stability of IL-containing colloidal systems. The importance and dynamic character of stability can be well illustrated by heterogeneous catalysis [30, 31]. Accordingly, a stable dispersion of primary particles is essential during the catalytic process, while these stable dispersions are destabilised after completion of the reaction due to aggregation and subsequent filtering to remove the particles. However, before addressing the potential interactions between particles dispersed in ILs, it is important to clarify the origin of the interparticle forces that are normally responsible for colloidal stability in aqueous suspensions, as well as the parameters that influence the stability of charged particles in the presence of electrolytes.

2.2.1. DLVO theory

The DLVO theory (after the initials of the famous theoretical physicists Boris Derjaguin, Lev Landau, Evert Verwey and Theo Overbeek) can be used to efficiently explain the stability of aqueous dispersions of charged particles [32, 33]. It describes the total interaction energy (V_T) between charged surfaces at a given separation distance (h) as the sum of the van der Waals (V_{vdW}) and the electric double layer forces (V_{EDL}):

$$V_T(h) = V_{EDL}(h) + V_{vdW}(h) \quad (1)$$

Van der Waals forces are always present, and they arise from the interactions of the rotating or oscillating dipoles of atoms and molecules. In principle, these interactions can be described using the Derjaguin approximation, which applies to particles that are larger than the interaction range [34]:

$$V_{vdW}(h) = -\frac{RH}{12h} \quad (2)$$

where R is the particle radius and H is the Hamaker constant, which specifies the strength of the interaction. In most cases, the Hamaker constant is positive, which means that the van der Waals force is attractive, and its value depends solely on the composition of the particle and the nature of the medium.

The explanation of the electric double layer force involves the complex behaviour of particles suspended in a polar liquid medium. Typically, these particles acquire a charge through the dissociation of surface groups, isomorphic substitution, or adsorption of charged species (e.g., ions, polymers) from the solution. A charged particle suspended in an electrolyte solution tends to be surrounded by a cloud of ions. The distribution of the ions around the particle is not uniform and results in a structure termed the electric double layer (EDL), as the surface charge requires balancing by ions with opposite charges to maintain electroneutrality [35]. This layer consists of an excess of counterions (opposite sign to the particle charge) and a deficiency of coions (same sign as the particle charge). The simplest representation of the EDL (see Figure 3) involves the notion that certain ions are loosely bound to the surface and form the Stern layer, while others are located further away in an ionic atmosphere characterised by continuous thermal motion and referred to as the diffuse layer.

In some cases, however, the separation of the EDL into a Stern layer and a diffuse layer may not provide sufficient insight for experimental interpretation. This is typically the case when a

distinction can be made between indifferent and specifically adsorbing ions. The Stern layer is then divided into two different regions: the inner Helmholtz layer (IHL) and the outer Helmholtz layer (OHL) [35]. The IHL is bounded by the surface and the inner Helmholtz plane (IHP), which passes through the centres of the specifically adsorbed ions, while the OHL lies between the IHP and the outer Helmholtz plane (OHP), which passes through the centres of the solvated ions at the distance of their closest approach to the charged surface and determines the beginning of the diffuse layer. The potential at the beginning of the diffuse part is called the diffuse-layer potential (ψ_D). Note that indifferent ions adhere solely through Coulomb forces, i.e., they are repelled by surfaces with the same charge, attracted to those with an opposite charge, and show no particular preference for adsorption on an uncharged surface. Conversely, specifically adsorbing ions exhibit a chemical or specific affinity for the surface in addition to Coulombic interactions. The term "chemical or specific" is a collective adjective that includes all interactions beyond purely Coulombic ones.

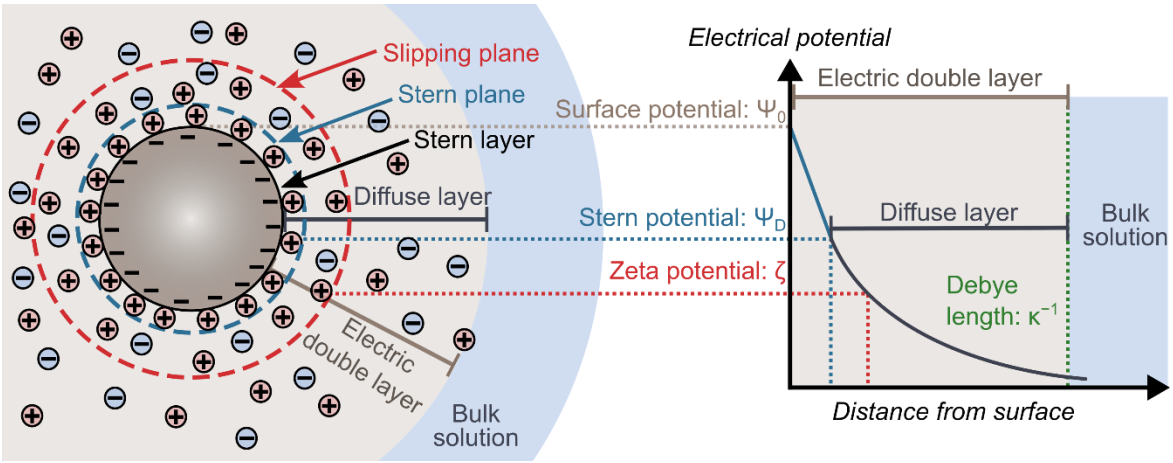

Figure 3. Schematic illustration of EDL structure and the characteristic distance-potential profile within the EDL.

In systems containing a charged solid-liquid interface, the movement of the particle or liquid creates a boundary within the diffuse layer, which is the so-called slipping plane. Within this, the particles behave like a dynamic unit, as it separates the liquid layer that adheres to the surface from the liquid layer that moves relative to the surface [35]. The potential difference between the slipping plane and the interior of the fluid is called the electrokinetic or zeta potential (ζ). This is an important parameter as its value can be directly determined empirically, e.g., using electrophoretic mobility, as explained later in section 4.2.2. In colloidal dispersions, the particles move by diffusion, which allows them to approach each other, and their EDLs may overlap,

leading to electrostatic repulsion between them, so that the interactions depend essentially on the EDL structure. The maximum potential occurs at the particle surface and decreases to zero at the boundary of the EDL, as it is electrically neutral. In general, there is a linear drop in potential in the inner layer, followed by an exponential decay to zero potential difference in an outer, diffuse layer (see Figure 3).

The mathematical equations describing the electrostatic interactions between charged surfaces in a liquid medium go back to the theory formulated by Gouy and Chapman [36]. They integrated thermal energy and Coulomb interactions into a statistical framework to describe these phenomena. For higher surface charge densities (i.e., particles with high electrostatic potential) and at smaller surface distances, the repulsion between the double layers can be quantified by applying the complex Poisson–Boltzmann equation between two identical plates [37]. In the simplest situation, when the surface charge density (i.e., the surface potential) is low, the Debye–Hückel approximation can be applied [38]:

$$V_{EDL}(h) = 2\pi\varepsilon_0\varepsilon R\psi_D^2 e^{-\kappa h} \tag{3}$$

where ε_0 and ε are the dielectric permittivity of the medium and the vacuum, respectively, while κ^{-1} is the Debye length, a fictitious constant used to estimate the thickness of the EDL, which depends on the ionic strength (I), among other parameters, as follows [35]:

$$\kappa^{-1} = \sqrt{\frac{\varepsilon\varepsilon_0 k_B T}{2N_A e^2 I}} \tag{4}$$

where k_B is the Boltzmann constant, T is the absolute temperature, N_A is the Avogadro number, and e is the elementary charge. The Debye length therefore depends only on the properties of the solution (ionic strength, dielectric constant, and temperature) and not on those of the surface. It is important to emphasise that the repulsion between the EDLs is not only of electrostatic origin. The potential profile that arises between two charged particles causes differences in the ion concentrations within the gap between these objects compared to the bulk solution [39]. These differences create an osmotic pressure that generates a force between the objects.

The structure and dimension of the EDL and thus the overall DLVO interactions can therefore be tuned by adding electrolytes to the samples [40]. Accordingly, surfaces with a high charge density in contact with a dilute electrolyte solution (low I) show a pronounced repulsion over large distances. This repulsion peaks at a certain distance, resulting in an energy barrier when considering the DLVO force (Figure 4a), which is the sum of the repulsive EDL and attractive

van der Waals forces. The potential energy well at contact is the thermodynamic equilibrium state for each system, while the particles that remain fully dispersed are in a kinetically determined stable state. As the ionic strength increases, the surface charges are compensated at a smaller distance, i.e., the thickness of the diffuse layer decreases. As a result, the energy barrier between the particles drops considerably, allowing them to approach each other in the range of van der Waals forces, which leads to aggregation. Once the surface charge density approaches zero (high I), the repulsive contribution is practically non-existent and the two surfaces attract each other strongly at all distances.

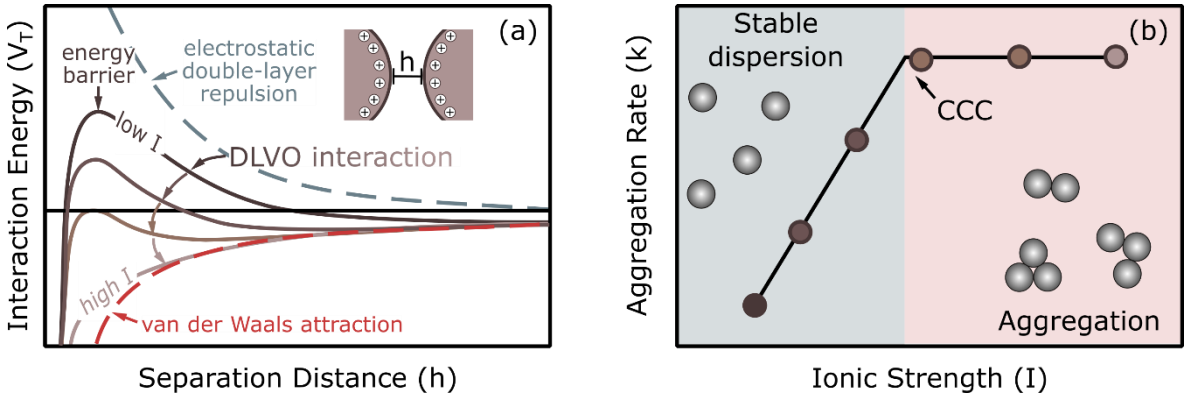

Figure 4. (a) Schematic DLVO plots show how the attractive van der Waals (red) and repulsive EDL forces (blue) together determine the total interaction potential (DLVO force, brown) between two charged surfaces in aqueous electrolyte solutions at different ionic strengths. (b) Variation of the aggregation rate constant of particle dimer formation with ionic strength.

When examining the aggregation rate as a function of electrolyte concentration, a distinct pattern can be observed (Figure 4b). At low ionic strength, charged particles have low or undetectable aggregation rates. However, as the salt concentration increases, the aggregation rate rises sharply as the energy barrier decreases, corresponding to the slow aggregation regime. Beyond a specific salt level, particles tend to aggregate rapidly, indicating the fast aggregation regime. The boundary between these two states is defined as the critical coagulation concentration (CCC) and marks a clear transition from slow to fast aggregation. The CCC serves as a precise measure to quantify the destabilising power of a particular electrolyte.

DLVO theory is often used to understand the stability and phase behaviour of lyophobic colloids, as it provides a good description of the interaction potential in simple colloidal dispersions. In complex aqueous systems, however, it has its limitations due to simplifications of the Poisson–Boltzmann theory. For example, the solvent is represented as a dielectric continuum, while the finite-size effects between ions, their chemical specificity, and the effect

of multivalent counterions are not taken into account. These shortcomings can cause the DLVO theory to fail in the interpretation of experimental data, especially in aqueous systems with high ionic strength. When the DLVO framework is not sufficient to explain certain experimental effects, non-DLVO forces come into play, such as hydration, hydrophobicity, specific ion effects, depletion, ion fluctuation, and polymer bridging [41-44].

2.2.2. Colloidal stability in ionic liquids

When explaining colloidal stability in IL-based particle dispersions, it becomes clear that the conventional DLVO theory faces major challenges. Due to the high ion concentration, it is expected that the surface charge of the particles is completely shielded so that electrostatic stabilisation cannot be assumed. This would mean that stable dispersions in ILs could not be prepared based on the DLVO theory. However, data from the literature indicate the opposite, i.e., stable dispersions exist in ILs [45, 46]. Moreover, the densely-packed ionic compounds in pure ILs behave far beyond the assumptions of Poisson–Boltzmann theory, which neglects the molecular nature of the solvent by representing it as a dielectric continuum medium. Consequently, it lacks any fluctuations in the ion concentration profile and does not take into account the local perturbations of the solvent structure around the particles. It also neglects any steric effects between the ions, which are considered to be point-like. However, regarding colloidal stability in ILs, these interactions are crucial and understanding them leads to many challenges that need to be addressed.

When a charged surface is immersed in a solvent composed entirely of ions, the prediction of the formation of an electric double layer, which is common in aqueous solutions, becomes unpredictable due to the complex interactions between ions in bulk ILs. Another issue is the uncertainties related to the dielectric constant, which is crucial for the description of electrostatic interactions. Surprisingly, ILs have moderate dielectric constants despite their ionic composition [47]. Moreover, the concept of ionic strength is also a matter of debate. There are questions regarding the complete dissociation of ILs and whether the dissociated fraction should be included in the calculation of ionic strength. Some authors rely on the definition of ionicity derived from the molar conductivity ratio ($\Lambda_{imp}/\Lambda_{NMR}$) [16], where Λ_{imp} is calculated from the ionic conductivity measured by the electrochemical impedance method and relies on the migration of charged species in an electric field, while Λ_{NMR} is estimated from the ionic self-diffusion coefficients obtained by nuclear magnetic resonance and assumes that each

diffusing species detected by this technique contributes to the molar conductivity. This ratio is therefore intended to represent the self-dissociativity of ILs, i.e., it indicates the proportion of ions (charged species) that contribute to the ionic conductivity out of all diffusing species. Others assume that the ILs are completely dissociated and that the ionic strength of the system can be determined from the molar concentration of the IL constituents [46]; while others treat ILs as dilute electrolytes consisting of neutral clusters with a low dissociation ratio [48].

The difficulty in defining the ionic force also leads to an ambiguous definition of the Debye length (as shown in eq 4). Attempts to calculate the Debye length in ILs have led to contradictory and often implausible results. When the ionic strength is determined based on the molar concentration of IL ions, κ^{-1} is estimated at an angstrom level [49]. Alternatively, when the ILs are considered dilute electrolytes with a low self-dissociation constant, the Debye length assumes more reasonable values of about 10 nm [48]. However, it remains doubtful whether such a description truly reflects the intrinsic nature of an IL.

It has been observed that solid particles form a stable colloidal system in corresponding ILs [45, 46, 49-51], which contradicts the DLVO theory – as it predicts the existence of unstable dispersions at high electrolyte (ion) concentrations. Various oxide nanoparticles [51, 52], clay minerals [53, 54] and transition metal nanoparticles [45, 55] were dispersed in ILs, which in many cases also served as a medium for particle synthesis [56, 57]. Note that in addition to ILs, stable colloids were also obtained in molten inorganic salts due to charge density oscillations around the dispersed particles [58]. To resolve the apparent contradiction between the DLVO theory and the stability of IL-based dispersions, extensive research has begun to investigate the origin of the stabilising forces in various IL-particle systems [6, 51, 59, 60].

In general, two main types of stabilisation mechanisms were assumed. Based on the results obtained by atomic force microscopy [46, 61], the first theory proposed that IL layering on the surface occurs by sequential adsorption of IL components at the interface, which is associated with the emergence of repulsive oscillatory (step-like) forces that cause stabilisation of particle dispersion (Figure 5a). The oscillations are measured for surface separations between 1–5 nm and have the dimensions of an ion pair. This suggests that more ordered interfacial arrangements decay into the bulk structure over a few ion-pair diameters.

Note that force-distance experiments do not distinguish between the limiting cases of fully charge-separated ion layers, such as discrete alternating cation-anion layers, and completely

charge-neutral mixed ion layers. The only limitation is that the film expelled from between the surfaces during each film-thickness transition is net neutral, which can be consistent with various ion arrangements. Recent studies suggest that most IL interfaces are likely to consist of ion layers that lie between these limits (Figure 6).

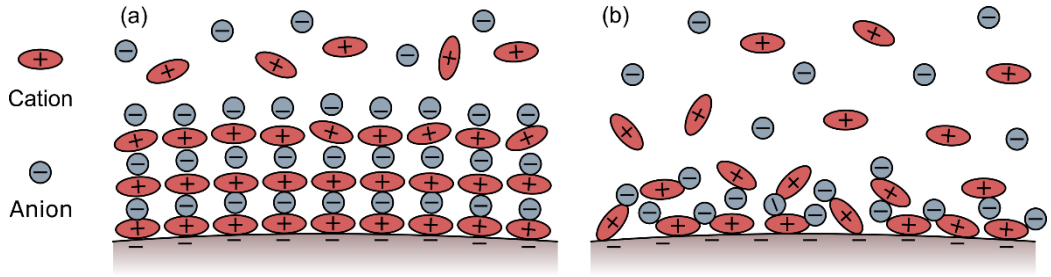

Figure 5. Schematic representation of the interfacial arrangement of ILs. (a) Layered adsorption leads to the formation of repulsive solvation forces, while (b) adsorption and partial dissociation of IL components lead to repulsion by electrostatic interactions.

The other theory is that ILs behave as an effectively neutral, coordinated cation-anion network that is in equilibrium with a small fraction of dissociated IL ions that screen charged surfaces by forming an electrical double layer (Figure 5b) [48]. Coordinated refers to specific interactions that may be present in addition to the electrostatic interactions, such as hydrogen bonding. In this case, long-range forces with a characteristic exponential decay length of about 10 nm were observed [62, 63], thus it is assumed that electrostatic interactions are responsible for the stability of the particles.

An emerging consensus is that non-electrostatic intermolecular forces play a crucial role and that their interplay with electrostatic forces leads to the formation of rich mesoscale structures that govern the surface-mediated interactions [64-66]. Accordingly, ILs appear to exhibit fundamental characteristics traditionally associated with both dilute electrolyte solutions – long-range, monotonic, exponentially decaying forces – and highly concentrated (aqueous) electrolyte solutions – short-range, oscillatory forces (Figure 6). When charged surfaces are placed in IL solutions, the dissolved ions form several bound ion layers immediately adjacent to the surfaces, which partially neutralise the surface charge. This regime typically extends between 1–5 nm from the surface and the bound ion layers lead to oscillatory forces that have similar range and amplitude to the short-range forces resulting from the IL nanostructure [63]. For molecularly smooth surfaces, the regime of short-range forces is always present, but the regime of long-range forces may or may not be present. Long-range forces appear to be more probable for highly charged surfaces and/or larger ions [66] and they can extend more than

10 nm beyond the short-range forces. In contrast, these interactions typically occur over shorter distances in concentrated aqueous electrolytes, as the decay length is between 0.5–2 nm [63]. This is related to the higher (bulk) dielectric permittivity of the electrolyte solutions relative to the dielectric permittivity measured for ILs. Although several systems have been studied recently using different methods, there is no consensus in the scientific community on whether any of these mechanisms can be generally applied or not [60, 64].

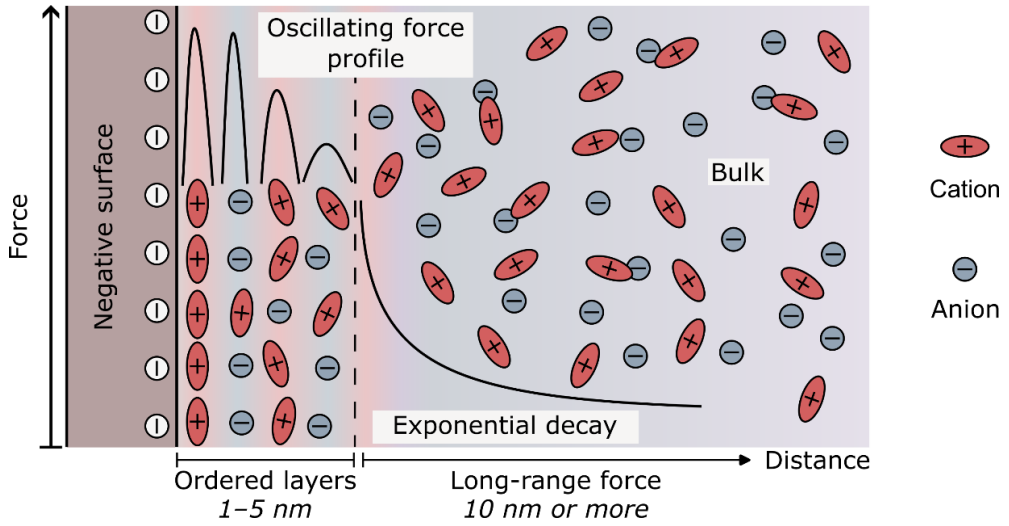

Figure 6. Schematic representation of the short-range oscillatory forces and long-range double layer forces for ionic liquids in contact with charged surfaces. The exact length of the regimes depends on the specific IL-surface combination.

To clarify the effect of interfacial self-assembly of IL constituents from a colloidal point of view, the aggregation mechanism of solid particles in ILs and their water mixtures was investigated by time-resolved light scattering [59]. It was found that aggregation rates vary systematically with the molar ratio of IL to water (Figure 7), and the mechanisms underlying particle stability are very different in dilute and concentrated ILs. On the water-rich side, the aggregation rate is initially insignificant but increases rapidly with increasing IL content, eventually reaching a plateau value. This behaviour is similar to that of inorganic salts (Figure 4b) and can be explained by the DLVO theory. The fact that dilute aqueous IL solutions closely resemble inorganic salts has been confirmed in several studies [67-70]. However, on the IL-rich side, aggregation proceeded slowly, with stabilisation occurring by two mechanisms. Viscous stabilisation – which predominates in highly viscous ILs – slowed down diffusion-controlled aggregation due to hindered diffusion in a viscous liquid. In contrast, on the IL-rich side, the solvation stabilisation led to a significant decrease in aggregation rates, which can be explained

by the previously introduced mechanism (Figure 6). Note that in studies dealing with colloidal stability in ILs, no evidence was found for the effect of long-range electrostatic repulsion between particles [6, 49, 71].

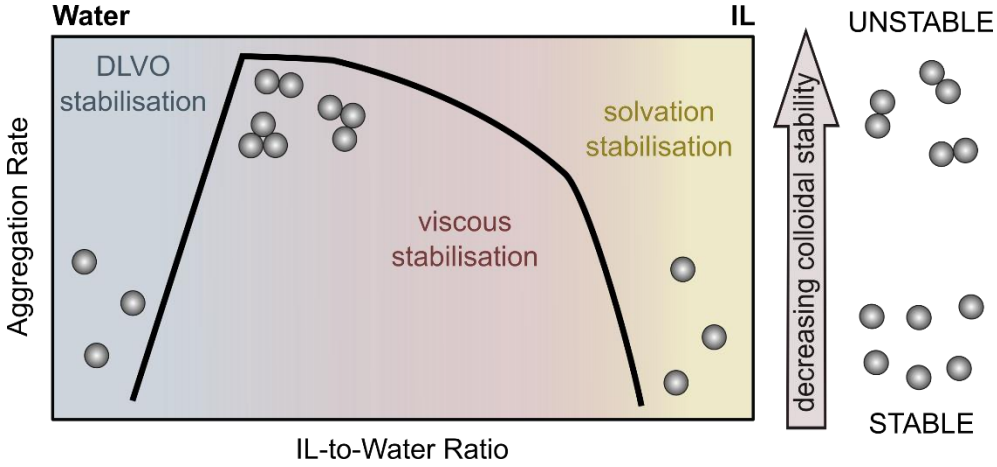

Figure 7. Illustration depicting how the rate and mechanism of aggregation vary with the IL-to-water ratio based on reference [59].

It is assumed that these two stabilisation mechanisms are generally valid, while the range in which these mechanisms are valid depends strongly on the quality of the ILs [59]. When the IL anions are miscible with water (e.g., SCN^-, DCA^-, right side in Figure 1), both stabilisation mechanisms can be observed, and solvation stabilisation can be effective even in ILs with a water content of 10 mass per cent. However, for water-immiscible IL anions (e.g., BF_4^-, left side in Figure 1), the main mechanism is viscous stabilisation, while solvation stabilisation plays no role unless the IL is extremely dry. Overall, the stability of IL-based colloidal dispersions is highly dependent on the cation-anion combinations, which is why the aggregation processes are neither fully understood nor predictable so far [60].

2.3. Effect of parameters on the colloidal stability of IL-containing dispersions

The previous sections illustrate the central role of interfacial structuration of ILs on solid surfaces, a factor of paramount importance for various phenomena, including colloidal stability. Therefore, it is essential to thoroughly consider the effects of all factors that can alter ion arrangement to ensure the success of applications. These factors include the presence of dissolved impurities, such as water or salt, and the distinct affinities of individual IL constituents to different particle surfaces (i.e., ion-specific effects), as these variables can significantly affect the formation and properties of IL layers at the interface.

2.3.1. Effect of trace water and salt impurities

The purity of the ILs used as a dispersion medium plays an important role in the aggregation mechanism of particles, as it can alter the forces between the particles in IL-based colloidal systems. Many applications of ILs require homogeneously dispersed (nano)particles in a wide range of experimental conditions [3, 72]. Therefore, the consequences caused by the presence of water and/or salt impurities or additives in such systems are of great importance.

Understanding the impact of water – whether intentionally introduced or occurring unintentionally in the system – is crucial from an application standpoint. Water not only alters the physicochemical properties of ILs [73, 74] but also affects the interfacial structuration of IL compounds at solid-liquid interfaces [75, 76] and thus the colloidal stability of an IL-based dispersion [45, 46, 59, 77, 78]. Note that water can often be present in ILs due to their hygroscopic nature [79]. Certain phenomena appear to be highly dependent on the water content of the IL medium, which has a profound effect on their bulk, and hence the interfacial properties [8, 80]. Water can also act as an additional ligand during synthesis and alter the kinetics of particle formation [81]. Conversely, ILs lose their fundamental properties when the water content predominates but can still function like conventional surfactants [56].

An important aspect is a substantial change in viscosity in an IL/water system – compared to pure IL – which greatly affects the transport properties of the medium. The presence of even a small amount of water in ILs can significantly reduce their viscosity [73, 74]. This property is beneficial for numerous industrial applications, as viscosity has an obvious impact on ionic conductivity, mixing, solute transfer, dispersion, filtration, and equipment selection [82]. The unique trait of nanoparticle dispersion with low viscosity in IL-water mixtures holds the potential to broaden their range of applications [83]. However, as mentioned above, the presence of water – even in trace amounts – can significantly affect the stability of dispersions in ILs and limit their applicability [46, 51]. Although such a small amount of water cannot influence the bulk properties significantly, water molecules penetrate the IL interfacial layer to interact directly with the particles. Water is believed to play a role in disrupting or displacing the IL ions within the solvation layer at the surface of the particles, which is considered to be the underlying cause of the instability observed in IL dispersions containing certain amounts of water.

Due to their high thermal stability, low volatility, and wide electrochemical window, ILs are suitable electrolytes for electrochemical applications. The addition of salts or nanoparticles can

further enhance conductivity and electrolyte stability, leading to improved performance and safety in energy storage devices [84, 85]. However, the presence of salt can impair the self-assembly of IL compounds on solid surfaces [86, 87]. Research merging IL dispersions and inorganic salts has mainly focused on the development of batteries and supercapacitors [85, 88]. To date, most of these studies have focused on the solvation of Li^+ in ILs due to the great interest in Li-ion batteries [89]. When adding inorganic salts to the IL dispersion, it is important to ensure that the mechanical performance is improved without compromising the transport properties and colloidal stability. It has been shown that the presence of Li^+ ions in colloidal silica–IL dispersion alters the microstructure of the system and has a strong influence on the structuring of the interface [86]. In contrast, an AFM study performed in an IL doped with LiCl on the Au(111) surface revealed that LiCl reduces the force required to rupture the near-surface layers, indicating a weakened IL structure [87]. The authors concluded that the presence of LiCl alters the interfacial nanostructure of ILs, either by weakening the electrostatic domains or by modifying the Hamaker constant near the surface, leading to stronger attraction. Nevertheless, there is a lack of comprehensive studies reporting on how dissolved salts affect the colloidal stability of IL-based dispersions, particularly concerning particle aggregation rates.

Overall, it can be generally stated that the presence of impurities alters the interactions and structure of the ILs, thereby affecting the stability of the colloidal dispersions. Furthermore, the specific behaviour of an IL/surface combination depends on the details of the molecular structure of the ions and the ion/surface interactions [90].

2.3.2. Ion-specific effect

The specific ion effects on interfacial features are universally observed in biological, chemical, medical, and industrial research. Besides, the dissolved ions in a solution have a direct effect on its physicochemical properties [91]. In this context, the key factor is the specific identity of the ions involved, rather than solely their charge or concentration, as suggested by widely accepted colloid theories, such as the Debye–Hückel theory. This phenomenon is classified as the Hofmeister series of ions – a concept initially formulated by Franz Hofmeister in 1888 to express the stabilising power of inorganic salts in protein solutions [92]. Accordingly, negatively charged proteins form stable solutions even in the presence of high concentrations of ions located on the right-hand side, while the ions on the left-hand side cause their precipitation even at low concentrations (Figure 8).

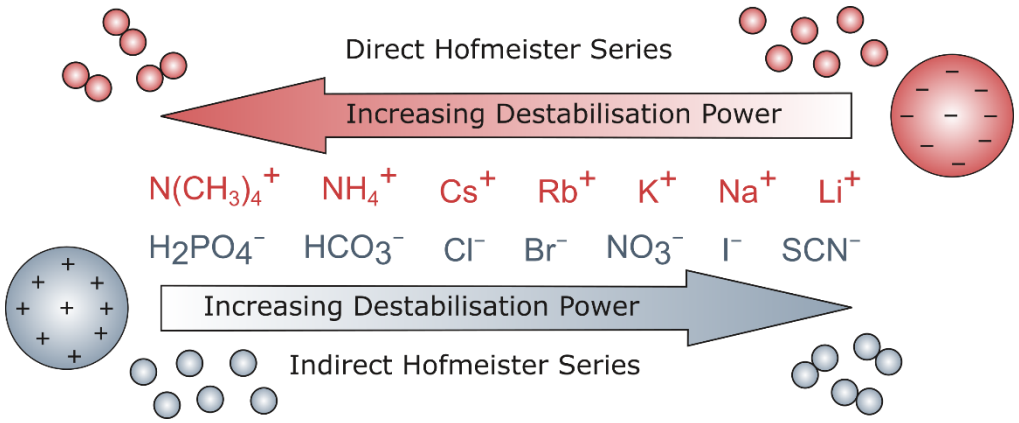

Figure 8. Hofmeister series for anions and cations. The series applies to hydrophobic particles with low surface charge in the presence of monovalent electrolytes.

Since then, it has been shown that ions can be ordered following the same sequence – completely or partially – based on many other phenomena, such as the surface tension or viscosity of electrolyte solutions, the dissolution heats of salts, the binding of ligands, and the charge of proteins or polyelectrolytes [93-97]. Particle aggregation typically follows the same series [67, 98-102], i.e., negatively charged hydrophobic particles (e.g., sulfonated latex [100], halloysite nanotubes [67]) follow the direct Hofmeister series (see above), with the less hydrated ions on the left inducing lower CCCs, while the ions on the right inducing higher ones. Conversely, positively charged particles (e.g., amidine latex [101]) follow the (reverse) indirect Hofmeister series and the ions on the left-hand side lead to higher CCCs, whereas the ones on the right induce lower values. For hydrophilic particle dispersions (e.g., protein-coated polystyrene particles [103]), the trend is reversed, meaning that ions have the opposite effect on the CCC values. Note that this tendency cannot be always unambiguously detected, and partially reversed sequences have also been reported [104].

To understand the Hofmeister effects, it is important to consider not only the properties of the dissolved ions but also the characteristics of the surface involved [103]. Although DLVO theory cannot distinguish between different types of ions of the same valence, ion specificity can be introduced by assuming that the salt components can interact specifically with the surface. This assumption is based on the fact that the affinity of the ions to the particle surfaces differs considerably so that their adsorption changes the surface charge to a different extent. In the case of counterions, adsorption reduces the charge and weakens the EDL forces [41, 105]. The position of an ion in the Hofmeister series can be qualitatively related to either its

hydrophobicity or its degree of solvation [106]. However, these effects cannot be strictly separated and are also dependent on the properties of the particles, so the observed series may differ to some extent [101, 104].

Ion specificity is of great importance in the case of ILs, as they consist entirely of ions. To place the IL constituents into the Hofmeister series, ion-specific effects were first studied on protein solubilisation and enzymatic activity in aqueous solutions of ILs [107, 108]. The influence of the ion-specific effect on the interfacial interactions was also systematically investigated using optical tweezers [109] and atomic force microscopy [69] in aqueous IL solutions. The main conclusion from these studies was that cations or anions have different affinities for certain surfaces, leading to different changes in the properties of the particle interface, which are reflected in the different electrostatic repulsive forces between the particles. On this basis, IL constituents can be classified based on their adsorption affinity for a particular surface, similar to conventional inorganic ions, according to the Hofmeister series.

Since the interfacial arrangement of the IL components is of crucial importance for the origin and magnitude of the resulting interparticle forces in IL dispersions, particle aggregation in aqueous IL media has been also studied [67, 68, 110]. Furthermore, the determination of the CCC for uniform particles provides a reliable measure of the position of the IL constituents within the Hofmeister series. Under these conditions, ILs tend to dissociate into individual ions, making them very similar to inorganic electrolytes. For negatively charged latex particles, an increase in the alkyl chain length of the IL cations, which increased their hydrophobicity, resulted in lower CCC values due to their higher affinity for the hydrophobic surface of the particles [110]. However, for positively charged latex particles, the lengthening of the carbon chain had no significant effect on the stability of the system. Similar results were obtained regarding the sensitivity of aggregation to the hydrophobicity of IL cations in the case of hydrophilic titanate nanoparticles, where the charge of the particles was modified by changing the pH instead of surface functionalisation [68]. However, the destabilising power of IL cations showed a reverse order to that observed in the case of hydrophobic latex particles. This underscores the significance of the hydrophobicity of the particles relative to the IL-forming ions concerning the accumulation of ILs at the interface. This type of evaluation of the particle/IL interactions made it possible to extend the original Hofmeister series with IL cations and anions [67, 110].

The importance of the ion-specific effect is also evident in the synthesis of particles in IL media, i.e., the preparation of gold and copper nanoparticles by thermal evaporation was significantly influenced by the composition of the ILs [111]. Methylimidazolium salts with short alkyl chains and with weakly coordinating perfluorinated counter anions (such as PF_6^-, BF_4^-, or Tf_2N^- (Tf=trifluoromethanesulfonyl)) are better stabilisers than ILs with cations bearing long alkyl chains (such as trihexyltetradecylphosphonium or 1-octyl-3-methylimidazolium) and anions of higher coordination strength (dicyanamide). The stability of the resulting colloids and the final particle size were notably influenced by the specific interactions between the metal and the IL, rather than by bulk properties such as viscosity and surface tension.

Ion specificity is also important in terms of the nature of the counterions present at the interface of nanoparticles in water at the initial stage of synthesis, as this has a strong influence on the physical properties of the particle dispersions when transferred to IL [51, 112]. Some of these ions remain close to the surface of the nanoparticle in the IL, modifying both the particle/particle and particle/IL interactions. The interface is modified by the charge-compensating ions compared to pure IL, due to the size mismatch between the counterion and IL, which disrupts the interfacial assembly of ILs and thus affects the stability of the dispersion.

Overall, in IL-based media, many ionic specificities – including ionic size and shape, hydrogen bonding, hydrophobicity, and the ability to form layers and structures via solvation forces – have been shown to impact local and global properties, both at interfaces and in bulk materials [111-113]. It also has a strong effect on the stability of IL-containing dispersions, which often hinders the applicability of colloidal systems. Therefore, precise measurements of aggregation rates and surface charges are required to further investigate the effects of IL constituents on interparticle forces and the colloidal stability of particle dispersions.

2.3.3. Tuning the colloidal stability

With the growing importance of IL-particle systems in various applications, fundamental research has increasingly focused on understanding and tuning the colloidal stability of nanoparticles in ILs. To obtain processable dispersions, nanoparticles often require stabilisation, whether they are synthesised directly in an IL or in another medium prior to transfer into the IL. Several approaches have been explored in the past to stabilise nanoparticles in ILs [60]. In certain instances, the particles could be stably suspended in ILs without the addition of classical stabilisers [46, 71, 86], while in other cases surface modification was required [114, 115].

For example, when maghemite nanoparticles were synthesised in water and later transferred to the IL $BMIMBF_4$, the dispersion was unstable unless the water was removed by vacuum pumping [116]. The stability was attributed to the formation of IL layers at the interface between nanoparticles and IL, which hindered the contact between the particles, while the water at the interface disrupted these layers, leading to aggregation. However, contradictory data can also be found in the literature regarding maghemite and ILs [70], where the bare nanoparticles lead to stable dispersions in the two ethyl-methylimidazolium ILs (namely EMIMAc and EMIMSCN) after the removal of water and sonication, but only to short-lived dispersions in $BMIMBF_4$. Note that the authors of reference [116] did not specify the pH conditions before transferring nanoparticles into the IL, making it impossible to determine the initial surface charge of the particles. This lack of information makes it difficult to compare the results of these two papers and to understand the reasons for their differing results.

If the bare particles are not stable in ILs, one approach is to graft polymers to their surface. When these polymer-grafted particles approach each other, the polymer layers can generally undergo some compression, resulting in a strong repulsion that is referred to as steric repulsion. The physical basis of this interaction is a combination of entropic and osmotic contributions [117, 118]. The adsorption of polyelectrolytes in the presence of IL can lead to a variety of conformations (Figure 9) that have a decisive influence on the degree of attraction and repulsion that occurs [49].

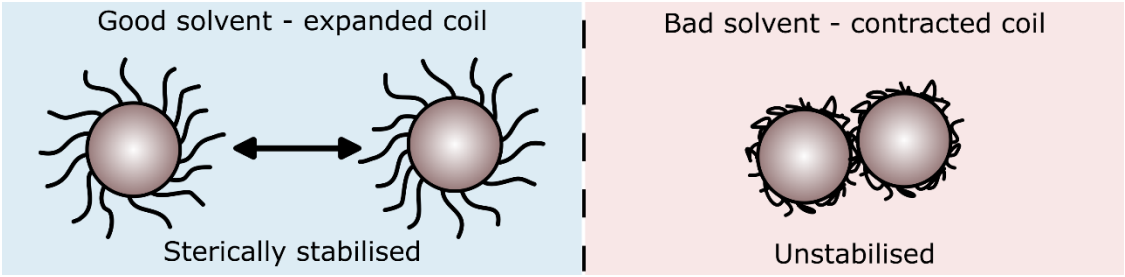

Figure 9. Schematic representation of the effect of the polymer coating on colloidal stability, depending on solvent interaction. Good solvent (left): Extended chains create a steric barrier that increases stability. Poor solvent (right): Collapsed chains provide limited repulsion and promote aggregation.

When the IL is a good solvent for the polymer – the interactions between the polymer segments and solvent molecules are energetically favourable – the polymer coils expand and generate steric repulsion [70]. Similar stabilisation can also be achieved by the adsorption of a long-chain surfactant on the particle surface [119]. However, this approach was ineffective when

the IL was a poor solvent for the polymer, as it led to collapsed polymer chains on the colloid surface, which caused limited steric repulsion and promoted aggregation [70].

An alternative approach is to coat the surface of the nanoparticles with one of the ions that form the ILs themselves [114]. For example, the surface of maghemite nanoparticles was modified by silanisation to introduce positively charged imidazolium moieties on their surface. This modification enabled stable dispersions in an imidazolium-based IL with up to 50 mass per cent. The resulting magnetic IL dispersion exhibited remarkable stability, even under high magnetic fields, due to a supramolecular structure that effectively prevents aggregation. In addition, IL-based polymers have also emerged as stabilising agents [120]. Yet, their effects on the colloidal stability of particles are not fully understood. Although there is some data in the literature on surface modification, stabilisation, and extraction of nanoparticles using IL polymers [121, 122], the aggregation properties of colloidal suspensions in the presence of IL polymers and the ion-specific effect in such systems have not been addressed.

Overall, many studies have attempted to shed some light on the mechanisms leading to the colloidal stabilisation of nanoparticles in the presence of ILs. However, further measurements are needed to resolve the existing contradictions and to gain a more comprehensive understanding of this topic.

2.4. Application of IL-containing particle dispersions

Nanoparticles possess distinctive physical characteristics that make them valuable in numerous applications such as catalysis, nanocomposites, electrochemistry, biotechnology, chemical analysis, diagnostics, drug delivery, and medicine [123, 124]. These applications benefit from novel properties like electronic and optical attributes, which stem from the large surface area-to-volume ratio and quantum confinement effect inherent in nanoparticles due to their nano-scale dimensions. ILs can form various structures with nanoparticles, depending on the balance of intra- and intermolecular interactions between them [60]. These novel functional materials demonstrate remarkable synergies, exploiting the combined properties of both components to achieve superior performance [3].

These hybrid systems hold significant promise for a range of electrochemical applications. By synergistically enhancing the properties of an electrolyte through a greater diffusion coefficient, higher electrical conductivity, and better thermal and electrochemical stability, they become promising for use in batteries and solar cells [84]. For this application, various structures

of IL and nanoparticle hybrids have been constructed, among which nanoparticle dispersions in ILs and IL-grafted nanoparticles are the most common [3]. For example, when 0.5 wt% of gold nanoparticles were incorporated into 1-ethyl-3-methylimidazolium ethylsulphate IL, the capacitance of the resulting electrolyte was increased by 190% and the ionic conductivity was also significantly enhanced [125]. Similarly, copper nanoparticles encapsulated within a carbon shell improved the performance of IL-based electrolytes in dye-sensitised solar cells by increasing the diffusion coefficient and electrical conductivity [3].

The unique characteristics of IL and nanoparticle hybrids show further promise in catalysis. For this use, nanoparticles (usually metal) can be simply dispersed (or synthesised) in ILs, or chemically bonded with ILs, which serve as a solvent, stabiliser, ligand and support for the nanoparticles. ILs provide a versatile liquid platform for hosting transition metal nanoparticle catalysts, offering steric and electrostatic stabilisation to prevent nanoparticle aggregation [31, 81]. These catalytic systems typically operate in multiphase environments in which the metal nanoparticles, dispersed in the ILs, form the denser phase and the substrates and product remain in the upper phase; hence the ionic catalytic solution is easily recovered by simple decantation. With the advantage of easy recovery, rationally designed metal nanoparticle/ILs hybrids have been successfully applied as catalysts for various reactions such as the hydrogenation of alkenes, arenes and ketones, hydrodehalogenation of aryl chlorides, and Heck, Suzuki, Stille, Sonogashira and Ullmann coupling reactions [31, 81]. The surrounding IL layer stabilises the nanoparticles, enabling their recyclability without compromising catalytic performance.

Nanoparticle-supported ILs offer another hybrid approach that combines the advantages of homogeneous and heterogeneous catalysis. For example, when TiO_2 was covalently functionalised with an IL, a remarkable improvement in the photoelectrochemical water oxidation performance was achieved [126]. This was demonstrated by a ten-fold increase in photocurrent compared to unmodified TiO_2 and a 37% increase in charge transfer efficiency. Long-term tests showed enhanced photo-stability of IL-TiO_2, which was attributed to synergistic effects between IL and TiO_2.

Moreover, ILs have emerged as a promising alternative to conventional solvents in the delamination of layered materials. Their main advantage lies in their ability to facilitate one-step delamination in a liquid phase and the subsequent stabilisation of the resulting 2D nanosheets in dispersions [9, 127-129]. The liquid phase delamination is preferred due to its simplicity,

efficiency, scalability, and ability to achieve uniform dispersion of nanomaterials. ILs achieve this by shielding attractive interactions between charged layers through repulsive solvation forces generated by the self-assembly of IL constituents on the surface, which promotes the collapse of stacked structures and subsequent delamination into unilamellar nanosheets. Such a phenomenon was first demonstrated in IL-graphene systems [9, 127]. Since then, ILs were successfully used to prepare stable and highly concentrated suspensions of a variety of layered materials, including black phosphorus [128], titanium disulphide [129] and boron nitride [130].

Among these layered materials, layered double hydroxides (LDHs) are one of the most intensively studied lamellar materials because the chemical composition of both the metal hydroxide layers and the intercalated anions can be precisely controlled, which is particularly advantageous for the desired application. They consist of positively charged mixed metal hydroxide layers – i.e., divalent (e.g., Mg^{2+}, Ca^{2+} or Zn^{2+}) and trivalent (e.g., Al^{3+}, Fe^{3+} or Cr^{3+}) metal ions coordinated by hydroxide groups – while in the interlamellar space, different types of charge-neutralising anions can be present together with water molecules [131]. The metal cations found in the LDH structure primarily belong to the third and fourth periods of the periodic table due to their ionic radii, which are suitable for this type of structure. Due to their distinctive anisotropic structure, they are among the few layered materials with a positive structural charge that enables the adsorption or intercalation of inorganic and organic anions [132-135]. In addition, LDHs can also be used as basic building blocks for functional materials used in catalysis [136, 137], drug delivery [133, 138, 139], and electrochemistry [140]. In addition, there is a growing contemporary interest in the application of LDH-IL systems. Accordingly, a solid electrolyte has been synthesised by impregnating LDH with IL and implemented in batteries for advanced energy storage applications [89]. The synthesis of LDH with the assistance of ILs resulted in the formation of particles with a high specific surface area, which were used for phosphate removal in water treatment processes [141]. LDH-IL systems also have potential applications in creating composite materials [142, 143] as the characteristics of the inorganic matrix can be combined with specific ILs to result in a synergistic effect, influencing the selection and adjustment of properties. However, although LDHs hold promise as potential sources of 2D materials and previous reports have investigated IL-LDH composites, there is a lack of comprehensive studies evaluating the potential delamination of layered LDHs into 2D double hydroxide materials in pure IL media.

3. Objectives

The main objective of this dissertation is to comprehensively investigate the colloidal stability and interfacial properties of ILs in colloidal dispersions to understand the fundamental mechanisms that determine their stability and interactions. The charge and aggregation relationships of the different particles in these dispersions are aimed to be understood, focusing on the effects of variables such as IL composition, water and salt content. By systematically exploring these physicochemical parameters, the factors that determine colloidal stability in both aqueous and pure IL dispersions may be elucidated, paving the way for their effective use in certain applications.

Our second aim is to unravel the influence of ion specificity on the stability of IL-containing dispersions. Accordingly, the affinity of IL constituents to the surfaces of latex particles with similar charge but different surface functionality was investigated. Based on the concept of the Hofmeister series, this exploration was carried out by following the charging and aggregation features in aqueous IL solutions, while the IL structures were systematically modified so that the IL compounds could be classified according to their affinity to the particle surface, and their destabilising power.

The third objective focuses on understanding the interactions between IL constituents and layered materials, specifically LDHs. Again, the charging and aggregation features in aqueous IL dispersions were studied to identify the most suitable ILs for efficient exfoliation and stabilisation of LDH materials in IL dispersions.

Building on the observed affinity of IL constituents to LDH surfaces, our fourth aim is to prove the concept of LDH delamination using ILs under ambient conditions. By selecting appropriate ILs with favourable interfacial properties and moderate viscosities, the goal was to demonstrate a one-step delamination process for LDHs leading to the preparation of 2D double hydroxide nanosheet dispersions.

Through these objectives, this dissertation aims to provide valuable insights into the complex world of IL-containing colloidal systems, bridging the gap in our understanding of their fundamental interactions. By addressing these objectives, this research seeks to improve the applicability and effectiveness of IL-based dispersions in various scientific and technological fields.

4. Experimental part

4.1. Materials

During sample preparation, ultrapure water was obtained from a Puranity TU+ (VWR) apparatus. The water and the electrolyte solutions were filtered with a 0.1 μm syringe filter (Millex) to remove insoluble impurities. The pH of the suspensions was adjusted by HCl (Sigma) and NaOH (VWR) and the measurements were carried out at 25 °C.

Spherical polystyrene latex particles functionalised with sulphate (SL) or amidine (AL) groups were purchased from Thermo Fischer Scientific, with a mean diameter of 430 nm and 510 nm, respectively. The manufacturer determined these values using transmission electron microscopy (TEM).

The LDHs discussed in the present thesis were prepared by the flash co-precipitation method followed by hydrothermal treatments [144, 145]. Briefly, a mixed metal ion solution was prepared by dissolving the appropriate amount of $Mg(NO_3)_2 \cdot 6H_2O$ (Sigma-Aldrich) and $Al(NO_3)_3 \cdot 9H_2O$ (Sigma-Aldrich) to obtain 0.2 M and 0.1 M concentrations, respectively. The salt solution was then mixed under an N_2 atmosphere, while the pH was adjusted to 10 with a 4.0 M NaOH solution (VWR). After being vigorously stirred for 30 minutes, the sample underwent centrifugation and was washed with water. The resulting slurry was then redispersed and transferred to an autoclave for treatment in an oven set at 120 °C for 24 hours. The sample was then allowed to cool to ambient temperature before being separated and dried overnight at 50 °C.

To prepare the mesoporous LDH particles for the delamination part, 100 mL of 30 mM sodium dodecyl sulphate (Sigma-Aldrich) was added to the original LDH dispersion [146]. The resulting slurry was stirred for 12 hours at 60 °C and pH 8.5. Subsequently, the surfactant content was removed by calcination at 510 °C for 12 hours, and the resulting layered double oxide compounds were rehydrated to reconstruct the LDH structure. The obtained slurry was then stirred at 50 °C for 96 hours, followed by repeated filtration, washing and drying steps to obtain the final product.

Analytical grade potassium chloride (KCl) was purchased from VWR. Among ILs 1-butyl-3-methylimidazolium chloride (BMIMCl), 1-butyl-2-methylpyridinium chloride (BMPYCl), 1-butyl-1-methylpiperidinium chloride (BMPIPCl), 1-butyl-1-methylpyrrolidinium chloride (BMPLCl) and ethylammonium nitrate (EAN) were bought from IoLiTec GmbH,

1-butyl-3-methylimidazolium bromide (BMIMBr), 1-butyl-3-methylimidazolium nitrate ($BMIMNO_3$), 1-butyl-3-methylimidazolium acetate (BMIMAc) and 1-butyl-3-methylimidazolium thiocyanate (BMIMSCN) were purchased from Sigma-Aldrich, while 1-butyl-3-methylimidazolium dicyanamide (BMIMDCA) was obtained from Merck. The structure of the investigated IL constituents can be seen in Figure 10.

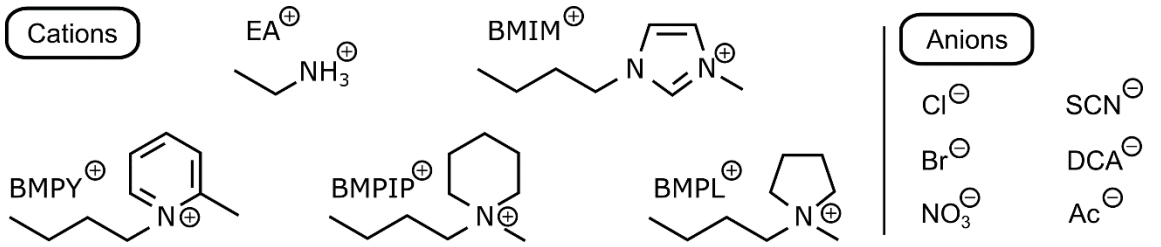

Figure 10. Constituent cations and anions of the investigated ILs.

The polyimidazolium-based polymer (IP-2) was obtained through a collaboration with Professor Paul J. Dyson (EPF Lausanne, Switzerland). In the synthesis [147], 1,4-bis(chloromethyl)benzene and 1-(trimethylsilyl)imidazole were dissolved in acetonitrile in a 1:1 molar ratio in a Schlenk-flask and the mixture was heated to reflux for 48 h. The white solid product was separated by filtration, washed with acetonitrile and diethyl ether, and then dried under vacuum for 24 h. All chemicals used for the synthesis were from Sigma-Aldrich.

4.2. Characterisation techniques

4.2.1. Characterisation of ionic liquid solutions

The refractive index (n) of IL solutions was determined using an Abbemat 3200 refractometer (Anton Paar, Austria) at a wavelength of 589 nm. To evaluate the light scattering measurements, the values of n were obtained by linear interpolation, based on the following equation:

$$n = c_{IL}a + b \tag{5}$$

where c_{IL} is the molar concentration of the IL solutions, a and b are fitted parameters, which are summarised in Table 1.

An LVDV-II+ ProC/P viscometer (Brookfield) was used to measure the dynamic viscosities of the IL solutions in a cone-plane geometry (CPE-40 cone). The viscosity of the different IL-water mixtures was determined by fitting shear stress versus shear rate data with the Casson model. The experimental η values were fitted as follows:

$$\eta/\eta_0 = 1 + A\sqrt{c_{IL}} + Bc_{IL} + Dc_{IL}^2 \quad (6)$$

where η_0 is the viscosity of water (8.90×10^{-4} Pa s at 25 °C), while A, B and D are constants summarised in Table 1. Note that the viscosity and refractive index data for EAN–water mixtures were taken from the literature [73].

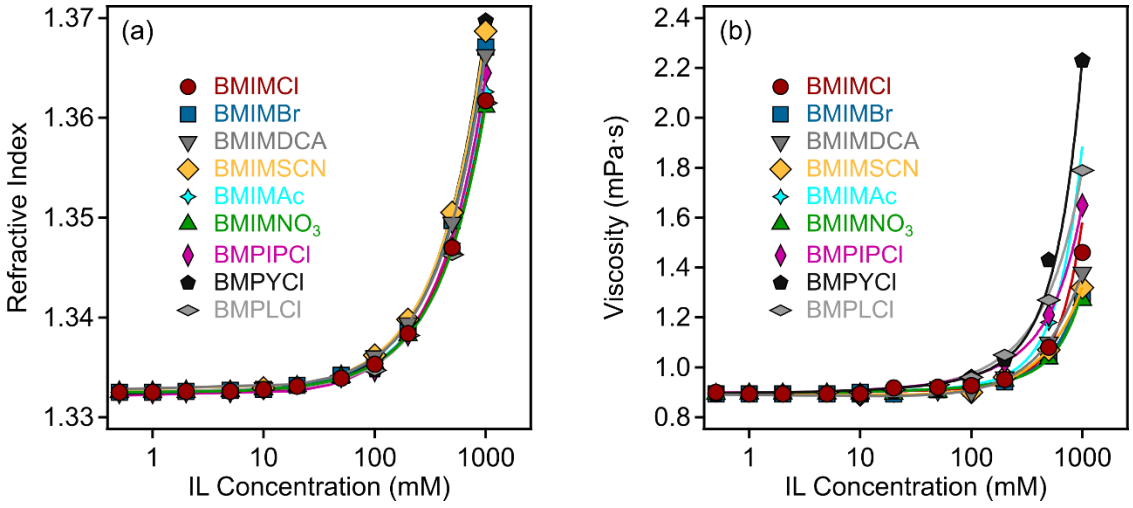

Figure 11. (a) Refractive indices and (b) viscosities of aqueous IL solutions at different concentrations. The solid lines represent the fits obtained with eq 5 (a) and eq 6 (b) [I, II].

Table 1. Fitting parameters for interpolating the refractive indices and viscosities of the IL solutions.

Composition	Refractive Index[a]		Viscosity[b]		
	a (M^{-1})	b	A ($M^{-1/2}$)	B (M^{-1})	D (M^{-2})
BMIMAc	3.01×10^{-5}	1.333	2.90×10^{-3}	6.72×10^{-9}	1.02×10^{-6}
$BMIMNO_3$	2.86×10^{-5}	1.333	2.94×10^{-3}	-3.40×10^{-10}	3.66×10^{-7}
BMIMBr	3.46×10^{-5}	1.333	2.93×10^{-3}	-3.30×10^{-10}	4.17×10^{-7}
BMIMCl	2.92×10^{-5}	1.333	2.87×10^{-3}	-1.00×10^{-4}	7.76×10^{-7}
BMIMSCN	3.61×10^{-2}	1.333	-1.08×10^{-1}	5.29×10^{-1}	5.52×10^{-2}
BMIMDCA	3.37×10^{-2}	1.333	-1.63×10^{-1}	6.86×10^{-1}	2.06×10^{-2}
BMPLCl	2.89×10^{-2}	1.333	5.52×10^{-2}	4.44×10^{-1}	1.54
BMPIPCl	3.21×10^{-2}	1.333	1.43×10^{-1}	3.08×10^{-1}	3.95×10^{-1}
BMPYCl	3.72×10^{-2}	1.333	-2.88×10^{-2}	4.38×10^{-2}	3.92

[a]Fitting parameters of eq 5. [b]Fitting parameters of eq 6

The water content (being present as an impurity) was determined by Karl-Fischer coulometric titrations using a KEM MKC-710 Karl Fischer Moisture Titrator for ILs that were used in pure form, without mixing with water. Accordingly, the water content proved to be 3.0 g/L for EAN and 3.9 g/L for BMIMSCN.

The structure of the synthesised IP-2 polymer was confirmed by Fourier-transform infrared spectroscopy (FTIR) recorded with a JASCO FT-IR-4700 spectrometer equipped with a DTGS detector in attenuated total reflectance mode. The spectral resolution was 4 cm^{-1} in the wavenumber range of 1800–1000 cm^{-1}.

4.2.2. Electrophoretic light scattering

Continuously monitored phase analysis light scattering (cmPALS) measurements are a powerful method of estimating the electrical properties of the surface of a charged colloidal particle in an electrolyte solution [148, 149]. The electrophoretic mobility (u) of the particles was determined using the LitesizerTM 500 (Anton Paar) equipped with a 40 mW semiconductor laser operating at a wavelength of 658 nm in backscattering mode using the phase analysis technique. During operation, the light source generates a coherent primary light beam, which is subsequently split by a beam splitter. One part is passed to the oscillating modulator, while the other part is used for the light scattering measurement. Then the scattered light is combined with the modulated reference beam from the modulator and detected on the primary scattering detector. In addition, a secondary detector continuously monitors a portion of the modulated reference beam from the modulator. This portion is used to correct for any instabilities in modulator frequency that may arise. The resulting monitor trace represents the reference beam, while the detector trace shows the interference (modulation) between the light scattered by the sample and the modulated reference beam. The phase plot obtained shows the phase difference between the detector and monitor traces due to the Doppler effect on the scattered light from moving scattering particles and the fit of the cmPALS to the data from which the electrophoretic mobility values were determined.

The mobility refers to the speed (v) – which can be determined by light scattering techniques (e.g., laser Doppler velocimetry or phase analysis light scattering) – at which charged particles migrate in an electric field (E) [37]:

$$v = uE \tag{7}$$

And since in a suspension, the particles move together with the stagnant layer of ions, the electrophoretic mobility values are proportional to the zeta potentials. Converting mobility to zeta potential relies on various models, but their applicability is limited and depends on the charge and size of the particles, as well as the ionic strength applied in the suspensions [35].

In this work, the electrokinetic potentials of the particles were always below 50 mV, and the EDL was assumed to be very thin compared to the particle radius, the Smoluchowski model was used for the conversion [35]:

$$\zeta = \frac{u\eta}{\varepsilon_0 \varepsilon} \tag{8}$$

The surface charge density of particles is a crucial parameter that can be estimated through the ionic strength dependence of potentials. The charge density at the slip plane (σ) was determined by fitting zeta potentials at different salt levels with the Debye−Hückel charge-potential relationship [150]:

$$\sigma = \varepsilon_0 \varepsilon \kappa \zeta \tag{9}$$

This model is applicable in low potential regions, and the ionic strength is considered through the Debye length (eq 4).

Samples were prepared by mixing the appropriate amount of electrolyte (salt or IL) stock solution and water to obtain the desired concentration. Particles were then added to the mixture by adding the calculated amount of stock dispersion to achieve the desired final particle concentration. The samples were allowed to settle at room temperature for 2 hours before measuring the electrophoretic mobilities, which occurred after 1 minute equilibration time in capillary cuvettes or with the Univette accessory (Anton Paar). The latter measuring cell is suitable for measuring high-conductivity samples, including those containing ILs. Five runs were performed and averaged.

4.2.3. Dynamic light scattering

The hydrodynamic radius (R_h) of the particles was measured by dynamic light scattering (DLS) technique. In the case of latex particles, the measurements were conducted with a NIBS High-Performance Particle Sizer (ALV) featuring a 3 mW He–Ne laser operating at a wavelength of 633 nm and a scattering angle of 173°. For LDH particles, a Litesizer 500 (Anton Paar) instrument was used, equipped with a 40 mW semiconductor laser with a wavelength of 658 nm and a scattering angle of 175°. The measurement concept of the two instruments is identical. The time-dependent scattering intensity was recorded for 20 seconds (Figure 12a), from which the intensity correlation function was derived (Figure 12b) and the cumulant method was used to obtain the decay rate constant (Γ) [151]. Based on this value, the translational diffusion

coefficient (D) can be determined, which can be further converted to R_h using the Stokes–Einstein relation [152]:

$$D = \frac{\Gamma}{q^2} = \frac{k_B T}{6\eta\pi R_h} \tag{10}$$

where q is the scattering vector obtained from the instrument parameters by the formula:

$$q = \frac{4\pi n}{\lambda} \sin\frac{\Theta}{2} \tag{11}$$

where λ is the wavelength of the laser beam and Θ is the scattering angle. The refractive indices and viscosity data for the IL solutions were determined as described in chapter 4.2.1.

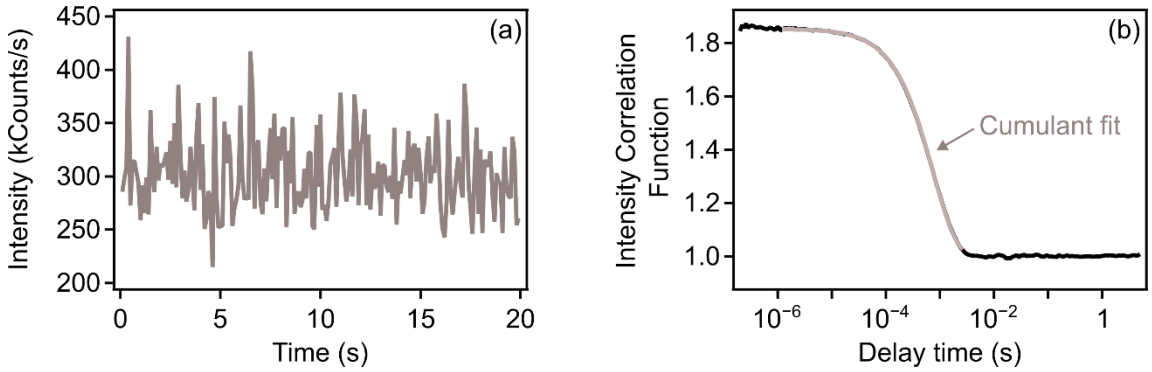

Figure 12. Fluctuation in scattering intensity (a) and the corresponding intensity correlation function with cumulant fit (b) for SL particles obtained by DLS.

To follow the aggregation processes time-resolved DLS measurements were carried out, which means that the change in R_h over time was followed. The apparent aggregation rate constant (Δ), which describes the initial increase of R_h in the early stages of aggregation, is given as [151]:

$$\Delta = \frac{1}{R_h^1}\left(\frac{dR_h}{dt}\right) = \left(\frac{I_2}{2I_1}\right)\left(1 - \frac{R_h^1}{R_h^2}\right) kN_0 \tag{12}$$

where t is the experiment time, N_0 is the initial number concentration of the particles, k is the absolute aggregation rate coefficient (in m^3/s unit), while R_h^1 and R_h^2 are the hydrodynamic radius of the monomer and dimer, respectively. The contribution of the form factors of the monomer (I_1) and the dimer (I_2) to the scattered intensity was predicted by the Rayleigh–Gans–Debye approximation [151].

The colloidal stability of the samples was further expressed in terms of stability ratio, which can be calculated as:

$$W = \frac{\Delta_{fast}}{\Delta} \tag{13}$$

where the fast subscript indicates fast or diffusion-controlled aggregation of the particles. The Δ_{fast} value was obtained separately for each system in the fast aggregation regime above the CCC. Note that unstable dispersions have a stability ratio close to 1, i.e., all particle collisions lead to the formation of dimers (Figure 13a). In contrast, higher values suggest slower particle aggregation, indicating a more stable sample. The standard error of the stability ratio measurement is about 10%.

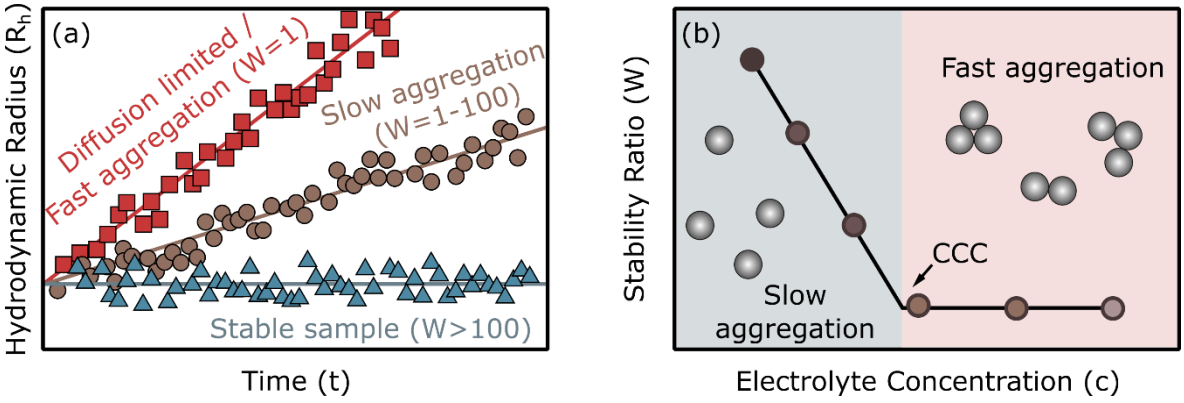

Figure 13. Illustration of the change in the particle size over time for dispersions with different levels of stability (a) and electrolyte concentration-dependent stability plots (b).

The CCC values were calculated from the electrolyte (salt or IL) concentration (c_{el}) dependent stability ratio plots (Figure 13b) with the following equation:

$$W = 1 + \left(\frac{CCC}{c_{el}}\right)^{-\beta} \tag{14}$$

where β can be obtained from the slope of the stability plot at the slow aggregation regime (i.e., before the CCC) as follows:

$$\beta = \frac{d \log 1/W}{d \log c_{el}} \tag{15}$$

4.2.4. Structural characterisation

X-ray diffraction (XRD) measurements were performed using a Bruker D8 Advanced diffractometer with CuKα (α = 0.1542 nm) as the radiation source in the range of 5–80° 2θ at step sizes of 0.02° and using a QT026 quartz XRD sample holder (cover plate: 20×20×0.5 mm). No background subtraction was performed. Based on the XRD results, the thickness of the LDH

crystals (L_C) was calculated using the Scherrer equation [145]:

$$L_C = \frac{\lambda K}{\beta \cos \theta} \tag{16}$$

where λ is the wavelength of the X-rays, K is the shape factor (0.9 for LDH), θ is the Bragg diffraction angle, and β is the full width at half maximum of the (003) reflection.

The morphology of the solids was characterised by transmission electron microscopy (TEM) and atomic force microscopy (AFM). The TEM images were acquired using a FEI Tecnai G2 type microscope. For sample preparation, the particle dispersions were dried on a copper-carbon mesh grid and 200 kV accelerating voltage was used for imaging in the bright field mode. AFM images were collected by a Multimode Nanoscope IIIa AFM instrument (Digital Instruments). The device was used in tapping mode in air at ambient temperature using a Si tip cantilever (PPP-NCHR-10, NanoSensors), with a nominal tip radius of less than 9 nm and a resonant frequency ranging 204–497 kHz. The samples were prepared by placing a drop of the dispersion on a freshly cleaved mica substrate (Ted Pella, Highest Grade V1) and allowing it to sediment for 1 hour. Then the IL solvent residue was removed by rinsing with acetonitrile and ultrapure water, followed by drying using N_2 gas. During the examination, height and amplitude images were simultaneously captured at a scan rate of 0.1 Hz.

Small-angle X-ray scattering (SAXS) and small- and wide-angle X-ray scattering (SWAXS) measurements were performed by Professor Matija Tomšič (University of Ljubljana) with two different laboratory-modified old-Kratky type cameras (Anton Paar) connected to a conventional X-ray generator (GE Inspection Technologies, SEIFERT ISO-DEBYEFLEX 3003). The generator contained a sealed X-ray tube with a Cu anode operating at 40 kV and 50 mA. Focusing multilayer optics (Goebel mirrors) were used to focus and monochromatize the primary X-ray beam to produce a high-intensity Cu-K_α line with a wavelength (λ), of 1.54 Å. Passing this beam through a block-collimation unit provided a well-defined line-collimated primary beam. Samples were measured at 25 °C in a standard quartz capillary (outer diameter of 1 mm and wall thickness of 10 μm). SWAXS measurements were recorded on a 2D imaging plate irradiated with scattered X-rays for 30 minutes and read out with a delay of 5 minutes using a Fuji BAS 1800II imaging-plate reader with a spatial resolution of 50×50 μm^2/px. SWAXS data were collected in the range of the scattering vector (q) from 0.1 to 30 nm^{-1}, while q can be calculated as:

$$q = \frac{4\pi}{\lambda} sin\left(\frac{\vartheta}{2}\right) \tag{17}$$

where ϑ is the scattering angle. Note that the scattering vector is different for DLS and SWAXS, as for DLS the formula includes the refractive index of the medium (eq 11), since there the scattering results from the interaction of the radiation with regions of different refractive indices, whereas in SWAXS it is the electron density. They were corrected for sample X-ray absorption and background scattering and transformed to absolute scale using water as the secondary standard [153]. The resulting SWAXS data were still experimentally smeared due to the finite dimensions of the primary beam [154].

The Indirect Fourier Transformation (IFT) method [155] with the Generalized Indirect Fourier Transformation software package [156] was used to analyse the experimental SAXS data. Since the maximum size of the scattering particles in the investigated liquid dispersions was close to the upper limit of our experimental resolution, the typical IFT analysis was first performed, yielding the pair distance distribution function $p(r)$, which is related to the scattering intensity $I(q)$ through the Fourier transform [155]:

$$I(q) = 4\pi \int_0^\infty p(r) \frac{sin(qr)}{qr} \, dr \tag{18}$$

where r is the distance in real space, i.e., the distance between two scattering centres within the scattering particle.

The $p(r)$ contains information about the geometric properties of the scattering particles. In the case of flat scattering particles with large lateral size with respect to their thickness, the structural information about the thickness of the nanosheets can be obtained from the scattering curves by applying a special cut-off-based mode of the IFT technique, which cosine-transforms the function $I(q)q^2$ into real space and yields the thickness $p_t(r)$ as follows [157]:

$$I(q)q^2 = 4\pi A \int_0^\infty p_t(r) \, cos(qr) \, dr \tag{19}$$

where A is the area of the basal plane. In this method, the scattering curves must be strongly truncated (cut-off) in the region of very small q values to exclude the part of the scattering curve that is strongly influenced by the scattering contribution resulting from the large lateral dimensions of the flat scattering particles. The resulting $p_t(r)$ function serves as an aid for determining the geometry of the scattering particles [157].

5. Results and discussion

5.1. Basic characterisation of the particles studied

First, the experimental conditions used for the light scattering techniques had to be optimised. Another fundamental step was the basic colloidal characterisation of the investigated particles, taking into account their interaction with inorganic salts. Therefore, the entire colloidal optimisation and characterisation of the systems are described in the following chapter.

5.1.1. Functionalised polystyrene latexes

Polystyrene-based latex beads were used to study charging, aggregation and interparticle forces in the presence of various IL-containing dispersions. Due to their homogeneous size and charge distribution, they have proven to be suitable for the investigation of fundamental colloidal phenomena [99, 158]. In addition, they are widely used in biotechnology [159], sensing [160], and materials science in the development of innovative composite materials [161, 162]. Latex particles are reported to be hydrophobic [163] and can have both a positive and a negative charge depending on their surface functionalities and pH. In the present work, the surface properties of the latex particles were altered either by their surface functional groups – amidine (AL) and sulphate (SL) groups were chosen to obtain a positive and negative surface charge, respectively – or by electrostatic functionalisation through adsorption of IP-2 polymer on the surface of the particles with opposite charge (SL-IP-2).

Prior to studying the aggregation mechanism in the dispersions in question, it was necessary to optimise the particle concentrations used in the light scattering experiments. DLS is suitable for studying the early stages of aggregation, i.e., the increase in the hydrodynamic radius of the particles should not exceed 40% during the measurements to determine the rate of aggregation accurately without the formation of higher-size clusters [151]. Such conditions are best found by varying the particle concentration in the presence of 1 M KCl, which corresponds to the fast, or diffusion-controlled aggregation regime. In the case of AL (Figure 14a), the particle concentration was varied in the range of 4–24 mg/L and the change in hydrodynamic radius was measured over time, as shown in Figure 14b. Note that the curves start at around 270 nm, which reflects the initial size of AL in a stable dispersion in the presence of 1 mM KCl at pH 4 (see the inset in Figure 14b).

At this high electrolyte concentration, there is no energy barrier upon collisions, thus the aggregation is solely diffusion-controlled, i.e., the value of the rate constant for dimer formation can be given by the Smoluchowski equation [164]:

$$k_S = \frac{8k_BT}{3\eta} \tag{20}$$

This allows the determination of the half-time of aggregation ($T_{1/2}$), which indicates the time interval required to aggregate half of the primary particles in the original dispersion. This parameter represents a useful time scale for the identification of the early stages in the aggregation process. In an unstable sample, in which diffusion-controlled particle aggregation takes place, this can be calculated as follows:

$$T_{1/2} = \frac{2}{k_S N_0} \tag{21}$$

Note that the aggregation half-time at a given temperature depends only on the initial particle concentration and the viscosity of the medium.

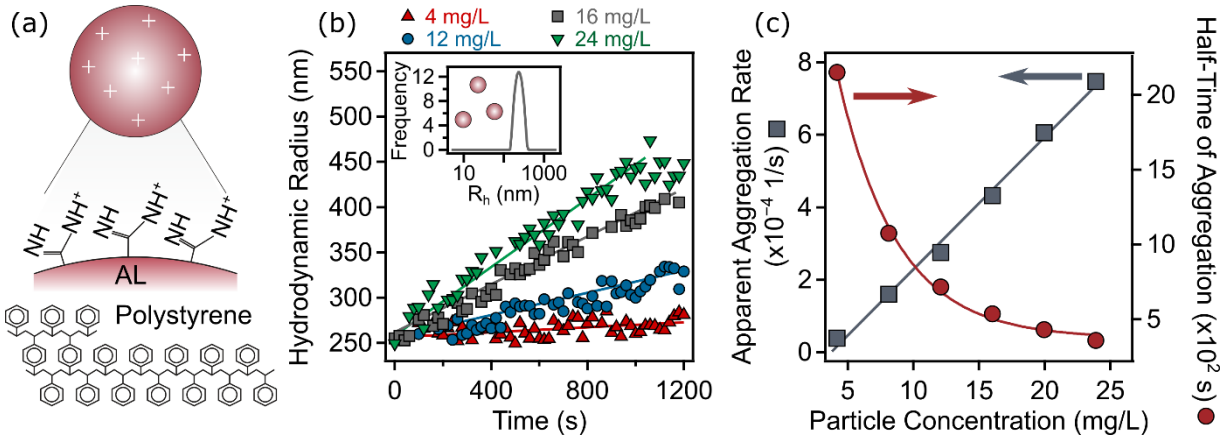

Figure 14. (a) Schematic representation of the structure of AL particle. (b) Variation of hydrodynamic radius versus time plots and (c) apparent dynamic aggregation rate (square, left axis) and half-time of aggregation (circle, right axis) for AL particles in the presence of 1 M KCl at pH 4, illustrating the dependence on particle concentration. The solid lines in (b) are linear fits to calculate the apparent aggregation rates using eq 12, while the lines in (c) are for illustrative purposes. The inset (b) shows the intensity-weighted size distribution of AL in a stable suspension, i.e., at 1 mM KCl and pH 4 [I].

Based on the data obtained, a concentration of 16 mg/L (2.18×10^{14} 1/m^3) of AL was determined to be optimal, since the resulting half-times are high enough to ensure that the measurements were performed at the early stages of the aggregation process (Figure 14c). At a lower concentration, the change in the hydrodynamic radius over time would not be well

observed (especially at low rates) and the aggregation half-time would be too long, requiring a long measurement time. In addition, the decrease in concentration would also be accompanied by a decrease in the intensity of the scattered light, which would have a negative effect on the accuracy of the hydrodynamic radius measurements by DLS. In contrast, the disturbing effect of the formation of larger aggregates (e.g., multiple scattering effect or phase separation) would be expressed at higher particle concentrations.

The optimisation of SL concentration was performed in a similar manner (Figure 15). The particle concentration was varied between 5 and 25 mg/L, while the time-dependent change in hydrodynamic radius was measured (Figure 15b). Based on the relation between the fast aggregation rates and half-times of aggregation (Figure 15c), time-resolved DLS measurements could be performed with good precision at a particle concentration of 20 mg/L (4.56×10^{14} 1/m^3).

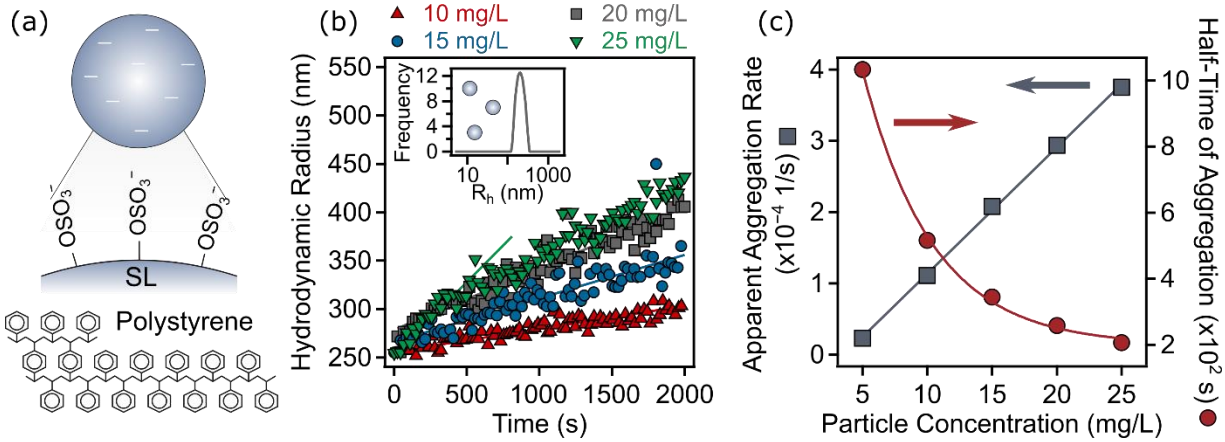

Figure 15. (a) Schematic representation of SL particle structure. (b) Variation of hydrodynamic radius versus time plots and (c) apparent dynamic aggregation rate (square, left axis) and half-time of aggregation (circle, right axis) for SL particles in the presence of 1 M KCl at pH 4, illustrating the dependence on particle concentration. The solid lines in (b) are linear fits to calculate the apparent aggregation rates using eq 12, while the lines in (c) are for illustrative purposes. The inset (b) shows the intensity-weighted size distribution of SL in a stable suspension, i.e., at 1 mM KCl and pH 4.

After optimising the experimental conditions, the commercially available SL particles were functionalised with oppositely charged IP-2 polymer to tune the charge and the surface character of the particles. The main goal was to develop an interfacial structure with IL functionalities. The successful synthesis of the polymer was confirmed by FT-IR spectroscopy (for the spectrum see Figure 16a) by identifying the characteristic vibrational peaks of IP-2 [147] at 1150 cm^{-1} (C=N$^+$), 1560 cm^{-1} (C=C) and 1625 cm^{-1} (C=N).

To determine the polymer dose required to fully coat the SL surface, the electrophoretic mobility, and the absolute aggregation rate values of SL at different IP-2 doses were determined (Figure 16b). The aim was to find the conditions under which the surface of the SL particles is completely covered with the polymer and, at the same time, forms a stable dispersion. In general, the mobilities changed from negative to positive, when the added amount of IP-2 polymer was increased indicating its strong affinity to the oppositely charged particle surface. The negative mobility values observed at low IP-2 doses were attributed to the presence of ionised sulphate functional groups, while the polymer only partially compensated the surface charge of the particles under these conditions. Increasing the amount of IP-2 led to charge neutralisation at the isoelectric point (IEP), where the particles have a net charge of zero. Thereafter, the process of adsorption progressed at higher doses and led to charge reversal resulting in a positive net charge on the particles. The mobility values remained constant at high IP-2 doses, where the surface of the particles contained a saturated IP-2 layer. Note that the coated particles exhibit a significantly lower magnitude of mobility on the plateau than the bare particles, indicating a lower surface charge density in the former case.

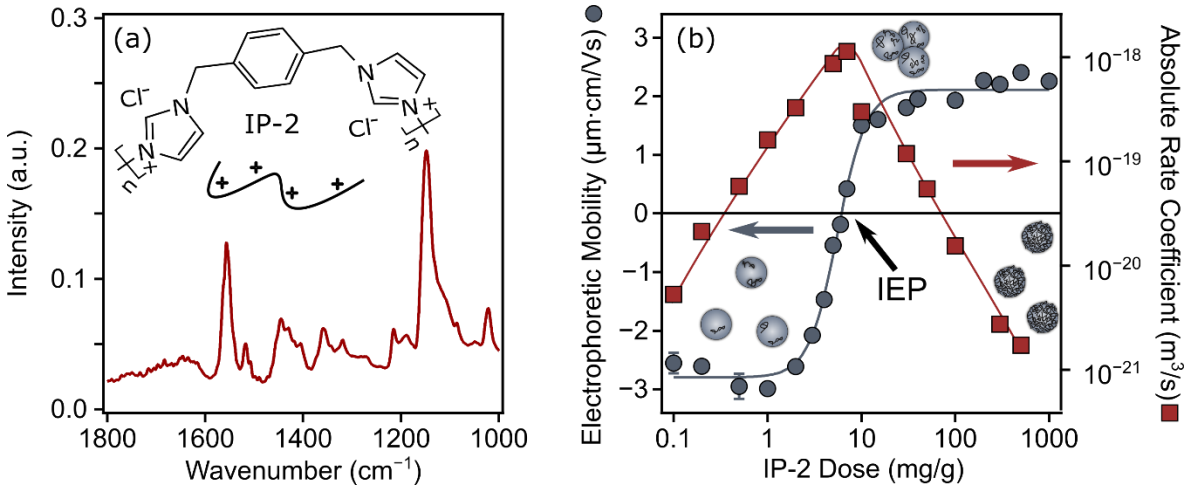

Figure 16. (a) FTIR spectrum of the IP-2 polymer. (b) Electrophoretic mobility (circles, left axis) and absolute rate coefficient (square, right axis) values of SL particles as a function of the IP-2 dose at 10 mM ionic strength adjusted by KCl and pH 4. The unit mg/g refers to mg IP-2 per one gram of SL. The lines serve to guide the eye [I, III].

Time-resolved DLS measurements were performed under the same experimental conditions as the electrophoretic mobility measurements, which allowed the precise determination of the aggregation processes within the dispersions. Figure 16b shows that the gradual trend in the mobility values corresponds to the changes in absolute aggregation rates, i.e., to the colloidal

stability of the dispersions. When the particles possess high electrophoretic mobility (either negative or positive), the aggregation rate values are low, indicating stable dispersions or slow aggregation. However, at IP-2 doses close to the IEP, there is an increase in the aggregation rates referring to rapid particle aggregation and hence, unstable samples.

Such charging and aggregation behaviour is in qualitative agreement with the DLVO theory [165, 166], which predicts stable dispersions in the case of high surface charge, and the corresponding repulsive double layer forces outweigh the attractive van der Waals interactions. Similar trends have been observed in systems containing oppositely charged latexes and polyelectrolytes [165-167], but this was the first report to include a polyimidazolium compound. Based on the above results, a dose of 500 mg/g (sample labelled SL-IP-2) was chosen for further studies, as under these circumstances the surface of the SL particles was completely coated with the IP-2 polymer, while the high positive charge ensured a very low aggregation rate, i.e., sufficiently high colloidal stability.

Moreover, the fundamental colloidal properties of the latex particles were investigated in the presence of an indifferent inorganic electrolyte, namely KCl. At low salt concentrations, negative and positive mobilities were observed for the SL and AL / SL-IP-2 particles, respectively (Figure 17a), reflecting the charge of the ionised surface functional groups at pH 4.

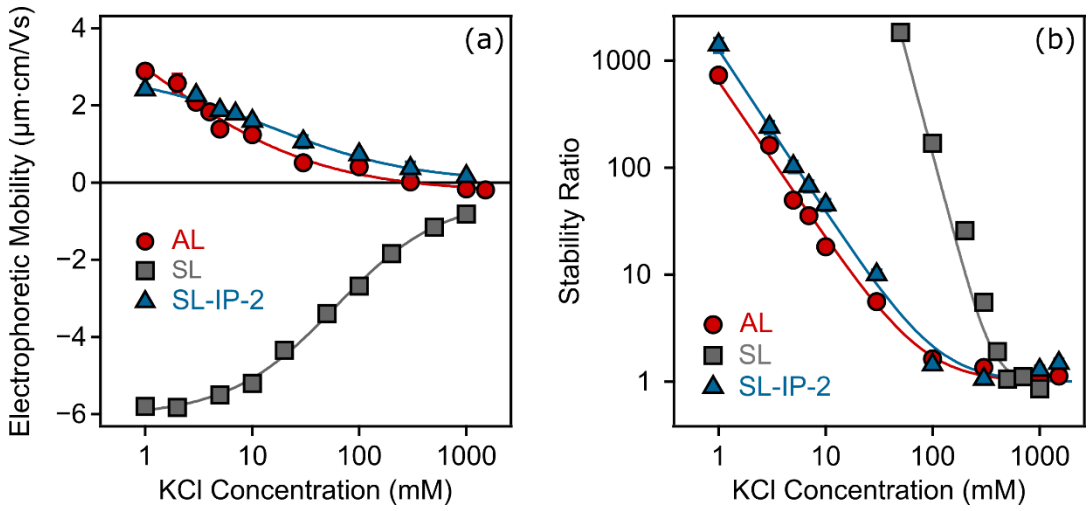

Figure 17. Electrophoretic mobilities (a) and stability ratios (b) of AL (circle), SL (square) and SL-IP-2 (triangle) particles as a function of the KCl concentration at pH 4. The lines on (a) just serve to guide the eye, while on (b) they were calculated using eq 14 [I].

In general, the absolute value of the electrophoretic mobilities decreased with KCl concentration in all cases, which can be attributed to the surface charge screening by the

counterions and the subsequent decrease in the absolute value of the electrostatic surface potential [7]. Note that in the case of SL, the mobility values passed through a minimum, a phenomenon typical of particles with high surface charge and well described by the electrokinetic effect [149, 168]. Accordingly, the electrophoretic retarding force acting on a particle increases at a faster rate with the particle charge than the driving force when an electric field is applied. The ionic strength-dependent potential data (eq 9) yielded surface charge densities at the slip plane of 3.5 mC/m^2 for AL, −27.8 mC/m^2 for SL, and 4.5 mC/m^2 for SL-IP-2. This value takes into account the pronounced influence of ions bound to the surface of the particle and therefore varies in the presence of different ions. As a result, it is useful for quantifying the adsorption affinity of ions and thus for arranging them into series based on their interaction with the surface, akin to the Hofmeister series [100].

The aggregation processes were followed by time-resolved DLS in the presence of KCl under the same experimental conditions (e.g., pH, particle/salt concentration range, and composition) as for electrophoresis, allowing direct comparison of the observed trends. The change in hydrodynamic radius (Figure 18) was remarkably different by increasing the KCl concentration.

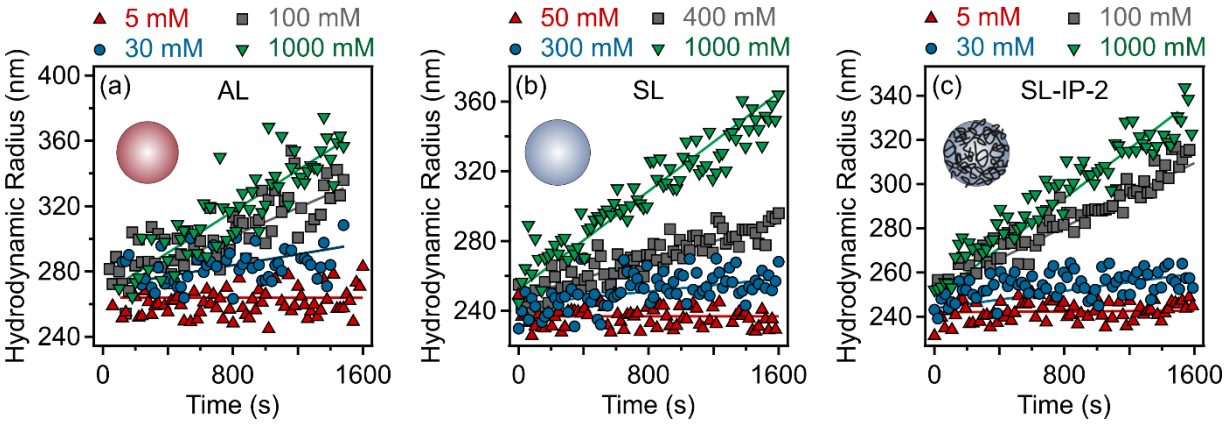

Figure 18. Hydrodynamic radius of (a) AL, (b) SL and (c) SL-IP-2 particles as a function of time at different KCl concentrations measured by time-resolved DLS at pH 4. The solid lines are linear fits to calculate the apparent aggregation rates using eq 12.

The samples were stable at low salt concentrations, as indicated by the high stability ratio values (Figure 17b), i.e., the particle size did not change significantly during the entire time of the measurement (Figure 18). By increasing the amount of KCl, moderate stability ratios were observed, referred to as the slow aggregation regime, while at higher electrolyte concentrations, the stability ratio was close to 1, indicating unstable samples and referred to as the fast aggregation regime. These two regimes are separated by the CCC, which was determined from

the stability ratio versus salt concentration plots using eq 14. The CCC values obtained were 80 mM for AL, 400 mM for SL, and 90 mM for SL-IP-2. Note that despite the similarity of the trends in the stability ratios, a divergence was observed in the slopes in the slow aggregation regime. In this region, the stability ratios decreased more rapidly with increasing ionic strength for SL particles, which can be attributed to the higher surface charge density leading to a stronger electrostatic interaction between the particle and salt constituent ions.

Overall, these trends in charging and aggregation properties are typical of aqueous colloidal systems where the main interparticle forces originate from DLVO-type interactions, such as van der Waals attraction and repulsion caused by overlapping electrical double layers [7].

5.1.2. Layered double hydroxides

The other particle system studied in this work was the Mg/Al–NO_3–LDH (see the scheme in Figure 19a). The general formula for the most common group of LDHs is $[M^{2+}_{1-x}M^{3+}_{x}(OH)_2][A^{n-}\cdot mH_2O]$, where M^{2+} and M^{3+} are the divalent and trivalent metal ions, while $A^{n-}\cdot mH_2O$ represents interlamellar charge-neutralising anions in a hydrated state [169]. The XRD patterns of the powder LDH samples (Figure 19b) unambiguously confirmed the successful synthesis as it contained all the characteristic peaks for LDH-based materials. The (003) reflection indicated an interlamellar distance of 0.83 nm (10.6°), in good agreement with the value reported in the literature [145]. The platelet-shaped particles had an average thickness of about 17.4 nm (based on eq 16) and a hydrodynamic radius of 120 nm (inset in Figure 19b). In addition, the morphology of the LDH was visualised by TEM (Figure 19c), which showed a typical hexagonal structure with some distortions.

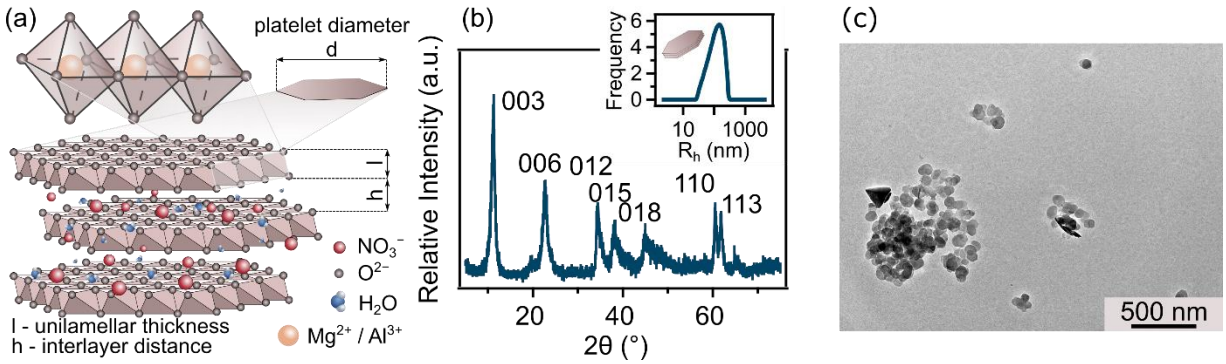

Figure 19. Schematic representation of the structure (a), powder XRD pattern (b), and TEM image (c) of LDH. The inset on (b) shows the intensity-weighted size distribution of LDH in stable suspension, i.e., at 1 mM KCl and pH 9 [II].

The particle concentration was optimised for time-resolved DLS studies in a similar way as for the latexes, and the optimal concentration of LDH was found to be 10 mg/L. Subsequently, the basic charging and aggregation properties were examined in the presence of KCl (Figure 20). The mobilities were positive due to the structural charge of the LDH particles (Figure 20a). Overall, similar trends were observed for the charge and aggregation characteristics as for the latexes, i.e. with increasing salt concentration, the mobility values decreased and the increase in particle size became steeper (Figure 20b), leading to a parallel decrease in stability ratios (Figure 20c). These trends – including the occurrence of slow and fast aggregation at low and high salt concentrations, respectively – were consistent with the DLVO theory and have been previously reported for LDH dispersions in the presence of inorganic salts [101, 170]. Based on these data, the surface charge density was set at 21.0 mC/m^2 and CCC values was 18.7 mM.

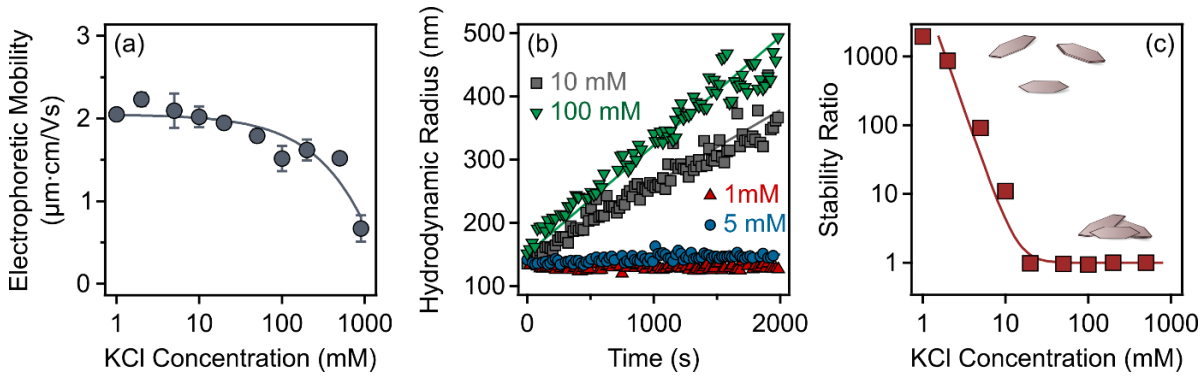

Figure 20. Electrophoretic mobilities (a) and stability ratios (c) of LDH particles as a function of the KCl concentration at pH 9. (b) Hydrodynamic radius of LDH as a function of time at different KCl concentrations measured by time-resolved DLS at pH 9.The lines on (a) just serve to guide the eye, on (b) they are linear fits to calculate the apparent aggregation rates using eq 12, while on (c) they were calculated using eq 14.

5.2. Colloidal stability in IL-containing dispersions

This chapter is concerned with the investigation of the colloidal stability and interfacial properties in IL dispersions, with a focus on the charge and aggregation relations of different particles. The influence of key variables, such as water and salt content, is also addressed, with a systematic analysis of their effects on colloidal stability. In this way, novel insights into the fundamental principles that govern the colloidal behaviour of IL-particle dispersions could be provided, thus promoting their effective use in a variety of applications, such as designing functional materials for energy storage devices or lubrication [66] or developing new catalysts [129].

5.2.1. Particle aggregation mechanisms in ILs

First, the aggregation behaviour of SL and SL-IP-2 particles in EAN and its water mixtures was studied. This investigation allowed an in-depth analysis of the fundamental colloidal properties in the presence of ILs for polymeric particles with different charges and functionalities over a wide range of EAN concentrations. Figure 21a and Figure 21b show that, in general, three main aggregation regimes have been identified for SL and SL-IP-2, respectively.

In the first regime, i.e., up to an EAN concentration of 1.0 M (water-rich side), aggregation rates were initially low but increased rapidly with increasing IL content until they reached a plateau. The observed trend mirrors that obtained in the presence of KCl (Figure 17), as ILs tend to completely dissociate and get hydrated in dilute aqueous solutions, similar to what is observed for inorganic salts [46, 67, 69]. Thus, this scenario is consistent with the predictions of DLVO theory, which leads to the term DLVO regime. The initial increase in aggregation rates signifies the onset of the slow aggregation regime, which is primarily determined by the gradual charge screening by EAN ions and surface adsorption of counterions. Note that for negatively charged SL particles, the counterion was the ethylammonium cation, whereas for positively charged SL-IP-2 particles, the counterion was the nitrate anion. The flat region observed at higher EAN concentrations indicates the fast aggregation regime, where the percentage of particle collisions forming dimers depends solely on their diffusion rate within the specific medium. The absolute aggregation rates in this fast aggregation regime (k_{fast}) were found to be 2.63×10^{-18} m^3/s for SL and 5.12×10^{-18} m^3/s for SL-IP-2 particles.

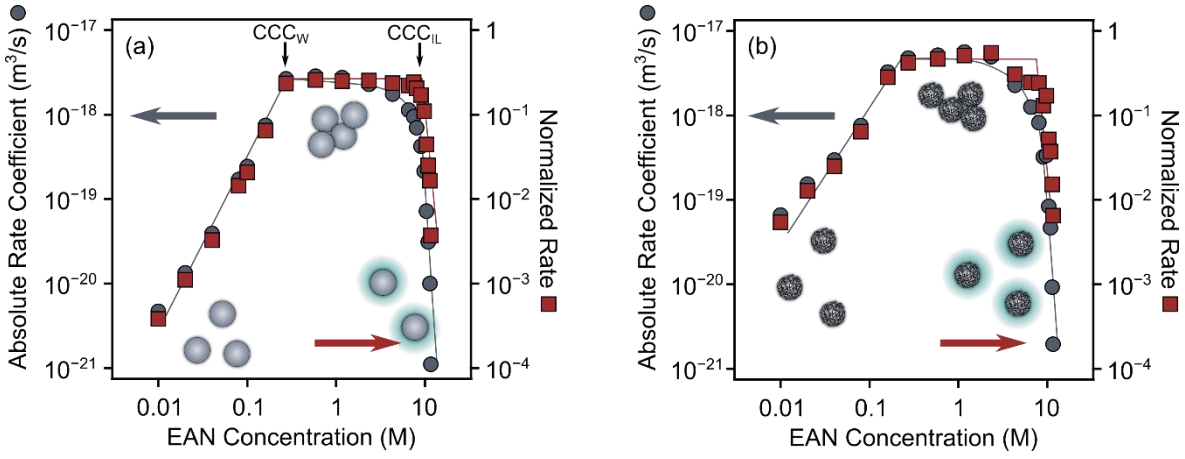

Figure 21. EAN concentration dependence of absolute aggregation rate coefficients (circles, left axes) and normalised aggregation rate coefficients (squares, right axes) for SL (a) and SL-IP-2 (b) particles. In (a) the CCCs corresponding to the water-rich (CCC_W) and EAN-rich (CCC_{IL}) concentration regimes are indicated. The solid lines serve as guides for the eye [III].

In the second regime, i.e., at intermediate EAN concentrations above 1.0 M, there was a gradual decrease in aggregation rates due to the increased viscosity of the mixture. The importance of the so-called viscous stabilisation can be confirmed by normalising the aggregation rate coefficients (k) with the Smoluchowski value (k_S) (given in eq 20), as it takes into account the dynamic viscosity of the solution for diffusion-controlled aggregation:

$$k_{norm} = \frac{k}{k_S} \tag{22}$$

Note that the viscosities of the mixtures increased sharply with increasing IL concentration (as illustrated in Figure 11b), while the Smoluchowski values decreased in parallel [73]. The fact that the normalised rate coefficients (k_{norm}) remained constant throughout the viscous stabilisation regime proves that the gradual slowdown of aggregation is indeed due to the increased viscosity of the medium, while aggregation remains diffusion-controlled. This mechanism could slow down the aggregation process in the studied systems by almost an order of magnitude. The experimental aggregation rate coefficients (k) were 2-3 times smaller than the calculated values (k_S) in the fast aggregation regime due to the influence of hydrodynamic and van der Waals interactions, which are neglected by the Smoluchowski theory. Similar discrepancies were also observed for the dispersion of other colloidal particles in aqueous solutions [59, 171-173].

In the third regime, there was a significant decrease in both absolute and normalised aggregation rates with an increase in EAN concentration, a phenomenon known as solvation stabilisation [59]. The onset of this distinct regime was marked by a sudden decrease in normalised aggregation rates at high IL concentrations where only a small amount of water was present. The stabilising effect in IL media was attributed to the formation of solvation layers, a concept that is further explored in this section. Interestingly, the presence of water in the samples disrupted the layering of IL constituents on the particle surface, highlighting the interference of water at the interface. This phenomenon mirrors the results of other studies and emphasises the disruptive role of water at interfaces [45, 59, 78].

The sharp transition between slow and fast aggregation within the DLVO regime on the water-rich side was quantified by the CCC. A similar critical concentration can be observed on the IL-rich side, indicating the transition from the viscous to the solvation stabilisation regime. These two CCCs are distinguished as CCC_W on the water-rich side and CCC_{IL} on the IL-side. To

follow the usual definition of CCC in water, CCC_W was expressed as the molar concentration of EAN, while CCC_{IL} is the molar concentration of water. The presented trends are generic for both SL (see Figure 21a) and SL-IP-2 particles (see Figure 21b), while the data obtained are summarised in Table 2.

Table 2. Characteristic aggregation data of latex particles measured in EAN-water mixtures.

	SL		SL-IP-2	
	CCC_W [a]	CCC_{IL} [b]	CCC_W [a]	CCC_{IL} [b]
EAN	0.23	7.1	0.15	15.0
EAN – 0.001 M $NaNO_3$	0.16	8.5	0.15	12.6
EAN – 0.01 M $NaNO_3$	0.15	7.3	0.14	16.2
EAN – 0.1 M $NaNO_3$	0.05	7.8	0.05	14.8

[a]Concentration of EAN in M. [b]Concentration of water in M. The accuracy of the CCC determination is about 10%.

An important note is that the CCC_W is much higher for SL, while the magnitude of the aggregation rate coefficients in the intermediate regime is higher for the SL-IP-2 particles. These observations are most likely due to the significantly higher surface charge of the bare SL particles compared to SL-IP-2 (see the magnitudes of mobility values in Figure 16b at low and high IP-2 doses), resulting in slightly stronger electrostatic repulsion between the particles, i.e., slower aggregation. In contrast, a higher water concentration is required for the destabilisation of SL-IP-2 particles compared to SL, as can be seen from the CCC_{IL} values in Table 2. This probably occurs because EAN acts as a good solvent for the coating polymer and forms a solvation sphere around the SL particle with polymer tails and loops, leading to an additional stabilising effect of steric origin between the adsorbed IP-2 layers [174, 175]. This additional repulsion led to an increased resistance to water-induced aggregation.

To further investigate the behaviour of ILs when interacting with charged particles, the electrophoretic mobility values for both particles were determined over the entire range of EAN-water mixtures. Figure 22a illustrates that although the sign of the mobility values was system-dependent, their magnitudes showed similar trends, i.e., the absolute values initially decreased with increasing EAN concentration due to surface charge screening, while they levelled off close to zero at higher EAN concentrations. This pattern reflects the behaviour commonly observed in charged colloids suspended in monovalent salt solutions and agrees well with established theories explaining the structure and the dimension of the electrical double layer [98].

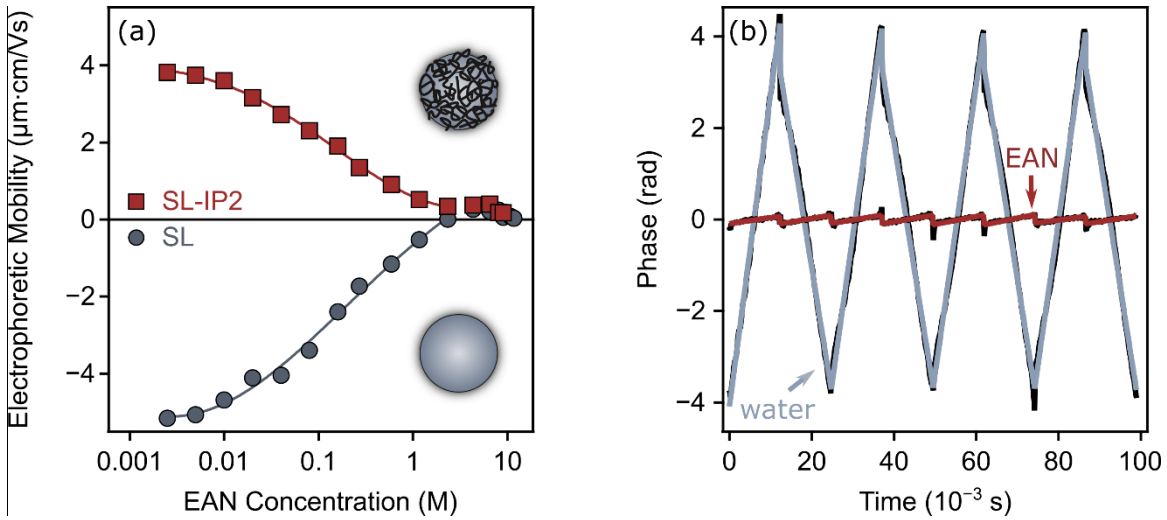

Figure 22. (a) Electrophoretic mobility values of SL and SL-IP-2 particles as a function of EAN concentration and (b) the phase plots in the presence of SL particles on the water-rich side (2.5 mM EAN concentration) and IL-rich side (0.17 M water concentration). The phase plots show the phase differences between the detector and the monitor traces (black lines), while the grey (water) and red (EAN) lines correspond to the fit of cmPALS to the data. The solid lines in (a) represent the interpolation based on eq 23 [III].

Based on the DLVO theory, the surface charge density values – obtained from the IL concentration-dependent electrophoretic mobility data using eq 9 – were further used on the water-rich side to calculate the CCC_W values as follows [176]:

$$CCC_W = \frac{1}{8\pi L_B}\left(\frac{24\pi}{He\varepsilon_0\varepsilon}\right)^{2/3}\sigma^{4/3} \tag{23}$$

The Hamaker constant used for the calculation was 9×10^{-21} J [176]. The CCC_W values obtained were 0.25 M for SL and 0.14 M for SL-IP-2, which is in good agreement with the values determined from the EAN concentration dependence of the aggregation rates (see Table 2). Based on the results, the aggregation processes on the water-rich side can indeed be explained by considering DLVO-type forces acting between the particles in both cases.

In addition, the phase plots shown in Figure 22b provide insight into the movement of the particles in the respective media. Accordingly, the charged particles on the water-rich side tend to move in the direction of the electrodes with opposite polarity. However, on the IL-rich side – where solvation stabilisation takes place – no particle movement could be detected by applying the electric field during the cmPALS measurements. These observations imply that electrostatic interactions between the particles play a negligible role in explaining successful stabilisation, as they appear to be suppressed by the prevailing ionic environment of the medium. In such cases,

it is highly probable that the colloidal stabilisation results from the formation of IL layers on the surface of the charged particles. However, electrostatic interactions still exist between all charged species within the system (anions, cations, and the charged particle surface), which are responsible for the nanostructural interfacial organisation [8].

5.2.2. Effect of salt content on the colloidal stability of IL-particle dispersions

Following the exploration of the fundamental colloidal properties of latex particles in a wide range of EAN concentrations, the effects of introducing $NaNO_3$ into the systems and its influence on the aggregation processes were investigated. The anticipation was that Na^+ ions should have a stronger influence on the interfacial properties considering that nitrate ions were already present in the mixtures as a component of EAN (NO_3^- was specifically chosen to avoid the introduction of additional anions into the systems). The Na^+ served as a counterion for the negatively charged SL particles, while it acted as a coion for the positively charged SL-IP-2.

Figure 23a illustrates the observed trends of aggregation rates for SL particles in EAN–water mixtures at three different $NaNO_3$ concentrations (i.e., 1 mM, 10 mM, and 100 mM). The general trend in the presence of salt was similar to that without salt, but salt concentration-dependent phenomena were observed, which deserves further discussion.

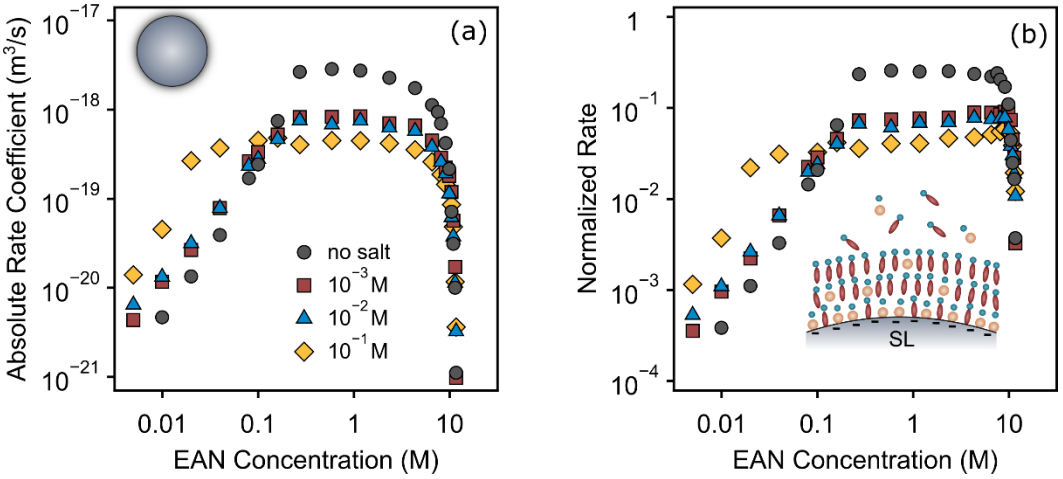

Figure 23. Absolute aggregation rate coefficients (a) and normalised rate (b) of SL as a function of EAN concentration in EAN–water mixtures with different concentrations of background $NaNO_3$ electrolyte [III].

The first remark was that with increasing salt concentration, the CCC_W values showed a consistent decrease, i.e., the presence of 0.1 M $NaNO_3$ resulted in the lowest CCC_W. The CCC values obtained after normalising the aggregation rates with the Smoluchowski value (see

Figure 23b) are summarised in Table 2. This decrease can be attributed to the increased charge screening due to the excess of counterions, which is consistent with the predictions of DLVO theory. In contrast, the CCC_{IL} value determined on the IL-rich side did not appear to be affected by the presence of $NaNO_3$, i.e., the values obtained were identical within experimental error, to those reported in previously studied systems without the added salt.

Furthermore, Figure 23a shows that the presence of Na^+ ions slows down the aggregation in the intermediate concentration range of the EAN-water system, where viscous stabilisation occurs. This effect is evident as the aggregation rates in the presence of salt constituent ions are nearly an order of magnitude lower than in the absence of added salt. Remarkably, this stabilisation becomes more pronounced with increasing concentration of Na^+ ions, i.e., aggregation rates were the lowest in the presence of 0.1 M $NaNO_3$. This pattern can be partially explained by the accumulation of Na^+ ions on the negatively charged SL particle surface, suggesting that they are likely involved in the formation of an initial cationic layer that neutralises the negative charge of the SL. Since sodium ions can interact with the components of EAN at the interface, they play an important role in the formation of structured solvation layers around the particles, which contributes to the development of more stable particle dispersions. A similar phenomenon has been observed at various solid/IL interfaces in the presence of inorganic ions [50, 86]. On the other hand, the Hamaker constant and its slight dependence on the ionic strength may also contribute somewhat to the above phenomena [177], since the effective ionic strength in this range is about 0.5–10 M. At such a high ionic strength, the range of the electrical double layer repulsion between two charged surfaces is much shorter than that of the attractive van der Waals forces, hence the effect on the Hamaker constant is more pronounced.

In contrast, for the SL-IP-2 particles – where the Na^+ ions have the same charge as the polymer-coated particles – the above-mentioned $NaNO_3$ concentration dependence was not observed in the intermediate IL concentration regime (see Figure 24). While the obtained trend in the determined CCC values mirrored that of the SL particles – i.e., the CCC_W values decreased with increasing salt levels, while the CCC_{IL} remained unaffected – the aggregation behaviour of SL-IP-2 particles seems to be largely unaffected by the presence of background salt, i.e., the determined fast aggregation rates remained unchanged within the experimental uncertainty, regardless of the $NaNO_3$ concentration. These observations indicate that Na^+ ions interact only

slightly with particles of the same charge so that their influence on the surface charge is negligible. The dependence of the Hamaker constant on the ionic strength, however, is probably not expressed because the particles cannot approach each other due to steric hindrance by the coating polymer.

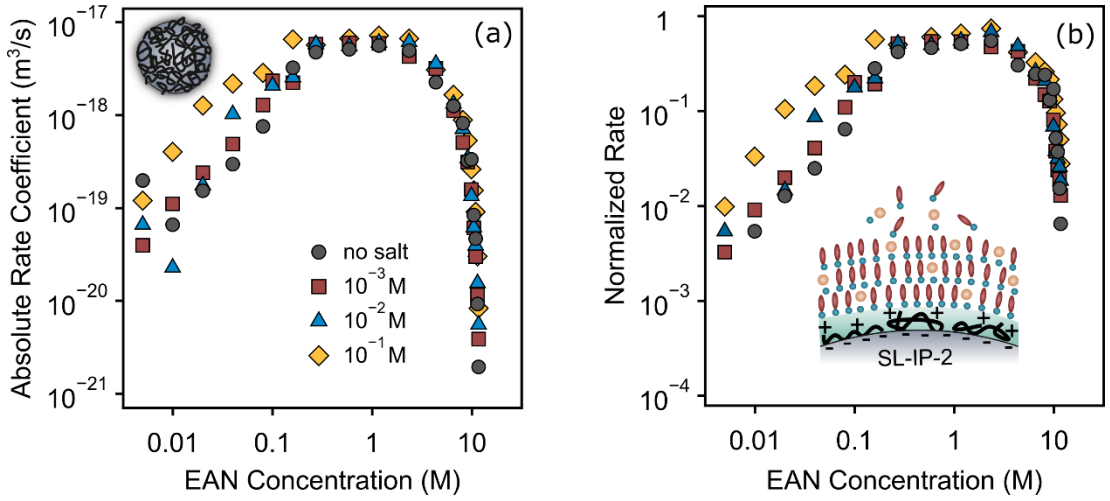

Figure 24. Absolute aggregation rate coefficients (a) and normalised rate (b) of SL-IP-2 as a function of EAN concentration in EAN–water mixtures with different concentrations of background $NaNO_3$ electrolyte [III].

The results indicate that Na^+ ions change the interfacial arrangement of IL ions in the system investigated, and thus influence the stability of colloidal dispersions. The extent of this influence varies and depends on the properties of the added ions and the surface charge of the particles. Overall, the presence of even small amounts of water or salt in the system (as an additive or unwanted impurity) can strongly alter the interfacial structuration of ILs, and thereby the aggregation mechanism in IL-containing particle dispersions. A similar alteration has already been reported for charged surfaces, such as mica [75] or graphene [76], where the changes in the interfacial structure were manifested by a reduction in the thickness of the adsorbed ion layer on mica during liquid drainage and significantly affected the zero charge potential of graphene.

5.3. Ion-specific effect of IL constituents

This chapter discusses the study of ion specificity and its effects on the stability of dispersions containing ILs. Using the Hofmeister series as a conceptual guide, the charge and aggregation characteristics in aqueous IL solutions in the presence of different types of particles were investigated. The systematic change of IL structures allowed the classification of IL compounds based on their affinity to the particle surface and their destabilising power.

5.3.1. Latex particles in aqueous IL dispersions

To investigate the ion-specific effects of IL compounds, the charging and aggregation properties of latex particles were first analysed in the presence of aqueous IL solutions containing chloride (Cl^-), bromide (Br^-), nitrate (NO_3^-) or acetate (Ac^-) anions and the 1-butyl-3-methylimidazolium cation ($BMIM^+$). Two types of positively charged particles, namely AL and SL-IP-2, were studied, thus the anions were the counterions and the $BMIM^+$ cation acted as the coion. This approach made it possible to study ion specificity using polymeric particles with the same sign of charge but different surface functionality.

First, the electrophoretic mobility of AL particles in aqueous IL solutions was measured, while the composition of the ILs was systematically varied to investigate the specific interfacial effects of the IL anions (Figure 25a). In general, the mobility values decreased with increasing IL concentration, similar to the case of the indifferent KCl electrolyte (Figure 17a). Such a decrease can be explained by the screening of the surface charge by the dissolved ions, while the deviation between the electrophoretic mobility plots when varying the IL composition indicates specific ion adsorption on the particle surface.

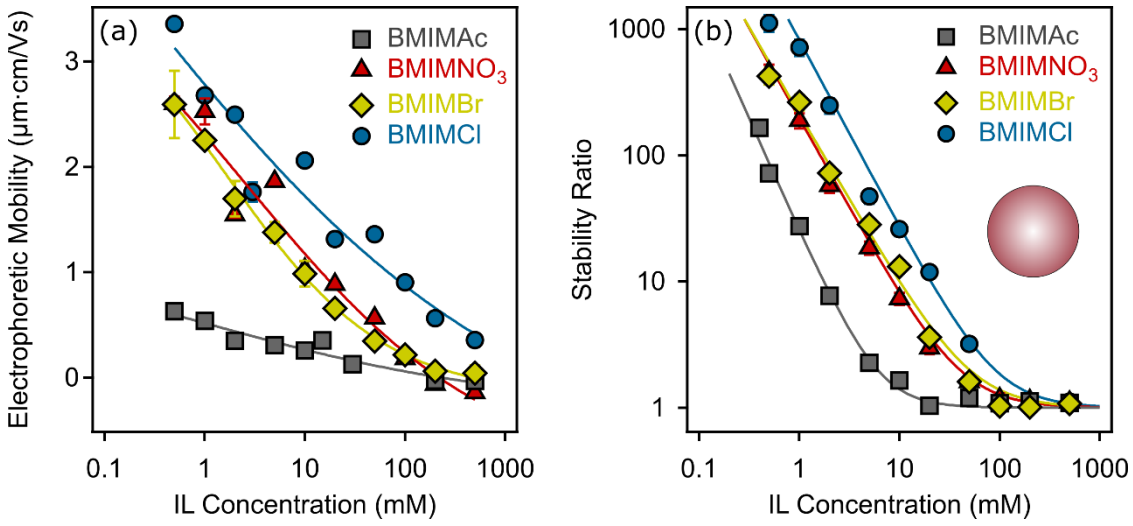

Figure 25. Electrophoretic mobility (a) and stability ratios (b) of AL as a function of IL concentration. The lines in (a) serve to guide the eyes, while in (b) they were calculated using eq 14. The measurements were performed at pH 4 and the AL concentration was 16 mg/L [I].

The stability ratios for the AL particles measured under the same experimental conditions as in the mobility studies are shown in Figure 25b. In each case, the overall trends were similar and resembled those obtained for inorganic salts described earlier (Figure 17b). Accordingly, slow (at low IL concentration) and fast (at high IL concentration) aggregation regimes were

identified, which were separated by the CCC as the transition point between the slow and fast aggregation regions. These tendencies are in good qualitative agreement with the DLVO theory, which states that the force between particles is the result of electrostatic repulsion and attractive van der Waals interactions [32, 33]. At low IL concentrations, the electrostatic repulsive forces decrease with increasing IL concentration, while the attractive forces remain unchanged, and therefore become dominant at higher ionic strengths. The presence of DLVO-type forces is also suggested by the low zeta potentials measured at CCC (Table 3).

Table 3. Characteristic aggregation and charging data of AL and SL-IP-2 particles measured in IL solutions.

ILs	AL			SL-IP-2		
	σ (mC/m^2)[a]	CCC (mM)[b]	u (μm·cm/Vs)[c]	σ (mC/m^2)[a]	CCC (mM)[b]	u (μm·cm/Vs)[c]
BMIMAc	0.5	6	0.21	7.5	100	0.78
$BMIMNO_3$	2.5	40	0.43	7.5	100	0.78
BMIMBr	3.0	50	0.46	7.5	100	0.78
BMIMCl	6.0	90	0.65	7.5	100	0.78

[a]Surface charge density determined with eq 9. [b]Critical coagulation concentration calculated by eq 14. [c]Electrophoretic mobility at the CCC.

Nevertheless, the variations of CCCs in the presence of different types of IL solutions shed light on the importance of ion-specific effects on the particle aggregation processes. This is also supported by the fact that the magnitude of the mobilities at the same IL concentrations and the surface charge density values (Table 3) – obtained from the IL concentration-dependent potential data using the Debye–Hückel model (eq 9) – decreased in the order $Cl^- > Br^- > NO_3^- > Ac^-$. This sequence is also illustrated by the evolution of the CCCs, which is consistent with the indirect Hofmeister series (Figure 8) [100, 178]. Accordingly, the larger and less hydrated Ac^- ions adsorbed most strongly on the hydrophobic, positively charged latex particle surface. The adsorption processes lead to a partial charge compensation, and thus to lower mobilities. However, the well-hydrated Cl^- ions had a lower affinity to the particle surface and preferred to remain in the bulk. Therefore, the magnitudes of surface charge and mobility are largest in the presence of this ion.

In contrast, in the case of SL-IP-2, the electrophoretic mobilities were the same within the experimental error for all systems (Figure 26a). After reaching an intermediate maximum, which is attributed to the electrokinetic effect [168], the mobility values decreased with increasing IL concentration in all cases, but no specific adsorption of IL anions was observed. The

insensitivity of the surface charge to the chemical composition of the surrounding anions in the SL-IP-2 systems is quite surprising, as specific adsorption of anions to positively charged bare latexes [100, 110] and to those functionalised with positively charged polyelectrolytes [179] has been reported in the past.

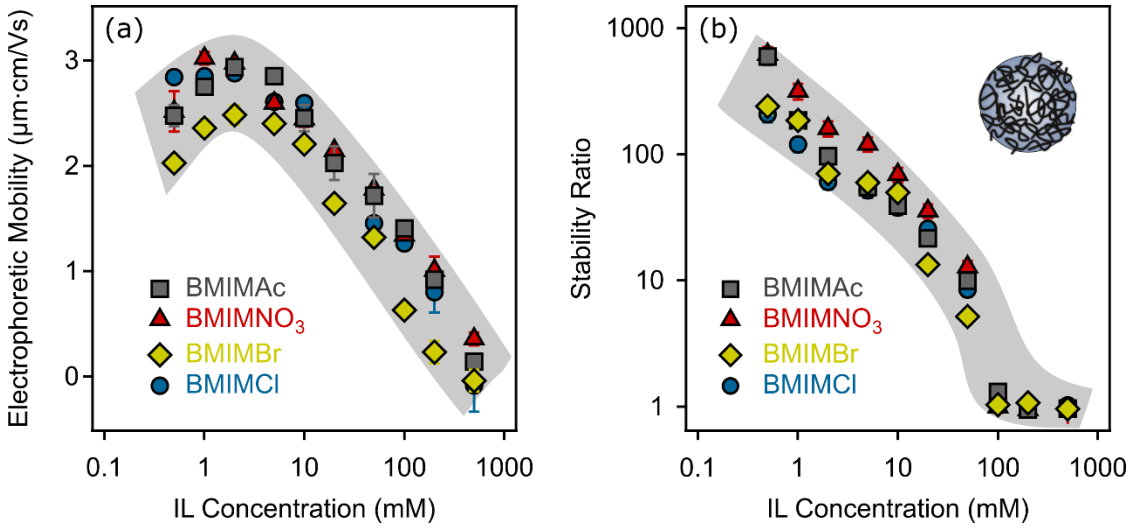

Figure 26. Electrophoretic mobility (a) and stability ratios (b) of SL-IP-2 as a function of IL concentration. The measurements were performed at pH 4 and SL-IP-2 concentration was 10 mg/L. The grey area shows the standard deviation of the data [I].

Furthermore, the stability plots were also identical within the experimental error regardless of the IL composition (Figure 26b), i.e., the onset of rapid particle aggregation was located at the same CCC for all systems (Table 3). It is important to note that in the slow aggregation regime, the decrease in stability ratio was not linear but curved, i.e., intermediate plateaus were observed at 10 mM IL concentrations. This occurrence is unusual for latex particles and is probably caused by the swelling of the adsorbed IP-2 layer, a phenomenon expected to take place within the same ionic strength range as the plateaus are situated [180]. Such swelling causes the formation of polyelectrolyte tails and loops on the surface, leading to a small rise in the stabilising steric forces [49], while the primary interactions between particles are still governed by DLVO forces.

Given the very similar surface charge density and CCC values for the AL and SL-IP-2 particles in the presence of indifferent KCl electrolyte (Figure 17), the striking contrast in charge and aggregation characteristics in IL solutions is very surprising. Figure 27a clearly shows the difference in the expression of the ion-specific effect for the latexes, as the presence of different IL anions led to different CCC values in the case of AL, whereas CCC did not depend on the IL

composition in the case of SL-IP-2. Remarkably, there are no similar findings in the existing literature, suggesting that the application of polyelectrolyte coating to mask ion-specific effects on particle aggregation is a unique and unexplored phenomenon. It could be exploited in applications where particles are dispersed in electrolyte mixtures, i.e., in the development of advanced composite materials for electrochemical purposes [181].

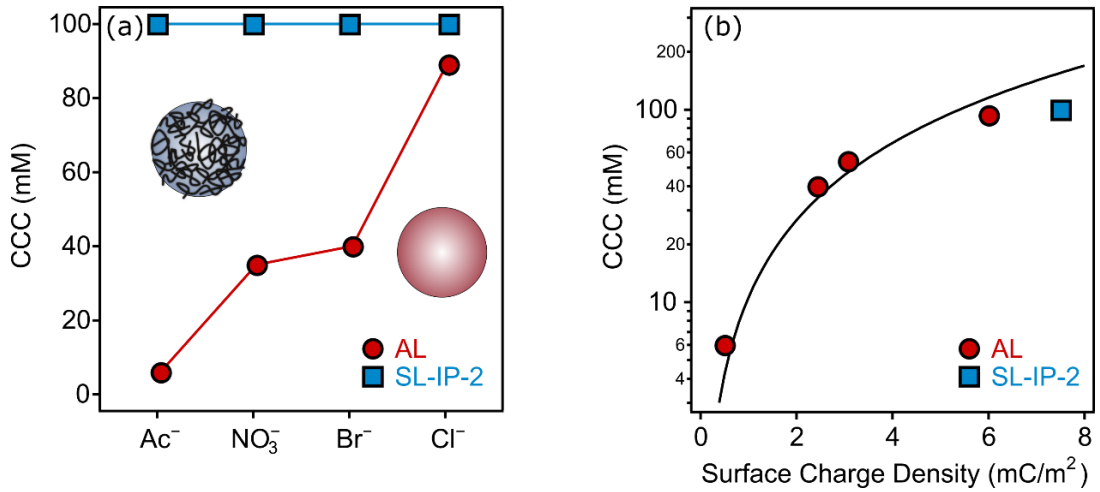

Figure 27. CCC values of AL (red circles) and SL-IP-2 (blue square) determined in the presence of ILs (a) and CCC versus the charge density data (b). The lines in (a) were added merely to guide the eyes, while (b) shows the DLVO prediction, which has been calculated by eq 24 [I].

In order to interpret the aggregation processes, the aggregation mechanism was further investigated using a relation derived from the DLVO theory [37, 176]:

$$CCC = \frac{0.365}{N_A L_B}(H\varepsilon_0\varepsilon)^{-2/3}\sigma^{4/3} \tag{24}$$

where L_B is the Bjerrum length corresponding to the distance, at which the electrostatic interaction between two charges is of the order of thermal energy. Note that the Hamaker constant of 1.0×10^{-21} J was used for both AL and SL-IP-2 particles. In this model, it was assumed that the energy barrier vanishes at the CCC and that beyond this concentration the attractive forces between the particles prevail. The relation calculates the CCC values from the charge densities and provides a clear and precise understanding of the charge and aggregation process that goes beyond a qualitative analysis based on DLVO theory alone. Accordingly, the experimental CCC values were plotted against the surface charge density data and compared to the CCCs calculated using eq 24. The data presented in Figure 27b show a relatively good agreement between the calculated and experimental values, proving that the predominant interparticle forces are of DLVO origin, as only DLVO-type forces were included in the

calculations to derive eq 24. However, specific ion adsorption resulted in different surface charge densities for AL – decreasing in the order $Cl^- > Br^- > NO_3^- > Ac^-$ – leading to weaker electrical double layer repulsion. Since the van der Waals forces are consistently present and are only slightly affected by the ionic strength [177], the decrease in CCC values in the specified sequence is attributed to the decreasing strength of the repulsive double layer forces. Overall, the DLVO forces determine the aggregation mechanism in aqueous IL dispersions, while the CCC is determined by the specific ion adsorption.

In the case of SL-IP-2 particles, however, there is no such specific ion effect. The basic phenomenon responsible for this result is probably related to the degree of hydration of the surface and the counterions. In previous studies, it was found that weekly hydrated ions have a stronger affinity for hydrophobic surfaces, resulting in stronger adsorption to hydrophobic latexes [110], which is consistent with the observed behaviour of the AL particles. Since the same counterions were used for the SL-IP-2 particles, the lack of ion-specific effects suggests that the hydrophobic nature of SL was reduced by surface functionalisation with IP-2, so that the different affinity of the counterions based on their hydration level is not pronounced. The reduced hydrophobicity may be also attributed to the stacking interaction between the imidazolium groups of $BMIM^+$ and IP-2. This interaction leads to an accumulation of $BMIM^+$ on the surface, resulting in a more ionic interfacial environment. Previous studies have also reported similar stacking interactions as evidenced by electronic structure analysis [182].

Although in this case mainly polymeric particles were investigated, the same coating technique could potentially be applied to various surfaces in contact with ILs [45, 183-185], as this approach is promising for the creation of ionophobic surfaces. Nevertheless, it is crucial to carefully optimise the experimental conditions such as pH, polymer concentration, and ionic strength before performing the coating procedure.

5.3.2. LDH particles in aqueous IL dispersions

The effect of IL cations and anions on the charge and aggregation properties of LDH particles in dilute aqueous IL solutions was investigated in a similar manner as above. The IL composition, i.e., the type of anions and cations, was systematically varied in the samples. Accordingly, different anions were applied through BMIMCl, BMIMBr, $BMIMNO_3$, BMIMSCN and BMIMDCA ILs, while the effects of the cations were studied in the presence

of BMIMCl, BMPYCl, BMPIPCl and BMPLCl. Note that for positively charged LDH, the anions were the counterions, while the cations acted as coions, thus the effect of both counter- and coions on the colloidal features of LDH was evaluated.

First, the impact of the IL anions on the colloidal stability of LDH was investigated at pH 9. The results on electrophoretic mobilities are shown in Figure 28a, which indicate that although the mobility values were system-specific, the trend in their concentration dependence is very similar in all cases. The values decreased with increasing IL concentration due to the surface charge screening by the IL components so that the mobility data approached zero at higher ionic strengths. However, they remained positive over the entire range studied due to the inherent structural charge of the particles. The observed peak in the trend of mobilities at low concentrations was attributed to the electrokinetic phenomenon, a typical occurrence for charged particles moving in an electric field [168].

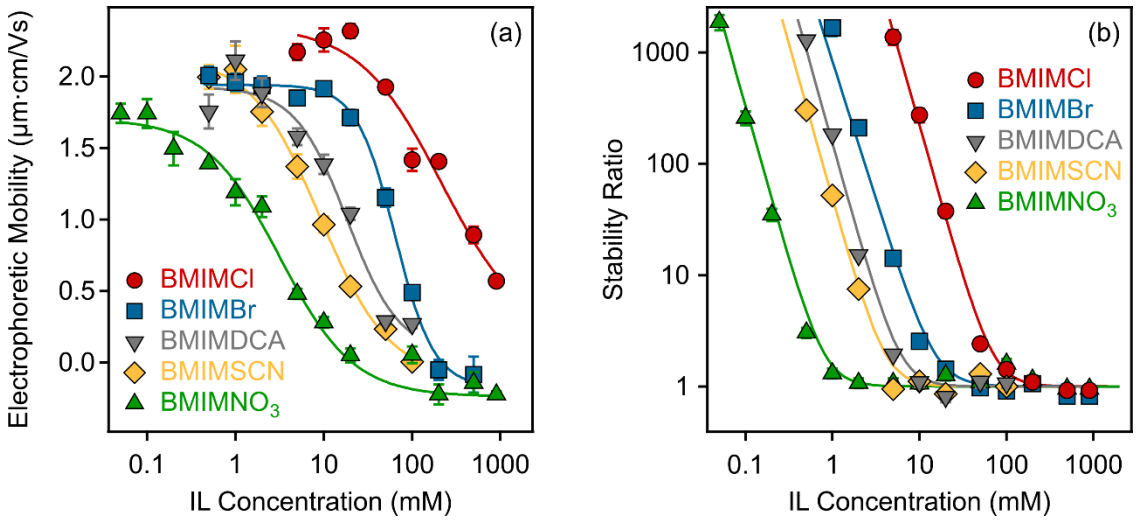

Figure 28. Electrophoretic mobility (a) and stability ratios (b) of LDH particles in the presence of ILs composed of different anions (Cl^-, Br^-, DCA^-, SCN^- and NO_3^-) and the $BMIM^+$ cation. The lines in (a) serve to guide the eyes, while in (b) they were calculated using eq 14. The measurements were performed at pH 9 and the LDH concentration was 10 mg/L [II].

The stability plots were then determined – under the same experimental conditions (e.g., particle concentration, pH, and IL concentration range) as in the electrophoretic studies – in the LDH-containing dispersions to enable a direct comparison of the charge and aggregation processes. The results shown in Figure 28b indicate that the general trend was the same as that experienced for inorganic electrolytes (Figure 19c). Accordingly, slow aggregation and stable samples were observed at low concentrations of IL, while the dispersions became unstable at

high ionic strength, as indicated by the stability ratio values close to one. As mentioned in the previous chapter, these charge and aggregation mechanism tendencies are typical for systems, in which the main interparticle forces arise from DLVO-type interactions, i.e., the colloidal stability of dispersions is determined by the superposition of attractive van der Waals and repulsive electrical double layer forces. However, the ion-specific effect also had a significant influence in the case of LDH, as shown by the fact that the magnitude of the mobility values at given IL concentrations decreased in the order $Cl^- > Br^- > DCA^- > SCN^- > NO_3^-$, which trend was also illustrated by the order of surface charge densities and CCCs shown in Table 4.

Table 4. Characteristic charging and aggregation data of LDH particles measured in diluted IL solutions.

IL cations	$BMIM^+$	$BMIM^+$	$BMIM^+$	$BMIM^+$	$BMIM^+$	$BMPL^+$	$BMPY^+$	$BMPIP^+$
IL anions	Cl^-	Br^-	DCA^-	SCN^-	NO_3^-	Cl^-	Cl^-	Cl^-
σ (mC/m^2)[a]	16	6	3	2	1	14	8	4
CCC (mM)[b]	70	15	6	4	0.8	50	30	10
Δ_{fast} ($\times 10^{-3}$ s^{-1})[c]	1.07	0.93	0.79	1.04	0.76	0.97	0.98	1.06

[a]Surface charge density determined with eq 9. [b]Critical coagulation concentration calculated by eq 14. [c]Apparent aggregation rate coefficient in the fast aggregation regime obtained by eq 12.

Subsequently, the effect of IL cations on the charging properties and aggregation behaviour of LDH particles was also studied. The electrophoretic mobility and stability ratio values of the positively charged particles were strongly influenced by the type of IL cations ($BMIM^+$, $BMPIP^+$, $BMPL^+$, and $BMPY^+$) when the same (Cl^-) counterion was used. Figure 29a shows that the general evolution of the charge features was similar to that described previously, i.e., the mobility values decreased as the concentration of the ILs increased due to charge screening. Besides, the shape of the stability plots (Figure 29b) was identical to the plots for varying anions (Figure 28b), i.e., slow aggregation occurred at low concentrations, fast aggregation at high concentrations, and these two regimes were separated by the CCC.

Although these observations are typical for colloidal systems containing charged particles in electrolyte solutions, the actual values of mobilities and stability ratios are sensitive and depend on the composition of the IL. Indeed, ion-specific interactions of IL cations with the like-charged surface of LDH particles were confirmed by the difference in the obtained surface charge density and CCC values, which decreased in the $BMIM^+ > BMPL^+ > BMPY^+ > BMPIP^+$ order (Table

4). Interestingly, the CCC values previously reported for colloidal particles in the presence of different monovalent inorganic coions did not show a clear correlation with the type of coion [100, 186]. Nevertheless, in a comprehensive study involving ILs, the aggregation processes were influenced by the nature of the coion [110], mainly due to the short-range attraction between the IL constituents, as suggested by direct force measurements [69].

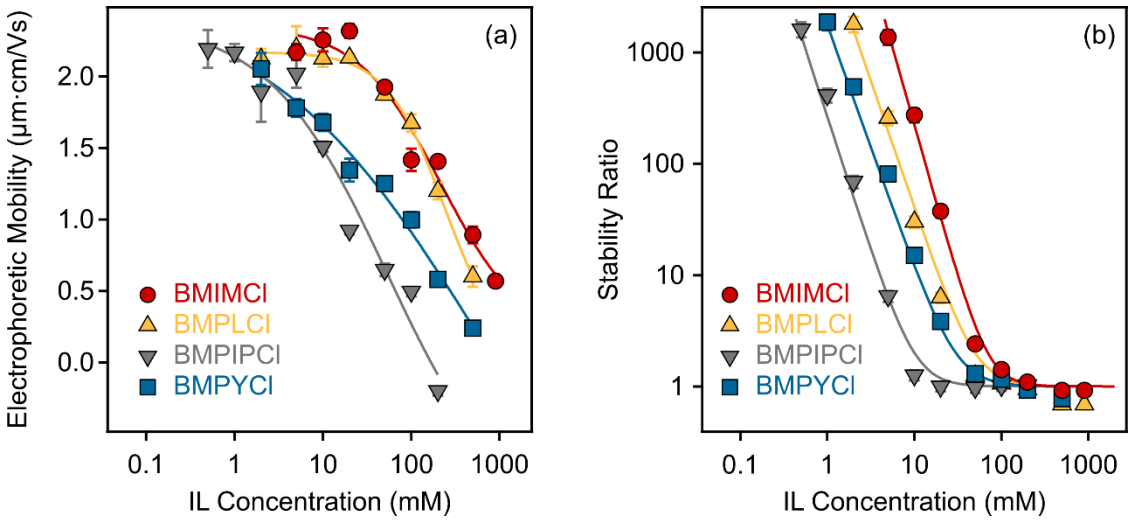

Figure 29. Electrophoretic mobility (a) and stability ratios (b) of LDH particles in the presence of ILs composed of different cations ($BMIM^+$, $BMPIP^+$, $BMPL^+$, and $BMPY^+$) and the Cl^- anion. The lines in (a) serve to guide the eyes, while in (b) they were calculated using eq 14. The measurements were performed at pH 9 and the LDH concentration was 10 mg/L [II].

The origin of the interaction forces between LDH particles in dilute IL solutions was also explored using the relationship derived from the DLVO theory, similar to the case of the latexes presented in the previous section. The experimentally determined CCCs as a function of charge densities are presented together with the fit obtained from eq 24 in Figure 30. To achieve the optimal fit to the experimental data, a Hamaker constant of 1.4×10^{-20} J was used in eq 24, which value aligns with the one obtained earlier for LDH particles [176]. The good agreement between the experimental and calculated data confirms that the predominant interparticle forces are of DLVO-type and have a similar origin regardless of the type of IL ions. However, the CCC values are governed by the change in the surface charge due to adsorbing IL constituents, whose affinity is different, leading to a variation in the strength of the stabilising electrical double layer forces.

In the aforementioned CCC sequence observed for the counterions (i.e., anions) – $Cl^- > Br^- > DCA^- > SCN^- > NO_3^-$ (Figure 31a) – the trend of the first four ions is consistent with the indirect Hofmeister series for positively charged hydrophobic particles determined in

inorganic salts [100], which was previously also established for LDH [101, 170] (see Figure 30b). Thus, the well-hydrated Cl^- ions prefer to remain in the bulk solution and lead to the highest CCC value, as they exhibit minimal adsorption on the hydrophobic LDH particles and thus retain a higher surface charge compared to the other anions studied. Conversely, the poorly hydrated SCN^- ions adhere strongly to the particle surface and result in partial charge compensation, leading to a lower surface charge and a lower CCC value.

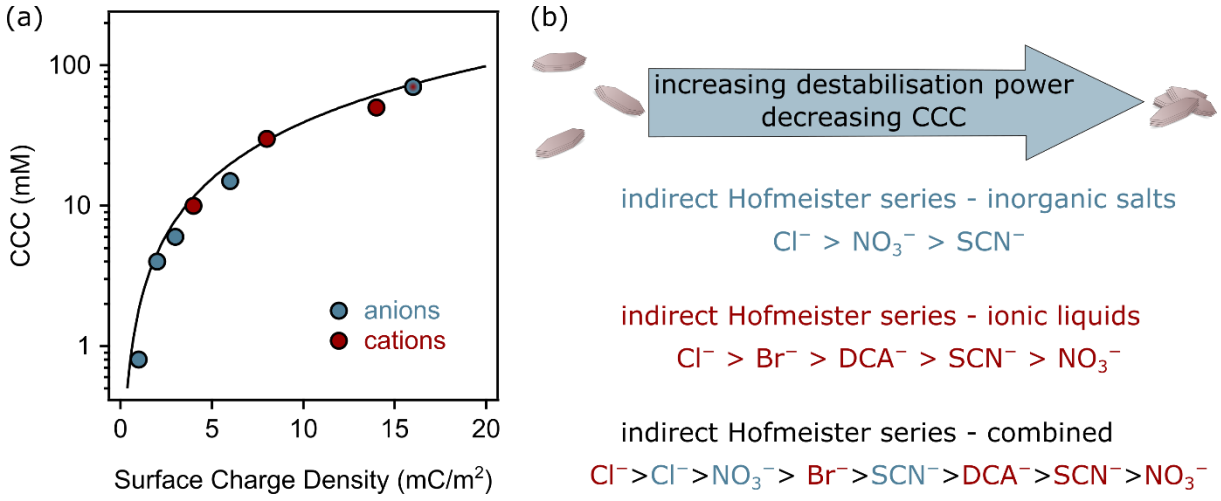

Figure 30. (a) Dependence of the CCC on the charge density at the slip plane in the presence of different IL anions (blue) and cations (red). The solid line shows the DLVO prediction, which was calculated by eq 24. (b) Schematic representation of the indirect Hofmeister series of anions that form inorganic salts (blue) and ILs (red) and the combination of these [II].

However, based on the order of the obtained parameters describing colloidal phenomena, the behaviour of NO_3^- ions is more complex. According to the indirect Hofmeister series for positively charged LDH, the CCC values in the presence of NO_3^- ions should be higher than those for the SCN^- anion, as in the case of inorganic electrolytes [170]. But on the contrary, the lowest values were obtained in its presence. Such a deviation from the conventional sequence could be attributed to the distinct counterion affinity towards the oppositely charged particles and the different degrees of ion pair formation of the IL on the surface. It is known that ions in different ILs can associate in the bulk [187, 188]. However, the IL constituents can also form ion pairs with the oppositely charged ions while adsorbed on the particle surface [110]. Accordingly, $BMIM^+$ cations can adsorb on the positively charged LDH surface, which could lead to a stronger co-adsorption of NO_3^- ions due to the associated IL molecules on the surface. This phenomenon then affects the surface charge and consequently the CCC.

Comparing the CCC data in the presence of ILs with literature values for LDH particles in the presence of dissolved inorganic salts with the same anions [101], it becomes evident that the CCCs in dilute ILs differ considerably, emphasizing the importance of the nature of cations (potassium or $BMIM^+$ coions) in the system. The combined sequence is shown in Figure 30b. Moreover, the highest CCC value in the case of $BMIM^+$ indicates the adsorption of these coions on the LDH surface, as already surmised in the discussion of the effects of IL anions in these systems. Such adsorption leads to a slightly higher surface charge density and consequently to stronger electric double layer forces and a higher CCC value.

Ion specificity was then further addressed in the case of both counterions and coion by comparing aggregation rates in the fast aggregation regime, i.e., above the CCCs. At such high IL concentrations, the viscosity of the IL solutions may differ significantly from that of pure water, which could lead to differences in the absolute aggregation rates. However, the viscosities of the investigated IL solutions were the same in the studied concentration range within the experimental error, so the apparent aggregation rates (eq 12) could be used for comparison to clarify system specificities. Accordingly, the fast aggregation rate coefficients remained almost identical regardless of the nature of the IL constituents, although the CCC depended strongly on the type of counterion (Figure 31a) and the coion (Figure 31b) present (see Table 4 for all data).

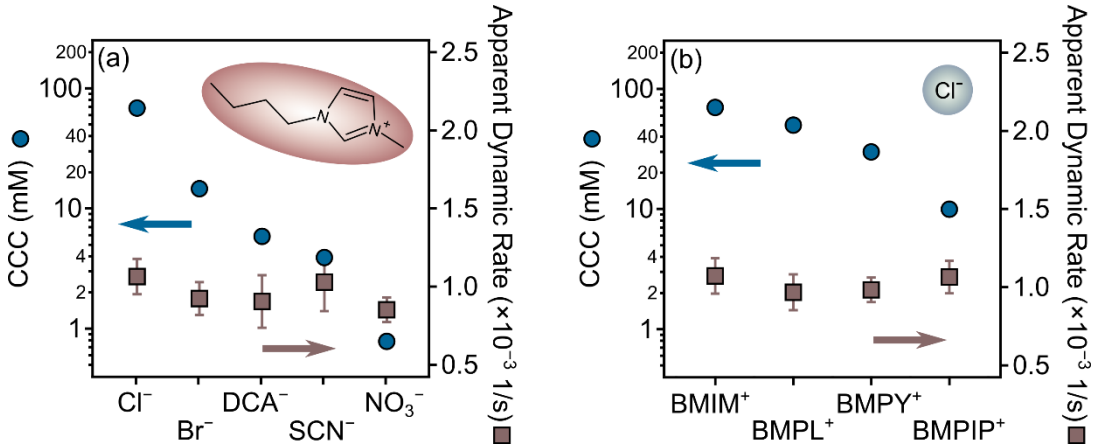

Figure 31. CCCs (circles, left axis) and apparent fast aggregation rate coefficients (squares, right axis) for LDH particles in the presence of (a) different IL anions and (b) cations. Rates were determined by averaging the aggregation rates obtained above the CCC in each system [II].

These observations suggest that the origin of the attractive forces (i.e., van der Waals and possible hydrophobic interactions) is similar regardless of the nature of the ions. This could be established because at such a high ionic strength, the electrostatic repulsion was completely

screened so that any differences in the fast aggregation rates could be attributed to forces other than the traditional DLVO interactions. Similar observations have already been reported for latex particles in the presence of various inorganic salts and ILs, when Cl^-, Br^-, $N(CN)_2^-$, and SCN^- anions were studied alongside Na^+, $BMIM^+$ and $BMPL^+$ cations [110].

The distinction between the impact of anions and cations on the CCC values is also important. The CCC values vary within two orders of magnitude for the anions (Figure 31a), being the highest for Cl^- and lowest for NO_3^-, while the changes in the cation series were moderate, decreasing by about one order of magnitude (Figure 31b). This difference can be explained by the fact that counterions tend to adsorb more strongly to surfaces, which increases the expression of ion specificity [189]. Consequently, changes in surface charge are more significant when counterions are adsorbed, leading to a broader range of CCCs due to the strong link between surface charge and aggregation properties. Similar differences were noted in surface charge density and CCC data when ionic liquid components were involved as counterions or coions in latex [110] and titanium dioxide [68] particle dispersions.

5.4. Concept of LDH delamination in IL media

Although previous studies have reported composites of ILs and LDHs [89, 142, 143, 190], no comprehensive investigations have been performed to assess the potential delamination of single-phase layered LDHs into 2D double hydroxide materials with a thickness of one or a few nanosheets. To fill in this gap, the delamination of mesoporous LDHs in ILs – namely EAN and BMIMSCN – under ambient conditions with minimal external energy input was investigated. The selected ILs have attracted considerable research attention and are predicted to offer benefits in delamination processes due to their favourable interfacial properties and moderate viscosities. In the liquid-phase delamination process, 20 mg of LDH powder was dispersed in 4 mL of solvent (water or various ILs), followed by sonication for 1 hour and subsequent mixing in a vertical rotator for 2 days.

First, XRD, SAXS, and SWAXS measurements were performed to confirm the layer formation and thus, to prove the successful synthesis of the mesoporous LDH structure. The XRD analysis of the LDH powder sample is shown as a black curve in Figure 32a and depicts the characteristic sharp diffraction peaks (003, 006, 012, 015, and 018), which are typical of LDH-based crystalline materials [145]. Using the Scherrer equation and the half-width of the (003) diffraction peak, the average crystallite size was determined to be 15.4 nm. Considering

that the basal interlayer spacing of LDH is about 0.8 nm [146], it was calculated that the LDH particles in this solid sample consist of approximately 19 layers stacked together.

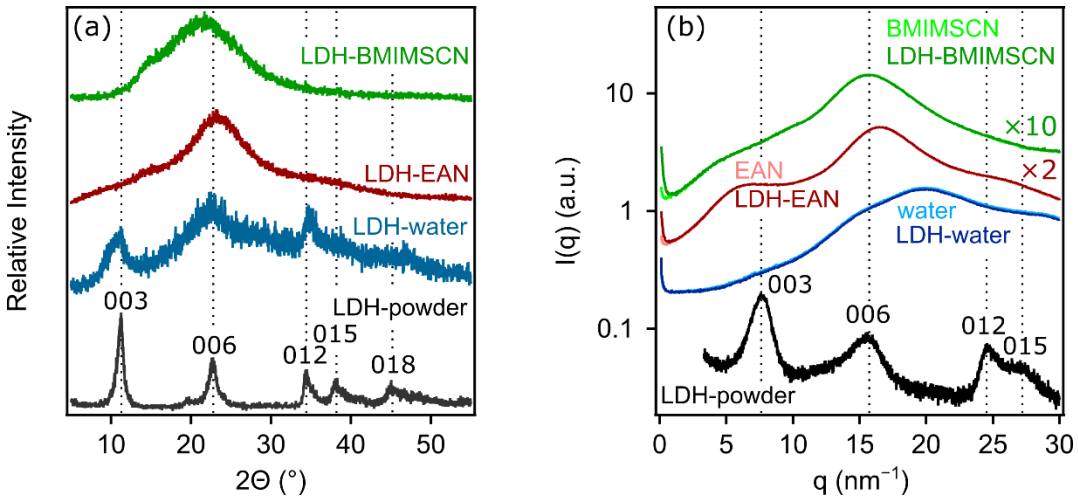

Figure 32. (a) XRD pattern of powder LDH (black), wet colloidal LDH aggregates from water-, EAN- and BMIMSCN-based suspensions. (b) Raw SWAXS curves of LDH samples in water, EAN, and BMIMSCN compared to the pure solvent curves and the SWAXS curve of the LDH powder sample in arbitrary units [IV].

Comparing the diffractogram of the powder (black curve) with the diffractogram of the aqueous LDH dispersion (blue curve) in Figure 32a, they show very similar patterns, indicating that the main crystalline phase of the LDH material remained unchanged after dispersion in water. However, the XRD patterns of the LDH dispersions in BMIMSCN and EAN (represented by green and red curves, respectively) lack distinct sharp peaks, suggesting that the LDH delamination in these samples occurred under ambient conditions with minimal external energy input. Note that the broad XRD peaks visible in Figure 32a for the dispersions (within the 2θ range of 10° to 30°) represent the background scattering contributions associated with the solvent structures [191], i.e., water, EAN, and BMIMSCN.

To confirm the presence of delaminated LDH nanosheets in the IL dispersions, SWAXS and SAXS techniques were applied. When the SWAXS results for LDH powder (black curve in Figure 32b) (with the characteristic 003, 006, 012, and 015 LDH patterns) are compared with the XRD data for the same sample (black curve in Figure 32a), it can be seen that the SWAXS peaks are slightly broader, which is due to the experimental smearing effects caused by the applied line-collimated primary beam in the SWAXS instrument (which causes some broadening of the scattering peaks) [154]. In order to elucidate the scattering contributions of the pure solvent, both the SWAXS data of the LDH dispersions and those of the corresponding

pure solvents are shown together in pairs. Figure 32b indicates that the scattering curves of the two water-based samples (light and dark blue curves) are practically identical and overlap, suggesting that no LDH particles were detected in the aqueous dispersion. At first sight, this may seem unexpected given the XRD results for the aqueous LDH dispersion (Figure 32a). However, it is important to note that the SWAXS measurements were performed on freshly prepared, low-viscosity liquid samples, in which the crystalline LDH particles can quickly settle to the bottom of the cylindrical measuring capillary. Therefore, these particles are not within the scattering volume, i.e., the main X-ray beam passing through the central part of the capillary. Conversely, the liquid samples were condensed before performing XRD measurements to obtain thick, gel-like samples. In this state, the crystalline LDH particles did not settle and remained in the main X-ray beam of the XRD instrument. The SWAXS data thus demonstrates the lack of delamination of LDH in aqueous dispersion.

In contrast, the delamination of LDH crystallites and the formation of stable LDH nanosheet dispersions were observed in both EAN and BMIMSCN. This observation was established from the fact that the pairwise scattering curves shown in Figure 32b for the two IL samples (light and dark red curves for EAN; light and dark green curves for BMIMSCN) were almost identical over the entire range of the scattering vector, except for the very low values, i.e., below 2 nm^{-1} in the SAXS region, indicating the presence of stable nanoparticles in these two dispersions. Moreover, in the SWAXS data of the IL-based LDH dispersions, no significant scattering was seen at the positions corresponding to the scattering peaks of the crystalline LDH powder sample (peaks 003, 006, 012, and 015 of the black curve), proving delamination.

In addition, the existence of the exfoliated LDH nanosheets in ILs was also evidenced by the broad scattering peaks in the SAXS data in Figure 33a after subtracting solvent scattering. To further corroborate these results, an IFT approach was used to analyse the SAXS data [155, 192]. The IFT fits are included in Figure 33a. The resulting pair distance distribution functions p(r) are shown for the IL-based delaminated LDH dispersions in Figure 33b, which provide information on the overall size of the nanoparticles. The total effective nanoparticle size – which represents the lateral dimensions of the delaminated LDH nanosheets – was found to be approximately 60 nm in both the BMIMSCN and EAN dispersions. Furthermore, the asymmetric p(r) function curves indicate the non-spherical shape of these particles, which is expected given their assumed 2D nanosheet structure.

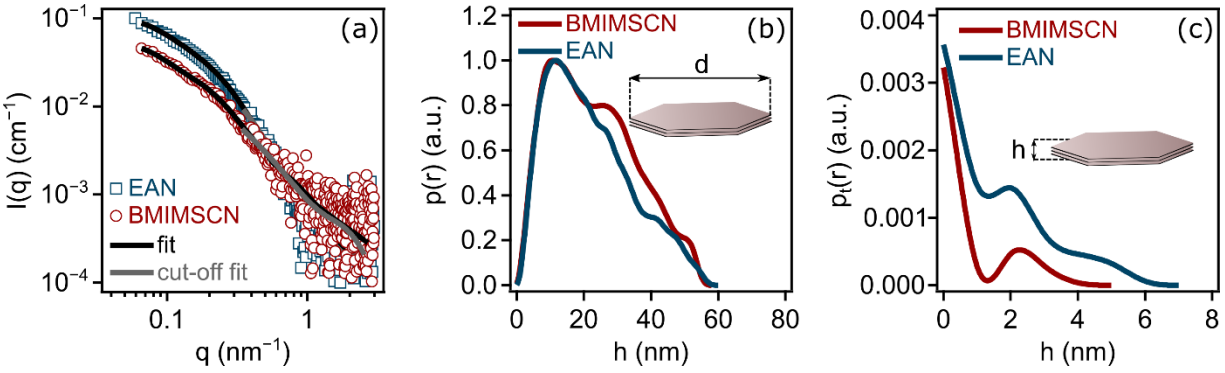

Figure 33. (a) Experimental SAXS curves (with IFT fit and cut-off IFT fit) of LDH dispersions in BMIMSCN and EAN. The background solvent scattering is subtracted. (b) Pair distance distribution function p(r) normalised to the maximum value of 1 and (c) the thickness pair distance distribution function $p_t(r)$ obtained by the IFT method from the SAXS data of the LDH dispersions in BMIMSCN and EAN [IV].

For platelet-shaped particles that are large in two dimensions, a special IFT analysis mode can be used that employs a cut-off at low values of the scattering vector to generate the $p_t(r)$ function, which provides information about the thickness of the scattering nanosheets. The $p_t(r)$ curves (depicted in Figure 33c) show a strong decrease from a thickness of 15.4 nm to about 1.5 nm, with some extended side wings reaching thicknesses of about 4 and 6 nm for BMIMSCN and EAN systems, respectively. This observation confirms the successful ultrasound-assisted delamination of LDHs in these particular IL dispersions.

The AFM technique was then used to obtain visual information about the particles and to further investigate the population of LDH nanosheets. Accordingly, large platelets – up to 300 nm in lateral dimensions – were found in the AFM images of the aqueous LDH dispersion (see Figure 34a). The corresponding height profiles indicate thicknesses of about 15–20 nm, which agrees well with the thickness of 15.4 nm determined from the XRD data of the crystalline powder sample (Figure 32a). This provides further evidence that there was no delamination of the LDH crystallites in the aqueous dispersion. However, the AFM results, i.e., the height/distance profiles obtained in EAN (Figure 34b) and BMIMSCN (Figure 34c), show that the lateral dimension and thickness of the LDH nanosheets in the IL-based dispersions were significantly smaller compared to the crystalline platelets observed in water.

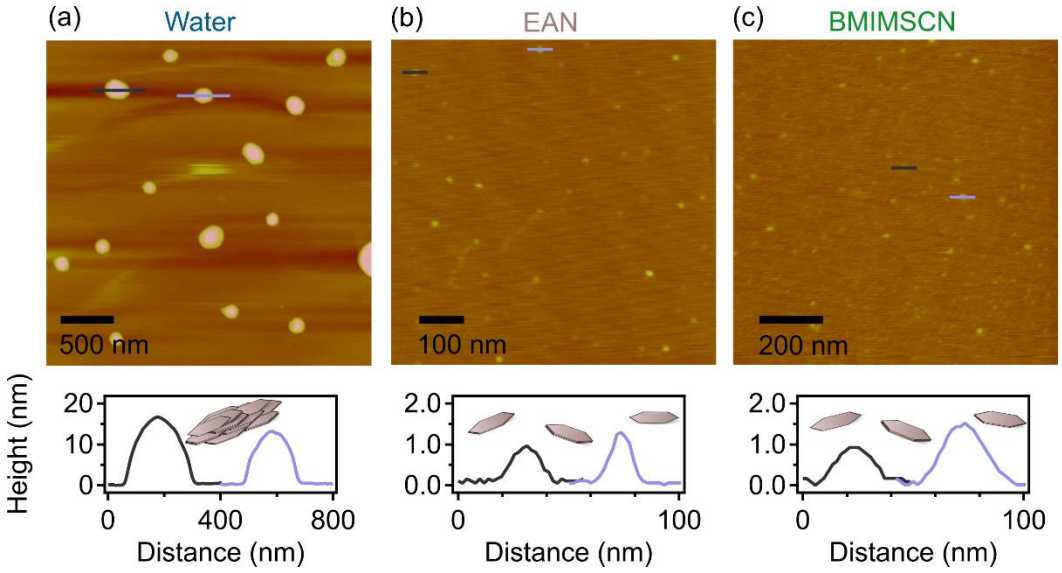

Figure 34. AFM images of LDHs along with the associated height profiles (corresponding to the labelled particles) derived from (a) water, (b) EAN, and (c) BMIMSCN dispersions [IV].

The distribution histograms – based on several AFM images – demonstrate that the average lateral size of LDH platelets decreased from 187 ± 50 nm in water (Figure 35a) to 32 ± 8 nm in EAN (Figure 35b) and 39 ± 8 nm in BMIMSCN (Figure 35c), while the thickness of the particles decreased from 12 ± 6 nm in water (Figure 35d) to 2 ± 1 nm and 1.7 ± 0.8 nm for EAN (Figure 35e) and BMIMSCN (Figure 35f), respectively. The nanosheets after sonication-assisted delamination in ILs have lateral dimensions of up to 60 nm and consist of up to 6 or 7 layers. Note that the majority consists of 2 or 3 layers, as shown in Figure 35h and Figure 35i. These results are in good agreement with the SAXS data described above. Based on the results, it can be concluded that either the LDH crystallites remain unchanged or that the large crystalline lamellar aggregates form when the LDH powder is dispersed in water. Besides, simultaneous disaggregation and delamination of the LDH particles occurred in the ILs after dispersion, which was accelerated by mild sonication.

Note that similar partial delamination and cleavage of aggregates were previously reported for LDH in an organic solvent [193]. In addition, similar results were reported for IL-assisted delamination of graphene [9, 127]. This phenomenon can be explained by the reduced attraction between the LDH layers, as IL constituents tend to arrange on charged surfaces in an ordered form consisting of cation and anion layers. Such an interfacial arrangement leads to the emergence of repulsive oscillatory forces that overcome the attractive van der Waals and electrostatic interactions between the LDH layers. This repulsion triggers delamination and

disaggregation, leading to the formation of well-dispersed LDH nanosheets. Importantly, the dispersions obtained in ILs were stable for at least 6 months, indicating a good stabilising effect of ILs for LDH nanosheets through interfacial structuration. This emphasizes the ability of ILs to influence surface interactions at the LDH-IL interface, thus preventing aggregation and ensuring long-term dispersion stability.

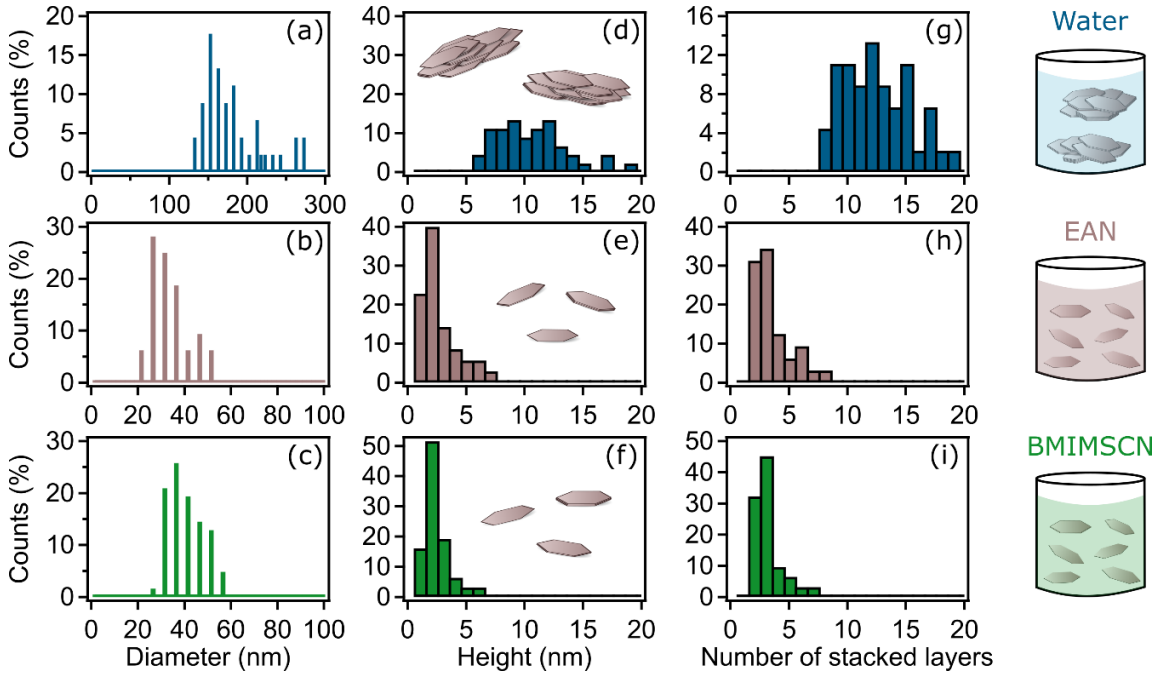

Figure 35. Distribution histograms of the diameter (a–c), thickness (d–f) and the stacked LDH layers (g–i) after sonication-assisted delamination of LDH in water (a, d, g), EAN (b, e, h) and BMIMSCN (c, f, i) [IV].

These findings prove the concept of delamination of LDH by ILs under ambient conditions, which is an excellent way to prepare 2D double hydroxide nanosheet dispersions in one step using a non-volatile solvent.

6. Summary

Ionic liquids, characterised by their ionic composition and liquid state below 100 °C, offer versatile solvents with advantageous properties, making them key in various applications. In particular, ILs play a crucial role in particle dispersions, either as the primary medium or as an additive. To optimise these applications, it is essential to understand the mechanisms that determine the stability of particle dispersions in ILs. Therefore, the overall aim was to investigate the fundamental stabilisation mechanisms and interactions of IL-containing dispersions, focusing in particular on the charge and aggregation relationships of the different particles.

First, time-resolved light scattering measurements in aqueous EAN solutions containing dissociated and hydrated IL ions have shown that the aggregation of both bare SL and polymer-coated SL-IP-2 particles is primarily driven by electrostatic forces. This electrostatic stabilisation regime shows an increased aggregation rate with IL content and reaches a plateau, analogous to the inorganic salts. By further increasing the IL concentration, the diffusion of the particles is limited by the increased viscosity of the medium, which leads to a slight increase in stability (viscous stabilisation). Remarkably, in pure EAN – with minimal water content – the particles exhibited high stability, contradicting theories that predict rapid aggregation at elevated ion concentrations. The absence of particle motion in neat EAN when applying an electric field during electrophoretic light scattering measurements, challenged the notion of electrostatic stabilisation observed in dilute IL solutions. Instead, the stability of these dispersions is attributed to repulsive oscillatory forces arising from the layer-by-layer assembly of the IL constituents on the particle surfaces (solvation stabilisation). These findings provide valuable insights into the origin of primary interparticle forces that determine the colloidal stability in both pure ILs and their aqueous solutions.

Secondly, the effect of the addition of sodium nitrate on the aggregation processes in SL/EAN dispersions was systematically investigated over a wide range of IL concentrations. In this way, the influence of sodium ions on the interfacial self-assembly was explored, since nitrate ions were naturally present in the IL studied. For negatively charged SL particles where sodium served as a counterion, the introduction of sodium nitrate led to a stabilisation of the dispersion in the intermediate IL concentration range, which is attributed to the accumulation of sodium ions at the interface. This stabilising effect was evidenced by significantly reduced aggregation

rates compared to systems containing only EAN, with the extent of stabilisation increasing proportionally with the amount of salt added. In contrast, the expected salt-dependent stabilisation pattern was not observed for the SL-IP-2 particles, where the sodium ions had the same sign of charge as the particle surface. The effect of the added ions is therefore mainly determined by their charge, size, affinity to the surface, and the surface characteristics of the tested particles.

Thereafter, the ion-specific effect of IL constituents on the colloidal stability of polymeric particles was investigated in aqueous IL dispersions featuring various anions and the $BMIM^+$ cation. The electrophoretic mobility and stability ratio values of positively charged AL particles were strongly influenced by the type of anion present, i.e., the CCC and surface charge density values followed the $Cl^- > Br^- > NO_3^- > Ac^-$ order. The observed trend is consistent with the reversed Hofmeister series of anions for positively charged hydrophobic surfaces. Ion-specific adsorption led to a reduction in surface charge density, resulting in lower CCC values, which was particularly pronounced for strongly adsorbing anions such as acetate. Overall, ion specificity played a crucial role in the adsorption process, while the aggregation mechanism together with the primary interparticle forces was consistent with the DLVO theory.

However, the effects of the ion-specific interactions could be mitigated by modifying the negatively charged surface of the latex particles with the positively charged IP-2 polymer. This modification “turned” the IL anions into indifferent salt components, which resulted in the electrophoretic mobility and stability ratio values of SL-IP-2 particles being the same in the presence of different ILs, i.e., the CCC values obtained were the same regardless of the type of anion being present. This unexpected behaviour suggests that coating a surface with a polyimidazolium compound can effectively mask the specific ion effects at the interface. These findings point to new ways of producing processable particle dispersions in ionic environments, regardless of their composition.

Given that ILs have shown considerable potential as a substitute for conventional organic solvents in exfoliation processes of layered materials, the interactions between IL components and LDH were investigated in both aqueous and pure IL environments. First, the ion-specific effect in IL-containing aqueous dispersions was investigated by systematically varying the IL anions and cations. The study showed a strong dependence of LDH particle stability, i.e., CCC values, on the chemical composition of both the counterions

(Cl^- > Br^- > DCA^- > SCN^- > NO_3^-) and the coions ($BMIM^+$ > $BMPIP^+$ > $BMPL^+$ > $BMPY^+$). Since the experimental aggregation kinetics were in good agreement with the predicted data, the origin of the interparticle forces was classified as electrostatic, in line with the classical DLVO theory. However, the distinct adsorption affinities of the IL constituents led to different modifications of the surface charge, which contributed to the observed differences in CCC values. A notable aspect was the comparison of CCCs measured in the presence of IL and inorganic salt-forming anions. The presence of $BMIM^+$ or K^+ cations in the system resulted in significant differences in the CCCs for chloride, nitrate, and thiocyanate anions. Particularly striking was the case of nitrate ions, where the CCC measured in BMIM-nitrate solutions was the lowest, contrary to expectations based on the indirect Hofmeister series. This discrepancy is attributed to the different degrees of IL ion pair formation, which is more pronounced in the BMIM-thiocyanate system, leading to lower concentrations of dissociated and adsorptive thiocyanate ions and consequently to higher CCC values. These results emphasise the complex interplay between IL composition, ion interactions, and colloidal stability in LDH particle dispersions.

Subsequently, the concept of LDH delamination using ILs under ambient conditions was supposed to be validated. For this purpose, two ILs were selected as delamination media based on the available information and the observed affinity of the IL constituents to the LDH surface. Successful delamination, i.e., the conversion of lamellar LDH into 2D double hydroxide nanosheets, in EAN and BMIMSCN was confirmed by the disappearance of characteristic diffraction peaks when LDH crystallites were dispersed in ILs. This transformation was further supported by SWAXS and SAXS results as well as by an evaluation of the height profiles of the nanoparticles using AFM. The results showed a reduction in both the thickness and lateral size of the dispersed particles in IL-based samples, indicating not only delamination but also cleavage of the LDH materials. These results confirm the feasibility of delaminating layered materials with ILs at room temperature and provide an efficient approach to prepare 2D double hydroxide nanosheet dispersions in a single step using “green” (non-volatile) solvents.

7. Összefoglalás

Az ionos folyadékok olyan, 100 °C alatti hőmérsékleten folyékony halmazállapotú anyagok, amelyek a hagyományos oldószerektől eltérően teljes egészükben ionokból állnak. Ebből adódóan rendkívül sajátos fizikai-kémiai tulajdonságokkal rendelkeznek, ami érdekessé teszik őket a számos alkalmazás szempontjából. A technológiák optimalizálásához elengedhetetlen a kolloidstabilitást befolyásoló tényezők megértése IL-ek jelenlétében. Általános célunk ezért az IL-tartalmú diszperziókban megfigyelhető alapvető stabilizációs mechanizmusok és kölcsönhatások feltárása volt különböző részecskék töltés és aggregációs viszonyainak nyomon követése által.

Időfüggő fényszórás mérések alapján híg vizes EAN közeg esetén, ahol a komponens ionok disszociált és hidratált formában vannak jelen, mind SL, mind a polimerrel bevont SL-IP-2 részecskék aggregációját elsősorban elektrosztatikus kölcsönhatások irányítják. Ebben a tartományban az aggregáció sebessége meredeken nőtt az IL tartalom növelésével egy adott határértékig, mely tendencia a szervetlen sókra is jellemző. Tovább növelve az EAN koncentrációt, a részecskék diffúziós sebességét limitálja a közeg megnövekedett viszkozitása, ami a stabilitás enyhe növekedésében nyilvánul meg (viszkózus stabilizáció). Majd tömény EAN közegben – amikor a víz csak kis mennyiségben van jelen – nagy stabilitású diszperziókat figyeltünk meg, ami ellentmond a magas iontartalom esetén gyors aggregációt jósló kolloidstabilitást leíró elméletnek. Tiszta EAN-ban nem lehetett kimutatni a részecskék elektroforetikus fényszórás mérések során alkalmazott elektromos tér hatására történő elmozdulását. Ez alapján az IL-ekben diszpergált részecskék töltését teljes mértékben árnyékolják az adszorbeálódó ionok, vagyis a tömény IL-ekben megfigyelt stabilizáció az IL komponensek határfelületi rétegeződése következtében kialakuló oszcillációs taszítóerők által értelmezhető (szolvatációs stabilizáció). Ezen eredmények rávilágítanak a részecskék kolloidstabilitásáért felelős fő kölcsönhatások eredetére mind tiszta IL-ekben, mind pedig azok vizes oldataiban.

Ezt követően az előzőekben tárgyalt széles EAN koncentrációtartományban vizsgáltuk a nátrium-nitrát hozzáadásának hatását a latex diszperziók kolloidstabilitására nézve. Mivel a nitrátionok már eleve jelen voltak a rendszerben az EAN komponenseként, nyomon követhetővé vált a nátriumionok határfelületi rendeződésre gyakorolt hatása. Negatív töltésű SL részecskék esetén jelentős stabilizáció volt megfigyelhető a köztes EAN koncentrációtartományban a só

hozzáadásának következtében, amit az aggregációs állandók jelentős csökkenése jelzett A nátriumionok határfelületen történő feldúsulásának eredményeképpen a stabilizáló hatás a hozzáadott só mennyiségének növelésével kifejezettebbé vált. Ezzel szemben, a pozitív töltésű SL-IP-2 részecskék esetén a meghatározott aggregációs állandók kísérleti hibán belül megegyeztek a hozzáadott só koncentrációjától függetlenül, vagyis a só jelenléte nem befolyásolta a kolloidstabilitást. A hozzáadott ionok hatását bizonyíthatóan azok töltése, mérete, felülethez való affinitása, illetve a vizsgált részecske felületének tulajdonságai határozzák meg elsősorban.

Ezután különböző anionokat és $BMIM^+$ kationokat tartalmazó vizes IL oldatok jelenlétében vizsgálva a polimer alapú latex részecskék kolloidstabilitását bebizonyosodott, hogy a pozitív töltésű AL részecskék elektroforetikus mobilitás és stabilitási arány értékei érzékenyek a jelenlévő anionok anyagi minőségére. Az ionspecifikus adszorpció a felületi töltéssűrűség eltérő mértékű módosításához vezet, ezáltal a CCC értékek a $Cl^- > Br^- > NO_3^- > Ac^-$ sorrendet követték. Az anionok ezen sorrendje megfelel a fordított Hofmeister-sorozatnak, amelyben az egyes ionok a pozitív töltésű hidrofób felületekhez való affinitásuk alapján foglalják el a helyüket. Amíg az eltérő destabilizáló hatásért az ionspecifikus adszorpció a felelős, addig a részecskeaggregáció mechanizmusa a DLVO-elméletbe foglalt vonzó- és taszító erőket feltételezve jól leírható.

Ezzel szemben az ionspecifikus kölcsönhatások elfedhetőnek bizonyultak a negatív töltésű SL részecske pozitív töltésű IP-2 polimerrel történő felületmódosítása révén. Ennek következtében a különböző anionok azonos mértékben befolyásolták a kolloidstabilitást, azaz az SL-IP-2 részecskék CCC értékei azonosak voltak különböző IL-ek jelenlétében, azok anyagi minőségétől függetlenül. Az eredmények alapján lehetőség van az ionspecifikus hatások elfedésére poliimidazóliummal történő funkcionalizálással, ami új lehetőségeket kínál részecskediszperziók ionos környezetben történő előállítására, függetlenül azok összetételétől.

Tekintettel arra, hogy az IL-ek potenciális oldószer, illetve adalékanyagjelöltek a réteges szerkezetű anyagok delaminálásra a szerves oldószerekkel szemben, vizsgáltuk az IL komponensek és az LDH részecskék közötti kölcsönhatásokat mind vizes, mind tiszta IL közegben. Először az IL-ek összetételét szisztematikusan változtatva vizsgáltuk az ionspecifikus hatást vizes IL közegű LDH diszperziókban. A kolloidstabilitás, és ezáltal a CCC értékek erős függést mutattak mind az ellenionok ($Cl^- > Br^- > DCA^- > SCN^- > NO_3^-$), mind

pedig a mellékionok ($BMIM^+ > BMPIP^+ > BMPL^+ > BMPY^+$) kémiai minőségétől. A mért és a DLVO elmélettel számolt adatok egyezése alapján megállapítható, hogy az aggregáció DLVO erők által vezérelt, viszont az ionok specifikus adszorpciója különböző mértékben módosítja a részecske felületi töltéssűrűségét, ami döntően befolyásolja az elektrosztatikus eredetű részecske-részecske kölcsönhatások erősségét és így a CCC értékeket. További értékes információt szolgáltatott az IL és a szervetlensó alkotó anionok jelenlétében mért CCC-k összehasonlítása. Attól függően, hogy milyen kation volt jelen a rendszerben mellékionként (BMIM+ vagy K+), a Cl^-, NO_3^- és SCN^- anionok esetében meghatározott CCC értékek jelentősen eltértek. Ez a nitrátionok esetén volt a legszembetűnőbb, ugyanis a $BMIMNO_3$ jelenlétében mért CCC volt legkisebb, holott a közvetett Hofmeister sorozat alapján ezt a BMIMSCN rendszer esetében várnánk. A jelenség mögött az eltérő mértékű IL ionpár képződése áll, amely a BMIMSCN rendszerben fokozottabban következik be, ezáltal pedig csökken a disszociált és adszorpcióra képes tiocianátionok koncentrációja, ami magasabb CCC értéket eredményez. Ezen megfigyelések hangsúlyozzák az IL összetétel, az ionok közötti kölcsönhatások és a kolloidstabilitás összetett kapcsolatát LDH-tartalmú diszperziókban.

Végül igazoltuk, hogy az LDH részecskék IL közegben történő delaminációja mérsékelt körülmények között egyetlen lépésben megvalósítható. Két IL-t választottunk delaminációs közegként a rendelkezésre álló információk és az IL-összetevők LDH felületéhez való affinitása alapján. A réteges szerkezet IL-ekben (EAN és BMIMSCN) történő megbontását az LDH – és annak vizes diszperziója – esetén megfigyelhető diffrakciós csúcsok eltűnése igazolta. A folyamat hatására mind a részecskék vastagsága, mind pedig átmérője jelentősen csökkent, amely az IL-ekben bekövetkező delamináció mellett a részecskék hasadását is jelzi, amit SAXS és SWAXS mérések is igazoltak. Ezen eredmények alátámasztják a réteges anyagok IL-ekben történő delaminálásának megvalósíthatóságát szobahőmérsékleten, és hatékony alternatívát kínálnak 2D kettős hidroxid nanolapok egy lépésben történő előállítására, "zöld" (nem illékony) oldószerekben.

8. References

[1] R.D. Rogers, K.R. Seddon: *Ionic liquids - Solvents of the future?*, Science, 302 (2003) 792-793.

[2] N.V. Plechkova, K.R. Seddon: *Applications of ionic liquids in the chemical industry*, Chem. Soc. Rev., 37 (2008) 123-150.

[3] Z.Q. He, P. Alexandridis: *Ionic liquid and nanoparticle hybrid systems: Emerging applications*, Adv. Colloid Interface Sci., 244 (2017) 54-70.

[4] S. Livi, J. Duchet-Rumeau, T.-N. Pham, J.-F. Gérard: *A comparative study on different ionic liquids used as surfactants: Effect on thermal and mechanical properties of high-density polyethylene nanocomposites*, J. Colloid Interface Sci., 349 (2010) 424-433.

[5] W.G. Lee, S.W. Kang: *Highly selective poly(ethylene oxide)/ionic liquid electrolyte membranes containing CrO_3 for CO_2/N_2 separation*, Chem. Eng. J., 356 (2019) 312-317.

[6] K. Ueno, M. Watanabe: *From colloidal stability in ionic liquids to advanced soft materials using unique media*, Langmuir, 27 (2011) 9105-9115.

[7] S.H. Behrens, M. Borkovec, P. Schurtenberger: *Aggregation in charge-stabilized colloidal suspensions revisited*, Langmuir, 14 (1998) 1951-1954.

[8] R. Hayes, G.G. Warr, R. Atkin: *Structure and nanostructure in ionic liquids*, Chem. Rev., 115 (2015) 6357-6426.

[9] A. Elbourne, B. McLean, K. Voitchovsky, G.G. Warr, R. Atkin: *Molecular resolution in situ imaging of spontaneous graphene exfoliation*, J. Phys. Chem. Lett., 7 (2016) 3118-3122.

[10] Z.P. Zheng, W.H. Fan, S. Roy, K. Mazur, A. Nazet, R. Buchner, M. Bonn, J. Hunger: *Ionic liquids: Not only structurally but also dynamically heterogeneous*, Angew. Chem. Int. Ed., 54 (2015) 687-690.

[11] M.J. Earle, J. Esperanca, M.A. Gilea, J.N.C. Lopes, L.P.N. Rebelo, J.W. Magee, K.R. Seddon, J.A. Widegren: *The distillation and volatility of ionic liquids*, Nature, 439 (2006) 831-834.

[12] P.T.P. Thi, C.W. Cho, Y.S. Yun: *Environmental fate and toxicity of ionic liquids: A review*, Water Res., 44 (2010) 352-372.

[13] T. Welton: *Room-temperature ionic liquids. Solvents for synthesis and catalysis*, Chem. Rev., 99 (1999) 2071-2083.

[14] H. Tokuda, S. Tsuzuki, M. Susan, K. Hayamizu, M. Watanabe: *How ionic are room-temperature ionic liquids? An indicator of the physicochemical properties*, J. Phys. Chem. B, 110 (2006) 19593-19600.

[15] M.S. Shannon, J.E. Bara: *Properties of alkylimidazoles as solvents for CO_2 capture and comparisons to imidazolium-based ionic liquids*, Ind. Eng. Chem. Res., 50 (2011) 8665-8677.

[16] K. Ueno, H. Tokuda, M. Watanabe: *Ionicity in ionic liquids: correlation with ionic structure and physicochemical properties*, Phys. Chem. Chem. Phys., 12 (2010) 1649-1658.

[17] K. Dong, S.J. Zhang, D.X. Wang, X.Q. Yao: *Hydrogen bonds in imidazolium ionic liquids*, J. Phys. Chem. A, 110 (2006) 9775-9782.

[18] Y.C. Pei, Y.X. Zhang, J. Ma, M.H. Fan, S.J. Zhang, J.J. Wang: *Ionic liquids for advanced materials*, Mater. Today Nano, 17 (2022) 23.

[19] G. Kaur, H. Kumar, M. Singla: *Diverse applications of ionic liquids: A comprehensive review*, J. Mol. Liq., 351 (2022) 19.
[20] M.V. Fedorov, A.A. Kornyshev: *Ionic liquids at electrified interfaces*, Chem. Rev., 114 (2014) 2978-3036.
[21] J. Luczak, M. Paszkiewicz, A. Krukowska, A. Malankowska, A. Zaleska-Medynska: *Ionic liquids for nano- and microstructures preparation. Part 1: Properties and multifunctional role*, Adv. Colloid Interface Sci., 230 (2016) 13-28.
[22] S. Sakthivel, R.L. Gardas, J.S. Sangwai: *Effect of alkyl ammonium ionic liquids on the interfacial tension of the crude oil-water system and their use for the enhanced oil recovery using ionic liquid-polymer flooding*, Energy Fuels, 30 (2016) 2514-2523.
[23] V. Vickackaite, A. Padarauskas: *Ionic liquids in microextraction techniques*, Cent. Eur. J. Chem, 10 (2012) 652-674.
[24] Z.H. Mou, B.G. Wang, H.S. Lu, S.S. Dai, Z.Y. Huang: *Synthesis of poly(ionic liquid)s brush-grafted carbon dots for high-performance lubricant additives of polyethylene glycol*, Carbon, 154 (2019) 301-312.
[25] S. Livi, J. Duchet-Rumeau, T.N. Pham, J.-F. Gérard: *Synthesis and physical properties of new surfactants based on ionic liquids: Improvement of thermal stability and mechanical behaviour of high density polyethylene nanocomposites*, J. Colloid Interface Sci., 354 (2011) 555-562.
[26] L.L. Yang, D.C. Kong, X.Y. Chang, G.C. Jiang, T. Ao, C.L. Xie, A.D.K. Moukoko, J.Y. Ma: *Counterion-specific shale hydration inhibiting performance of vinylimdazolium ionic liquids*, J. Mol. Liq., 335 (2021) 116544.
[27] Y.J. Yang, S.M. Yaakob, N.E. Rabat, M.R. Shamsuddin, Z. Man: *Release kinetics study and anti-corrosion behaviour of a pH-responsive ionic liquid-loaded halloysite nanotube-doped epoxy coating*, RSC Adv., 10 (2020) 13174-13184.
[28] D.S. Silvester, R. Jamil, S. Doblinger, Y.X. Zhang, R. Atkin, H. Li: *Electrical double layer structure in ionic liquids and its importance for supercapacitor, battery, sensing, and lubrication applications*, J. Phys. Chem. C, 125 (2021) 13707-13720.
[29] Z.J. Huang, J.G. Uranga, S.L. Zhou, H.Y. Jia, Z.F. Fei, Y.F. Wang, F.D. Bobbink, Q.H. Lu, P.J. Dyson: *Ionic liquid containing electron-rich, porous polyphosphazene nanoreactors catalyze the transformation of CO2 to carbonates*, J. Mater. Chem. A, 6 (2018) 20916-20925.
[30] S. He, Z. An, M. Wei, D.G. Evans, X. Duan: *Layered double hydroxide-based catalysts: nanostructure design and catalytic performance*, Chem. Commun., 49 (2013) 5912-5920.
[31] J.D. Scholten, B.C. Leal, J. Dupont: *Transition metal nanoparticle catalysis in ionic liquids*, ACS Catal., 2 (2012) 184-200.
[32] B. Derjaguin, L.D. Landau: *Theory of the stability of strongly charged lyophobic sols and of the adhesion of strongly charged particles in solutions of electrolytes*, Acta Phys. Chim., 14 (1941) 633-662.
[33] E.J.W. Verwey, J.T.G. Overbeek: *Theory of stability of lyophobic colloids*, Elsevier, Amsterdam, 1948.
[34] J. Israelachvili: *Intermolecular and surface forces*, 3 ed., Academic Press, London, 2011.
[35] A.V. Delgado, F. Gonzalez-Caballero, R.J. Hunter, L.K. Koopal, J. Lyklema: *Measurement and interpretation of electrokinetic phenomena*, J. Colloid Interface Sci., 309 (2007) 194-224.

[36] I.H. Harding, T.W. Healy: *Electrical double-layer properties of amphoteric polymer latex colloids*, J. Colloid Interface Sci., 107 (1985) 382-397.
[37] D.F. Evans, H. Wennerstrom: *The colloidal domain*, John Wiley, New York, 1999.
[38] S.H. Behrens, D.I. Christl, R. Emmerzael, P. Schurtenberger, M. Borkovec: *Charging and aggregation properties of carboxyl latex particles: Experiments versus DLVO theory*, Langmuir, 16 (2000) 2566-2575.
[39] G. Trefalt, I. Szilagyi, G. Tellez, M. Borkovec: *Colloidal stability in asymmetric electrolytes: Modifications of the Schulze-Hardy rule*, Langmuir, 33 (2017) 1695-1704.
[40] B. Derjaguin: *On the repulsive forces between charged colloid particles and on the theory of slow coagulation and stability of lyophobe sols*, Trans. Faraday Soc., 35 (1940) 0203-0214.
[41] F.J.M. Ruiz-Cabello, G. Trefalt, T. Oncsik, I. Szilagyi, P. Maroni, M. Borkovec: *Interaction forces and aggregation rates of colloidal latex particles in the presence of monovalent counterions*, J. Phys. Chem. B, 119 (2015) 8184-8193.
[42] M.M. Gudarzi, G. Trefalt, I. Szilagyi, P. Maroni, M. Borkovec: *Forces between negatively charged interfaces in the presence of cationic multivalent oligoamines measured with the atomic force microscope*, J. Phys. Chem. C, 119 (2015) 15482-15490.
[43] A. Zaccone, H. Wu, M. Lattuada, M. Morbidelli: *Correlation between colloidal stability and surfactant adsorption/association phenomena studied by light scattering*, J. Phys. Chem. B, 112 (2008) 1976-1986.
[44] G. Fritz, V. Schadler, N. Willenbacher, N.J. Wagner: *Electrosteric stabilization of colloidal dispersions*, Langmuir, 18 (2002) 6381-6390.
[45] E. Vanecht, K. Binnemans, S. Patskovsky, M. Meunier, J.W. Seo, L. Stappers, J. Fransaer: *Stability of sputter-deposited gold nanoparticles in imidazolium ionic liquids*, Phys. Chem. Chem. Phys., 14 (2012) 5662-5671.
[46] J.A. Smith, O. Werzer, G.B. Webber, G.G. Warr, R. Atkin: *Surprising particle stability and rapid sedimentation rates in an ionic liquid*, J. Phys. Chem. Lett., 1 (2010) 64-68.
[47] T. Singh, A. Kumar: *Static Dielectric Constant of Room Temperature Ionic Liquids: Internal Pressure and Cohesive Energy Density Approach*, J. Phys. Chem. B, 112 (2008) 12968-12972.
[48] M.A. Gebbie, M. Valtiner, X. Banquy, E.T. Fox, W.A. Henderson, J.N. Israelachvili: *Ionic liquids behave as dilute electrolyte solutions*, Proc. Natl. Acad. Sci. U. S. A., 110 (2013) 9674-9679.
[49] K. Ueno, A. Inaba, M. Kondoh, M. Watanabe: *Colloidal stability of bare and polymer-grafted silica nanoparticles in ionic liquids*, Langmuir, 24 (2008) 5253-5259.
[50] M. Mamusa, J. Siriex-Plenet, F. Cousin, E. Dubois, V. Peyrea: *Tuning the colloidal stability in ionic liquids by controlling the nanoparticles/liquid interface*, Soft Matter, 10 (2014) 1097-1101.
[51] J.C. Riedl, M.A.A. Kazemi, F. Cousin, E. Dubois, S. Fantini, S. Lois, R. Perzynski, V. Peyre: *Colloidal dispersions of oxide nanoparticles in ionic liquids: elucidating the key parameters*, Nanoscale Adv., 2 (2020) 1560-1572.
[52] R. Bhandary, J.G. Alauzun, P. Hesemann, A. Stocco, M. In, P.H. Mutin: *Phase transfer of TiO_2 nanoparticles from water to ionic liquid triggered by phosphonic acid grafting*, Soft Matter, 13 (2017) 8023-8026.
[53] G.K. Dedzo, C. Detellier: *Clay minerals-ionic liquids, nanoarchitectures, and applications*, Adv. Funct. Mater., 28 (2018) 1703845.

[54] D. Brondani, C.W. Scheeren, J. Dupont, I.C. Vieira: *Halloysite clay nanotubes and platinum nanoparticles dispersed in ionic liquid applied in the development of a catecholamine biosensor*, Analyst, 137 (2012) 3732-3739.

[55] P. Migowski, J. Dupont: *Catalytic applications of metal nanoparticles in imidazolium ionic liquids*, Chem.-Eur. J., 13 (2007) 32-39.

[56] M. Antonietti, D.B. Kuang, B. Smarsly, Z. Yong: *Ionic liquids for the convenient synthesis of functional nanoparticles and other inorganic nanostructures*, Angew. Chem. Int. Ed., 43 (2004) 4988-4992.

[57] M. Ramalakshmi, P. Shakkthivel, M. Sundrarajan, S.M. Chen: *Novel method of room temperature ionic liquid assisted Fe3O4 nanocubes and nanoflakes synthesis*, Mater. Res. Bull., 48 (2013) 2758-2765.

[58] H. Zhang, K. Dasbiswas, N.B. Ludwig, G. Han, B. Lee, S. Vaikuntanathan, D.V. Talapin: *Stable colloids in molten inorganic salts*, Nature, 542 (2017) 328-331.

[59] I. Szilagyi, T. Szabo, A. Desert, G. Trefalt, T. Oncsik, M. Borkovec: *Particle aggregation mechanisms in ionic liquids*, Phys. Chem. Chem. Phys., 16 (2014) 9515-9524.

[60] Z.Q. He, P. Alexandridis: *Nanoparticles in ionic liquids: interactions and organization*, Phys. Chem. Chem. Phys., 17 (2015) 18238-18261.

[61] R. Atkin, G.G. Warr: *Structure in confined room-temperature ionic liquids*, J. Phys. Chem. C, 111 (2007) 5162-5168.

[62] M.A. Gebbie, H.A. Dobbs, M. Valtiner, J.N. Israelachvili: *Long-range electrostatic screening in ionic liquids*, Proc. Natl. Acad. Sci. U. S. A., 112 (2015) 7432-7437.

[63] A.M. Smith, A.A. Lee, S. Perkin: *The electrostatic screening length in concentrated electrolytes increases with concentration*, J. Phys. Chem. Lett., 7 (2016) 2157-2163.

[64] M.A. Gebbie, A.M. Smith, H.A. Dobbs, A.A. Lee, G.G. Warr, X. Banquy, M. Valtiner, M.W. Rutland, J.N. Israelachvili, S. Perkin, R. Atkin: *Long range electrostatic forces in ionic liquids*, Chem. Commun., 53 (2017) 1214-1224.

[65] A. Elbourne, K. Voitchovsky, G.G. Warr, R. Atkin: *Ion structure controls ionic liquid near-surface and interfacial nanostructure*, Chem. Sci., 6 (2015) 527-536.

[66] M. Radiom: *Ionic liquid-solid interface and applications in lubrication and energy storage*, Curr. Opin. Colloid Interface Sci., 39 (2019) 148-161.

[67] B. Katana, D. Takács, E. Csapo, T. Szabo, A. Jamnik, I. Szilagyi: *Ion specific effects on the stability of halloysite nanotube colloids-inorganic salts versus ionic liquids*, J. Phys. Chem. B, 124 (2020) 9757-9765.

[68] P. Rouster, M. Pavlovic, T. Cao, B. Katana, I. Szilagyi: *Stability of titania nanomaterials dispersed in aqueous solutions of ionic liquids of different alkyl chain lengths*, J. Phys. Chem. C, 123 (2019) 12966-12974.

[69] V. Valmacco, G. Trefalt, P. Maroni, M. Borkovec: *Direct force measurements between silica particles in aqueous solutions of ionic liquids containing 1-butyl-3-methylimidazolium (BMIM)*, Phys. Chem. Chem. Phys., 17 (2015) 16553-16559.

[70] N. Jain, X.L. Zhang, B.S. Hawkett, G.G. Warr: *Stable and water-tolerant ionic liquid ferrofluids*, ACS Appl. Mater. Interfaces, 3 (2011) 662-667.

[71] K. Ueno, S. Imaizumi, K. Hata, M. Watanabe: *Colloidal interaction in ionic liquids: Effects of ionic structures and surface chemistry on rheology of silica colloidal dispersions*, Langmuir, 25 (2009) 825-831.

[72] M.A. Minea, S.M.S. Murshed: *Ionic liquids-based nanocolloids-A review of progress and prospects in convective heat transfer applications*, Nanomaterials, 11 (2021) 1039.

[73] R. Zarrougui, M. Dhahbi, D. Lemordant: *Transport and thermodynamic properties of ethylammonium nitrate-water binary mixtures: Effect of temperature and composition*, J. Solution Chem., 44 (2015) 686-702.

[74] B. Mokhtarani, A. Sharifi, H.R. Mortaheb, M. Mirzaei, M. Mafi, F. Sadeghian: *Density and viscosity of pyridinium-based ionic liquids and their binary mixtures with water at several temperatures*, J. Chem. Thermodyn., 41 (2009) 323-329.

[75] M.W. Han, R.M. Espinosa-Marzal: *Influence of water on structure, dynamics, and electrostatics of hydrophilic and hydrophobic ionic liquids in charged and hydrophilic confinement between mica surfaces*, ACS Appl. Mater. Interfaces, 11 (2019) 33465-33477.

[76] Q.L. Zheng, Z.A.H. Goodwin, V. Gopalakrishnan, A.G. Hoane, M.W. Han, R.X. Zhang, N. Hawthorne, J.D. Batteas, A.A. Gewirth, R.M. Espinosa-Marzal: *Water in the electrical double layer of ionic liquids on graphene*, ACS Nano, (2023) 14.

[77] R. Hayes, G.G. Warr, R. Atkin: *At the interface: solvation and designing ionic liquids*, Phys. Chem. Chem. Phys., 12 (2010) 1709-1723.

[78] J.C. Rubim, F.A. Trindade, M.A. Gelesky, R.F. Aroca, J. Dupont: *Surface-enhanced vibrational spectroscopy of tetrafluoroborate 1-n-butyl-3-methylimidazolium ($BMIBF_4$) ionic liquid on silver surfaces*, J. Phys. Chem. C, 112 (2008) 19670-19675.

[79] R. Qiao: *Water at ionic liquids-solid interfaces*, Curr. Opin. Electrochem., 13 (2019) 11-17.

[80] Y. Gao, N. Li, L.Q. Zheng, X.Y. Zhao, J. Zhang, Q. Cao, M.W. Zhao, Z. Li, G.Y. Zhang: *The effect of water on the microstructure of 1-butyl-3-methylimidazolium tetrafluoroborate/TX-100/benzene ionic liquid microemulsions*, Chem.-Eur. J., 13 (2007) 2661-2670.

[81] J. Dupont, J.D. Scholten: *On the structural and surface properties of transition-metal nanoparticles in ionic liquids*, Chem. Soc. Rev., 39 (2010) 1780-1804.

[82] N. Hjalmarsson, R. Atkin, M.W. Rutland: *Is the boundary layer of an ionic liquid equally lubricating at higher temperature?*, Phys. Chem. Chem. Phys., 18 (2016) 9232-9239.

[83] J.M.P. Franca, S.I.C. Vieira, M.J.V. Lourenco, S.M.S. Murshed, C.A.N. de Castro: *Thermal conductivity of C(4)mim (CF3SO2)(2)N and C(2)mim EtSO4 and their ionanofluids with carbon nanotubes: Experiment and theory*, J. Chem. Eng. Data, 58 (2013) 467-476.

[84] W.J. Zhou, M. Zhang, X.Y. Kong, W.W. Huang, Q.C. Zhang: *Recent advance in Ionic-liquid-based electrolytes for rechargeable metal-ion batteries*, Adv. Sci., 8 (2021) 2004490.

[85] A. Ray, B. Saruhan: *Application of ionic liquids for batteries and supercapacitors*, Materials, 14 (2021) 2942.

[86] J. Nordstrom, L. Aguilera, A. Matic: *Effect of lithium salt on the stability of dispersions of fumed silica in the ionic liquid $BMImBF_4$*, Langmuir, 28 (2012) 4080-4085.

[87] R. Hayes, N. Borisenko, B. Corr, G.B. Webber, F. Endres, R. Atkin: *Effect of dissolved LiCl on the ionic liquid-Au(111) electrical double layer structure*, Chem. Commun., 48 (2012) 10246-10248.

[88] M. Vranes, N. Cvjeticanin, S. Papovic, M. Pavlovic, I. Szilagyi, S. Gadzuric: *Electrochemical study of anatase TiO2 nanotube array electrode in electrolyte based on 1,3-diethylimidazolium bis(trifluoromethylsulfonyl)imide ionic liquid*, Ionics, 25 (2019) 5501-5513.

[89] Z.J. Wu, Z.K. Xie, J. Wang, T. Yu, Z.D. Wang, X.G. Hao, A. Abudula, G.Q. Guan: *Lithium-salt-containing ionic liquid-incorporated Li-Al-layered double hydroxide-based solid electrolyte with high-performance and safety in solid-state lithium batteries*, ACS Sustain. Chem. Eng., 8 (2020) 12378-12387.

[90] J. Vatamanu, O. Borodin, G.D. Smith: *Molecular insights into the potential and temperature dependences of the differential capacitance of a room-temperature ionic liquid at graphite electrodes*, J. Am. Chem. Soc., 132 (2010) 14825-14833.

[91] K.P. Gregory, G.R. Elliott, H. Robertson, A. Kumar, E.J. Wanless, G.B. Webber, V.S.J. Craig, G.G. Andersson, A.J. Page: *Understanding specific ion effects and the Hofmeister series*, Phys. Chem. Chem. Phys., 24 (2022) 12682-12718.

[92] W. Kunz, J. Henle, B.W. Ninham: *'Zur lehre von der wirkung der salze' (about the science of the effect of salts): Franz Hofmeister's historical papers*, Curr. Opin. Colloid Interface Sci., 9 (2004) 19-37.

[93] B.B. Kang, H.C. Tang, Z.D. Zhao, S.S. Song: *Hofmeister series: Insights of ion specificity from amphiphilic assembly and interface property*, ACS Omega, 5 (2020) 6229-6239.

[94] H. Robertson, J.D. Willott, K.P. Gregory, E.C. Johnson, I.J. Gresham, A.R.J. Nelson, V.S.J. Craig, S.W. Prescott, R. Chapman, G.B. Webber, E.J. Wanless: *From Hofmeister to hydrotrope: Effect of anion hydrocarbon chain length on a polymer brush*, J. Colloid Interface Sci., 634 (2023) 983-994.

[95] S. Manet, Y. Karpichev, D. Bassani, R. Kiagus-Ahmad, R. Oda: *Counteranion effect on micellization of cationic gemini surfactants 14-2-14: Hofmeister and other counterions*, Langmuir, 26 (2010) 10645-10656.

[96] H.D.B. Jenkins, Y. Marcus: *Viscosity B-coefficients of ions in solution*, Chem. Rev., 95 (1995) 2695-2724.

[97] G. Hantal, J. Kolafa, M. Sega, P. Jedlovszky: *Polarization effects at the surface of aqueous alkali halide solutions*, J. Mol. Liq., 385 (2023) 122333.

[98] T. Lopez-Leon, A.B. Jodar-Reyes, D. Bastos-Gonzalez, J.L. Ortega-Vinuesa: *Hofmeister effects in the stability and electrophoretic mobility of polystyrene latex particles*, J. Phys. Chem. B, 107 (2003) 5696-5708.

[99] T. Lopez-Leon, J.L. Ortega-Vinuesa, D. Bastos-Gonzalez: *Ion-specific aggregation of hydrophobic particles*, ChemPhysChem, 13 (2012) 2382-2391.

[100] T. Oncsik, G. Trefalt, M. Borkovec, I. Szilagyi: *Specific ion effects on particle aggregation induced by monovalent salts within the Hofmeister series*, Langmuir, 31 (2015) 3799-3807.

[101] M. Pavlovic, R. Huber, M. Adok-Sipiczki, C. Nardin, I. Szilagyi: *Ion specific effects on the stability of layered double hydroxide colloids*, Soft Matter, 12 (2016) 4024-4033.

[102] P. Rouster, M. Pavlovic, I. Szilagyi: *Destabilization of titania nanosheet suspensions by inorganic salts: Hofmeister series and Schulze-Hardy rule*, J. Phys. Chem. B, 121 (2017) 6749-6758.

[103] J.M. Peula-Garcia, J.L. Ortega-Vinuesa, D. Bastos-Gonzalez: *Inversion of Hofmeister series by changing the surface of colloidal particles from hydrophobic to hydrophilic*, J. Phys. Chem. C, 114 (2010) 11133-11139.

[104] F. Dumont, J. Warlus, A. Watillon: *Influence of the point of zero charge of titanium-dioxide hydrosols on the ionic adsorption sequences*, J. Colloid Interface Sci., 138 (1990) 543-554.

[105] J. Morag, M. Dishon, U. Sivan: *The governing role of surface hydration in ion specific adsorption to silica: An AFM-based account of the Hofmeister universality and its reversal*, Langmuir, 29 (2013) 6317-6322.

[106] C. Calero, J. Faraudo, D. Bastos-Gonzalez: *Interaction of monovalent ions with hydrophobic and hydrophilic colloids: Charge inversion and ionic specificity*, J. Am. Chem. Soc., 133 (2011) 15025-15035.

[107] D. Constantinescu, H. Weingartner, C. Herrmann: *Protein denaturation by ionic liquids and the Hofmeister series: A case study of aqueous solutions of ribonuclease A*, Angew. Chem. Int. Ed., 46 (2007) 8887-8889.

[108] A.A. Tietze, F. Bordusa, R. Giernoth, D. Imhof, T. Lenzer, A. Maass, C. Mrestani-Klaus, I. Neundorf, K. Oum, D. Reith, A. Stark: *On the nature of interactions between ionic liquids and small amino-acid-based biomolecules*, ChemPhysChem, 14 (2013) 4044-4064.

[109] M.M. Elmahdy, C. Gutsche, F. Kremer: *Forces within single pairs of charged colloids in aqueous solutions of ionic liquids as studied by optical tweezers*, J. Phys. Chem. C, 114 (2010) 19452-19458.

[110] T. Oncsik, A. Desert, G. Trefalt, M. Borkovec, I. Szilagyi: *Charging and aggregation of latex particles in aqueous solutions of ionic liquids: Towards an extended Hofmeister series*, Phys. Chem. Chem. Phys., 18 (2016) 7511-7520.

[111] K. Richter, A. Birkner, A.V. Mudring: *Stability and growth behavior of transition metal nanoparticles in ionic liquids prepared by thermal evaporation: how stable are they really?*, Phys. Chem. Chem. Phys., 13 (2011) 7136–7141.

[112] T. Fiuza, M. Sarkar, J.C. Riedl, M. Beaughon, B.E. Torres Bautista, K. Bhattacharya, F. Cousin, E. Barruet, G. Demouchy, J. Depeyrot, E. Dubois, F. Gélébart, V. Geertsen, G. Mériguet, L. Michot, S. Nakamae, R. Perzynski, V. Peyre: *Ion specific tuning of nanoparticle dispersion in an ionic liquid: a structural, thermoelectric and thermo-diffusive investigation*, Phys. Chem. Chem. Phys., 25 (2023) 28911-28924.

[113] S. Dozic, N. Zec, A. Tot, S. Papovic, K. Pavlovic, S. Gadzuric, M. Vranes: *Does the variation of the alkyl chain length on N1 and N3 of imidazole ring affect physicochemical features of ionic liquids in the same way?*, J. Chem. Thermodyn., 93 (2016) 52-59.

[114] A. Medeiros, A.L. Parize, V.M. Oliveira, B.A.D. Neto, A.F. Bakuzis, M.H. Sousa, L.M. Rossi, J.C. Rubim: *Magnetic ionic liquids produced by the dispersion of magnetic nanoparticles in 1-n-Butyl-3-methylimidazolium bis(trifluoromethanesulfonyl)imide (BMI.NTf$_2$)*, ACS Appl. Mater. Interfaces, 4 (2012) 5458-5465.

[115] J.S. Gao, R.S. Ndong, M.B. Shiflett, N.J. Wagner: *Creating nanoparticle stability in ionic liquid [C$_4$mim][BF$_4$] by inducing solvation layering*, ACS Nano, 9 (2015) 3243-3253.

[116] F.C.C. Oliveira, L.M. Rossi, R.F. Jardim, J.C. Rubim: *Magnetic fluids based on γ-Fe$_2$O$_3$ and CoFe$_2$O$_4$ nanoparticles dispersed in ionic liquids*, J. Phys. Chem. C, 113 (2009) 8566-8572.

[117] A.V. Dobrynin, A. Deshkovski, M. Rubinstein: *Adsorption of polyelectrolytes at oppositely charged surfaces*, Macromolecules, 34 (2001) 3421-3436.

[118] I. Szilagyi, G. Trefalt, A. Tiraferri, P. Maroni, M. Borkovec: *Polyelectrolyte adsorption, interparticle forces, and colloidal aggregation*, Soft Matter, 10 (2014) 2479-2502.

[119] C. Vollmer, C. Janiak: *Naked metal nanoparticles from metal carbonyls in ionic liquids: Easy synthesis and stabilization*, Coord. Chem. Rev., 255 (2011) 2039-2057.

[120] D. Mecerreyes: *Polymeric ionic liquids: Broadening the properties and applications of polyelectrolytes*, Prog. Polym. Sci., 36 (2011) 1629-1648.
[121] I. Biondi, V. Laporte, P.J. Dyson: *Application of a versatile nanoparticle stabilizer in phase transfer and catalysis*, ChemPlusChem, 77 (2012) 721-726.
[122] X. Yang, Z.F. Fei, D.B. Zhao, W.H. Ang, Y.D. Li, P.J. Dyson: *Palladium nanoparticles stabilized by an ionic polymer and ionic liquid: A versatile system for C-C cross-coupling reactions*, Inorg. Chem., 47 (2008) 3292-3297.
[123] P.G. de Gennes: *Ultradivided matter*, Nature, 412 (2001) 385-385.
[124] T.L. Moore, L. Rodriguez-Lorenzo, V. Hirsch, S. Balog, D. Urban, C. Jud, B. Rothen-Rutishauser, M. Lattuada, A. Petri-Fink: *Nanoparticle colloidal stability in cell culture media and impact on cellular interactions*, Chem. Soc. Rev., 44 (2015) 6287-6305.
[125] S.C. Hamm, S. Basuray, S. Mukherjee, S. Sengupta, J.C. Mathai, G.A. Baker, S. Gangopadhyay: *Ionic conductivity enhancement of sputtered gold nanoparticle-in-ionic liquid electrolytes*, J. Mater. Chem. A, 2 (2014) 792-803.
[126] L. Jing, M. Wang, X.Y. Li, R.Y. Xiao, Y.F. Zhao, Y.X. Zhang, Y.M. Yan, Q. Wu, K.N. Sun: *Covalently functionalized TiO_2 with ionic liquid: A high-performance catalyst for photoelectrochemical water oxidation*, Appl. Catal. B-Environ., 166 (2015) 270-276.
[127] X.Q. Wang, P.F. Fulvio, G.A. Baker, G.M. Veith, R.R. Unocic, S.M. Mahurin, M.F. Chi, S. Dai: *Direct exfoliation of natural graphite into micrometre size few layers graphene sheets using ionic liquids*, Chem. Commun., 46 (2010) 4487-4489.
[128] W.C. Zhao, Z.M. Xue, J.F. Wang, J.Y. Jiang, X.H. Zhao, T.C. Mu: *Large-scale, highly efficient, and green liquid-exfoliation of black phosphorus in ionic liquids*, ACS Appl. Mater. Interfaces, 7 (2015) 27608-27612.
[129] C.J. Pang, J.G. Liu, R. Peng, Y.Y. Guo, Z.Y. Li, H.Y. Wang: *Liquid-phase exfoliation of titanium disulfide nanosheets in aqueous ionic liquid solutions for highly efficient CO_2 electroreduction*, J. Mol. Liq., 381 (2023) 121814.
[130] T. Morishita, H. Okamoto, Y. Katagiri, M. Matsushita, K. Fukumori: *A high-yield ionic liquid-promoted synthesis of boron nitride nanosheets by direct exfoliation*, Chem. Commun., 51 (2015) 12068-12071.
[131] Z.B. Cao, B. Li, L.Y. Sun, L. Li, Z.P. Xu, Z. Gu: *2D layered double hydroxide nanoparticles: Recent progress toward preclinical/clinical nanomedicine*, Small Methods, 4 (2019) 1900343.
[132] F.L. Theiss, S.J. Couperthwaite, G.A. Ayoko, R.L. Frost: *A review of the removal of anions and oxyanions of the halogen elements from aqueous solution by layered double hydroxides*, J. Colloid Interface Sci., 417 (2014) 356-368.
[133] G. Mishra, B. Dash, S. Pandey: *Layered double hydroxides: A brief review from fundamentals to application as evolving biomaterials*, Appl. Clay Sci., 153 (2018) 172-186.
[134] C. Forano, S. Vial, C. Mousty: *Nanohybrid enzymes - Layered double hydroxides: Potential applications*, Curr. Nanosci., 2 (2006) 283-294.
[135] C. Vasti, D.A. Bedoya, L.V. Bonnet, E. Ambroggio, C.E. Giacomelli, R. Rojas: *Synthetic and biological identities of layered double hydroxides nanocarriers functionalized with risedronate*, Appl. Clay Sci., 199 (2020) 105880.
[136] F. Song, X.L. Hu: *Exfoliation of layered double hydroxides for enhanced oxygen evolution catalysis*, Nat. Commun., 5 (2014) 4477.

[137] S. Murath, T. Varga, A. Kukovecz, Z. Konya, P. Sipos, I. Palinko, G. Varga: *Morphological aspects determine the catalytic activity of porous hydrocalumites: the role of the sacrificial templates*, Mater. Today Chem., 23 (2022) 100682.
[138] V. Rives, M. del Arco, C. Martin: *Intercalation of drugs in layered double hydroxides and their controlled release: A review*, Appl. Clay Sci., 88-89 (2014) 239-269.
[139] Z. Gu, J.J. Atherton, Z.P. Xu: *Hierarchical layered double hydroxide nanocomposites: structure, synthesis and applications*, Chem. Commun., 51 (2015) 3024-3036.
[140] Z.J. Yuan, S.M. Bak, P.S. Li, Y. Jia, L.R. Zheng, Y. Zhou, L. Bai, E.Y. Hu, X.Q. Yang, Z. Cai, Y.M. Sun, X.M. Sun: *Activating layered double hydroxide with multivacancies by memory effect for energy-efficient hydrogen production at neutral pH*, ACS Energy Lett., 4 (2019) 1412-1418.
[141] T.R. Zhan, Y.M. Zhang, Q. Yang, H.H. Deng, J. Xu, W.G. Hou: *Ultrathin layered double hydroxide nanosheets prepared from a water-in-ionic liquid surfactant-free microemulsion for phosphate removal from aquatic systems*, Chem. Eng. J., 302 (2016) 459-465.
[142] F. Seidi, M. Jouyandeh, S.M.R. Paran, A. Esmaeili, Z. Karami, S. Livi, S. Habibzadeh, H. Vahabi, M.R. Ganjali, M.R. Saeb: *Imidazole-functionalized nitrogen-rich Mg-Al-CO_3 layered double hydroxide for developing highly crosslinkable epoxy with high thermal and mechanical properties*, Colloid Surf. A-Physicochem. Eng. Asp., 611 (2021) 125826.
[143] T.F. Li, W. Zhang, W. Chen, H.N. Miras, Y.F. Song: *Layered double hydroxide anchored ionic liquids as amphiphilic heterogeneous catalysts for the Knoevenagel condensation reaction*, Dalton Trans., 47 (2018) 3059-3067.
[144] Q. Wang, D. O'Hare: *Recent advances in the synthesis and application of layered double hydroxide (LDH) nanosheets*, Chem. Rev., 112 (2012) 4124-4155.
[145] D.G. Evans, R.C.T. Slade: *Structural aspects of layered double hydroxides*, in: X. Duan, D.G. Evans (Eds.) Layered Double Hydroxides2006, pp. 1-87.
[146] G. Varga, Z. Somosi, A. Kukovecz, Z. Konya, I. Palinko, I. Szilagyi: *A colloid chemistry route for the preparation of hierarchically ordered mesoporous layered double hydroxides using surfactants as sacrificial templates*, J. Colloid Interface Sci., 581 (2021) 928-938.
[147] W. Zhong, F.D. Bobbink, Z.F. Fei, P.J. Dyson: *Polyimidazolium salts: Robust catalysts for the cycloaddition of carbon dioxide into carbonates in solvent-free conditions*, ChemSusChem, 10 (2017) 2728-2735.
[148] A.V. Delgado, E. Gonzalez-Caballero, R.J. Hunter, L.K. Koopal, J. Lyklema: *Measurement and interpretation of electrokinetic phenomena - (IUPAC technical report)*, Pure Appl. Chem., 77 (2005) 1753-1805.
[149] R.W. O'Brien, L.R. White: *Electrophoretic mobility of a spherical colloidal particle*, J. Chem. Soc.-Faraday Trans., 74 (1978) 1607-1626.
[150] W.B. Russel, D.A. Saville, W.R. Schowalter: *Colloidal dispersions*, Cambridge University Press, Cambridge, 1989.
[151] H. Holthoff, S.U. Egelhaaf, M. Borkovec, P. Schurtenberger, H. Sticher: *Coagulation rate measurements of colloidal particles by simultaneous static and dynamic light scattering*, Langmuir, 12 (1996) 5541-5549.
[152] B.J. Berne, R. Pecora: *Dynamic light scattering*, Robert E. Krieger Publishing, Malabar, 1990.

[153] D. Orthaber, A. Bergmann, O. Glatter: *SAXS experiments on absolute scale with Kratky systems using water as a secondary standard*, J. Appl. Crystallogr., 33 (2000) 218-225.
[154] O. Glatter: *Numerical methods*, Scattering methods and their application in colloid and interface science, Elsevier, Amsterdam, 2018, 137-174.
[155] O. Glatter: *Evaluation of small-angle scattering data from lamellar and cylindrical particles by the indirect transformation method*, J. Appl. Crystallogr., 13 (1980) 577-584.
[156] G. Fritz, O. Glatter: *Structure and interaction in dense colloidal systems: evaluation of scattering data by the generalized indirect Fourier transformation method*, J. Phys.-Condes. Matter, 18 (2006) S2403-S2419.
[157] T. Sato, H. Sakai, K. Sou, M. Medebach, O. Glatter, E. Tsuchida: *Static structures and dynamics of hemoglobin vesicle (HbV) developed as a transfusion alternative*, J. Phys. Chem. B, 113 (2009) 8418-8428.
[158] C. Schneider, M. Hanisch, B. Wedel, A. Jusufi, M. Ballauff: *Experimental study of electrostatically stabilized colloidal particles: Colloidal stability and charge reversal*, J. Colloid Interface Sci., 358 (2011) 62-67.
[159] J. Ramos, J. Forcada, R. Hidalgo-Alvarez: *Cationic Polymer Nanoparticles and Nanogels: From Synthesis to Biotechnological Applications*, Chem. Rev., 114 (2014) 367-428.
[160] Y.N. Xia, B. Gates, Y.D. Yin, Y. Lu: *Monodispersed colloidal spheres: Old materials with new applications*, Adv. Mater., 12 (2000) 693-713.
[161] M.A.M. Mballa, S.I. Ali, J.P.A. Heuts, A.M. van Herk: *Control of the anisotropic morphology of latex nanocomposites containing single montmorillonite clay particles prepared by conventional and reversible addition-fragmentation chain transfer based emulsion polymerization*, Polym. Int., 61 (2012) 861-865.
[162] S. Saringer, R.A. Akula, A. Szerlauth, I. Szilagyi: *Papain adsorption on latex particles: Charging, aggregation, and enzymatic activity*, J. Phys. Chem. B, 123 (2019) 9984-9991.
[163] J.L. Trompette, J.F. Lahitte: *Influence of the counterion nature on the stability sequence of hydrophobic latex particles*, J. Phys. Chem. B, 123 (2019) 3859-3865.
[164] J. Gregory: *Monitoring particle aggregation processes*, Adv. Colloid Interface Sci., 147-48 (2009) 109-123.
[165] G. Gillies, W. Lin, M. Borkovec: *Charging and aggregation of positively charged latex particles in the presence of anionic polyelectrolytes*, J. Phys. Chem. B, 111 (2007) 8626-8633.
[166] I. Popa, G. Gillies, G. Papastavrou, M. Borkovec: *Attractive and repulsive electrostatic forces between positively charged latex particles in the presence of anionic linear polyelectrolytes*, J. Phys. Chem. B, 114 (2010) 3170-3177.
[167] I. Szilagyi, D. Rosicka, J. Hierrezuelo, M. Borkovec: *Charging and stability of anionic latex particles in the presence of linear poly(ethylene imine)*, J. Colloid Interface Sci., 360 (2011) 580-585.
[168] M. Borkovec, S.H. Behrens, M. Semmler: *Observation of the mobility maximum predicted by the standard electrokinetic model for highly charged amidine latex particles*, Langmuir, 16 (2000) 5209-5212.
[169] P.J. Sideris, U.G. Nielsen, Z.H. Gan, C.P. Grey: *Mg/Al ordering in layered double hydroxides revealed by multinuclear NMR spectroscopy*, Science, 321 (2008) 113-117.

[170] W.Y. Yu, N. Du, Y.T. Gu, J.G. Yan, W.G. Hou: *Specific ion effects on the colloidal stability of layered double hydroxide single-layer nanosheets*, Langmuir, 36 (2020) 6557-6568.

[171] M. Schudel, S.H. Behrens, H. Holthoff, R. Kretzschmar, M. Borkovec: *Absolute aggregation rate constants of hematite particles in aqueous suspensions: A comparison of two different surface morphologies*, J. Colloid Interface Sci., 196 (1997) 241-253.

[172] P. Sinha, I. Szilagyi, F.J.M. Ruiz-Cabello, P. Maroni, M. Borkovec: *Attractive forces between charged colloidal particles induced by multivalent ions revealed by confronting aggregation and direct force measurements*, J. Phys. Chem. Lett., 4 (2013) 648-652.

[173] M. Kobayashi, F. Juillerat, P. Galletto, P. Bowen, M. Borkovec: *Aggregation and charging of colloidal silica particles: Effect of particle size*, Langmuir, 21 (2005) 5761-5769.

[174] A. Fuchs, E. Killmann: *Adsorption of polyelectrolytes on colloidal latex particles, electrostatic interactions and stability behaviour*, Colloid. Polym. Sci., 279 (1998) 53-60.

[175] E. Seyrek, J. Hierrezuelo, A. Sadeghpour, I. Szilagyi, M. Borkovec: *Molecular mass dependence of adsorbed amount and hydrodynamic thickness of polyelectrolyte layers*, Phys. Chem. Chem. Phys., 13 (2011) 12716-12719.

[176] M. Galli, S. Saringer, I. Szilagyi, G. Trefalt: *A simple method to determine critical coagulation concentration from electrophoretic mobility*, Colloid Interfac., 4 (2020) 20.

[177] M. Elzbieciak-Wodka, M. Popescu, F.J. Montes Ruiz-Cabello, G. Trefalt, P. Maroni, M. Borkovec: *Measurements of dispersion forces between colloidal latex particles with the atomic force microscope and comparison with Lifshitz theory*, J. Chem. Phys., 140 (2014) 104906.

[178] N. Schwierz, D. Horinek, R.R. Netz: *Reversed anionic Hofmeister series: The interplay of surface charge and surface polarity*, Langmuir, 26 (2010) 7370-7379.

[179] T. Lopez-Leon, A.B. Jodar-Reyes, J.L. Ortega-Vinuesa, D. Bastos-Gonzalez: *Hofmeister effects on the colloidal stability of an IgG-coated polystyrene latex*, J. Colloid Interface Sci., 284 (2005) 139-148.

[180] J. Hierrezuelo, I. Szilagyi, A. Vaccaro, M. Borkovec: *Probing nanometer-thick polyelectrolyte layers adsorbed on oppositely charged particles by dynamic light scattering*, Macromolecules, 43 (2010) 9108-9116.

[181] W.C. Wei: *Hofmeister effects shine in nanoscience*, Adv. Sci., (2023) 18.

[182] R.P. Matthews, T. Welton, P.A. Hunt: *Hydrogen bonding and pi-pi interactions in imidazolium-chloride ionic liquid clusters*, Phys. Chem. Chem. Phys., 17 (2015) 14437-14453.

[183] P.P. Arquilliere, I.S. Helgadottir, C.C. Santini, P.H. Haumesser, M. Aouine, L. Massin, J.L. Rousset: *Bimetallic Ru-Cu nanoparticles synthesized in ionic liquids: Kinetically controlled size and structure*, Top. Catal., 56 (2013) 1192-1198.

[184] D.A. Beattie, R.M. Espinosa-Marzal, T.T.M. Ho, M.N. Popescu, J. Ralston, C.J.E. Richard, P.M.F. Sellapperumage, M. Krasowska: *Molecularly-thin precursor films of imidazolium-based ionic liquids on mica*, J. Phys. Chem. C, 117 (2013) 23676-23684.

[185] S. Kondrat, A.A. Kornyshev: *Pressing a spring: what does it take to maximize the energy storage in nanoporous supercapacitors?*, Nanoscale Horizons, 1 (2016) 45-52.

[186] T. Hegedus, D. Takács, L. Vasarhelyi, I. Szilagyi, Z. Konya: *Specific ion effects on aggregation and charging properties of boron nitride nanospheres*, Langmuir, 37 (2021) 2466-2475.

[187] H.K. Stassen, R. Ludwig, A. Wulf, J. Dupont: *Imidazolium salt ion pairs in solution*, Chem.-Eur. J., 21 (2015) 8324-8335.

[188] A. Stoppa, J. Hunger, G. Hefter, R. Buchner: *Structure and dynamics of 1-N-Alkyl-3-N-methylimidazolium tetrafluoroborate plus acetonitrile mixtures*, J. Phys. Chem. B, 116 (2012) 7509-7521.

[189] T. Sugimoto, T.C. Cao, I. Szilagyi, M. Borkovec, G. Trefalt: *Aggregation and charging of sulfate and amidine latex particles in the presence of oxyanions*, J. Colloid Interface Sci., 524 (2018) 456-464.

[190] S. Livi, V. Bugatti, L. Estevez, J. Duchet-Rumeau, E.P. Giannelis: *Synthesis and physical properties of new layered double hydroxides based on ionic liquids: Application to a polylactide matrix*, J. Colloid Interface Sci., 388 (2012) 123-129.

[191] T.L. Greaves, D.F. Kennedy, N. Kirby, C.J. Drummond: *Nanostructure changes in protic ionic liquids (PILs) through adding solutes and mixing PILs*, Phys. Chem. Chem. Phys., 13 (2011) 13501-13509.

[192] O. Glatter: *New method for evaluation of small-angle scattering data*, J. Appl. Crystallogr., 10 (1977) 415-421.

[193] Y. Zhao, W.D. Yang, Y.H. Xue, X.G. Wang, T. Lin: *Partial exfoliation of layered double hydroxides in DMSO: a route to transparent polymer nanocomposites*, J. Mater. Chem., 21 (2011) 4869-4874.

Papers related to the dissertation

[I] B. Katana, D. Takács, F.D. Bobbink, P.J. Dyson, N.B. Alsharif, M. Tomšič, I. Szilagyi: *Masking specific effects of ionic liquid constituents at the solid–liquid interface by surface functionalization*, Phys. Chem. Chem. Phys., 22 (2020) 24764-24770.

[II] D. Takács, B. Katana, A. Szerlauth, D. Sebők, M. Tomšič, I. Szilagyi: *Influence of adsorption of ionic liquid constituents on the stability of layered double hydroxide colloids*, Soft Matter, 17 (2021) 9116-9124.

[III] D. Takács, M. Tomšič, I. Szilagyi: *Effect of water and salt on the colloidal stability of latex particles in ionic liquid solutions*, Colloid Interfac., 6 (2022) 2.

[IV] D. Takács, G. Varga, E. Csapo, A. Jamnik, M. Tomsic, I. Szilagyi: *Delamination of layered double hydroxide in ionic liquids under ambient conditions*, J. Phys. Chem. Lett., 13 (2022) 11850-11856.

Acknowledgement

First and foremost, I would like to express my sincere gratitude to Dr. István Szilágyi, my supervisor and the leader of Biocolloids Research Group, for his constant guidance, invaluable advice, and support during my doctoral studies.

I am also grateful to Prof. Ágota Tóth, head of the Department of Physical Chemistry and Materials Science for the opportunity to finish my doctoral studies at the department.

I would like to express my gratitude to Prof. Matija Tomšič for his assistance with the SAXS measurements, which significantly contributed to the quality and depth of my research. I am also thankful to Prof. Paul Dyson for his collaboration and for providing the IP-2 polymer, which added a valuable dimension to my work.

I cannot forget to extend my gratitude to my colleagues at the Biocolloids Research Group for the friendly and supportive working environment, as well as the great memories that will always be cherished.

In closing, I would like to wholeheartedly thank my loving parents, my supportive brother, and my feline companions for the tremendous support and reassuring background they have given me. I am also deeply grateful for my extraordinary friends, who have provided me with much-needed and pleasant distraction when I needed it the most through engaging conversations, thorough investigations of random topics, infectious laughter, and delightful cat videos.

To summarise: Köszönök mindenkinek mindent!